Forschungszentrum Jülich
in der Helmholtz-Gemeinschaft

Institute of Energy Research (IEF)
Photovoltaics (IEF-5)

Microcrystalline silicon layers for thin film solar cells prepared with Hot Wire Chemical Vapour Deposition and Plasma Enhanced Chemical Vapour Deposition

Yaohua Mai

Jül-4254

Microcrystalline silicon layers for thin film solar cells prepared with Hot Wire Chemical Vapour Deposition and Plasma Enhanced Chemical Vapour Deposition

Yaohua Mai

Berichte des Forschungszentrums Jülich ; 4254
ISSN 0944-2952
Institute of Energy Research (IEF)
Photovoltaics (IEF-5) Jül-4254

(Tianjin, V.R. China, Nankai Univ., Diss., 2006)

The complete volume is freely available on the Internet on the Jülicher Open Access Server (JUWEL) at http://www.fz-juelich.de/zb/juwel

Zu beziehen durch: Forschungszentrum Jülich GmbH · Zentralbibliothek, Verlag
D-52425 Jülich · Bundesrepublik Deutschland
☎ 02461/61-5220 · Telefax: 02461/61-6103 · e-mail: zb-publikation@fz-juelich.de

Contents

Abstract

High rate growth process, material quality and related solar cell performance of hydrogenated microcrystalline silicon (μc-Si:H) were investigated in this work. High deposition rate (R_D) was achieved by very high frequency (VHF) plasma-enhanced chemical vapor deposition (PECVD) working at high pressure and high power (hphP). Compared to the μc-Si:H material deposited with conventional low pressure, low power (lplP), the hphP films showed equivalent optical and electrical properties, indicating their abilities as absorbers in thin film silicon solar cells. The influences of the deposition parameters on the solar cell deposition rate and performance were systematically investigated in this thesis. It was found that optimum cells were always found close to the transition from highly microcrystalline to the amorphous growth and with medium crystallinity. Variations of many deposition parameters can tune the crystallinity. Among them, varying silane concentration (SC) is the most easy and straightforward way. Under optimized conditions, high efficiency of 9.8% was obtained at R_D over 1 nm/s for a single junction p-i-n solar cell. Efforts were also made to find out the correlation between the material properties and solar cell performance. The Raman structure depth profile method revealed that hphP solar cells consisted of a more amorphous incubation layer at the p/i interface, which was found to reduce the short wavelength light response of the solar cells.

Besides PECVD, Hot Wire (HW) CVD is an alternative method for μc-Si:H deposition. It was found that HWCVD μc-Si H cells showed higher V_{OC} and FF than the PECVD cells in a wide range of i-layer crystallinity. This was attributed to the better p/i interface quality in the HWCVD cells. Inserting an intrinsic microcrystalline p/i interface layer deposited by HWCVD into PECVD cells nearly eliminated the above differences. Raman structure depth profile, transmission electron microscopy and selective area electron diffraction were applied to investigate the structure properties of the solar cells. However, differences could hardly be found in the already homogeneous i-layers of PECVD and HWCVD cells. Thus the positive effect of the HW-buffer for facilitating nucleation was not observed. An amorphous HW-buffer layer in PECVD cells resulted in a more amorphous p/i interface and an increasing crystallinity along the growth axis. However, such amorphous interface layer still enhanced the V_{OC} and FF of the resulting cells. Therefore, it was concluded that structure homogeneity was not the reason for the better performance of the HWCVD cells. Applying the HW-buffer concept to the PECVD hphP cells, we obtained a high efficiency of 10.3% at a high R_D of 1.1 nm/s. This is the highest efficiency reported so far for the single junction μc-Si:H solar cells in p-i-n configuration.

Chapter 1

Introduction

1.1 Solar energy and solar cells

Nowadays, more than 85 % of our commercial energy supplies are produced from the combustion of fossil fuels, i.e. coal, oil and natural gases [*Goetzberger 2003*]. The increasing demand and consumption of fossil energy resources are now causing severe economical and environmental problems. Due to its almost infinite energy source and the environment friendly nature, photovoltaics, converting the sun light directly into electricity, has been regarded as a promising technique for future power supply.

The photovoltaic effect was first discovered by E. Becquerel in 1839 [*E. Becquerel 1839*]. However, considerable progress had not been made until the first single crystalline silicon (c-Si) solar cell was invented by Chapin et al. in 1954 [*Chapin 1954*]. In the past several decades, different types of solar cells have been developed. Among them the conventional Si wafer based c-Si or multi-Si solar cells were classified as the first generation cells [*Green 2002*]. The efficiency of c-Si solar cells has been improved a lot from 6 % of the first cell to today's 24.7 % [*Zhao 1999*]. At present, the world photovoltaic market is dominated by the first generation cells. The production cost of these solar cells is mainly determined by the material cost from silicon wafers and encapsulant. This makes it difficult to largely reduce the production cost and thus will limit the large-scale application of such cells. Thin film solar cells, like cadmium-telluride (CdTe), copper-indium-gallium-selenide (CIGS) and amorphous or microcrystalline silicon cells, are considered to be the second generation. Thin film technologies are promising in the cost reduction since they do not need the expensive silicon wafers, and they can be deposited on large area, low cost substrates, such as glass, stainless steel and plastic foils. The hydrogenated amorphous silicon (a-Si:H) solar cells, fabricated from largely available elements, are the first industrialized thin film photovoltaic products. Compared to a-Si:H solar cells, hydrogenated microcrystalline silicon solar (μc-Si:H) cells show a number of advantages, such as wider spectral response and better stability against light soaking, etc. μc-Si:H thin films and solar cells deposited by plasma-enhanced chemical vapor deposition (PECVD) and hot wire chemical vapor

deposition (HWCVD) are the research subjects of this work.

1.2 Amorphous and microcrystalline silicon material and solar cells

Hydrogenated amorphous and microcrystalline silicon thin films consist of a large amount of hydrogen atoms, and thus are usually regarded as the alloy of silicon and hydrogen. For simplicity, they are referred to be amorphous and microcrystalline silicon in this thesis. In this section, only a brief introduction to the history and current status of amorphous silicon and microcrystalline silicon thin films and solar cells will be given. For detailed information of such material and devices, see Chapter 2.

1.2.1 Amorphous silicon thin films and solar cells

Compared to the rigid periodic atomic structure in crystalline silicon, a-Si:H material shows no long range order and translation symmetry. The absence of long range order and translation symmetry result in unique characteristics in the material, such as the presence of band tail states and dangling bonds, etc.

Amorphous silicon has been deposited by many techniques. Among them, PECVD was the first one to produce high quality a-Si:H thin films with high photosensitivity [*Chittick 1969*]. Nowadays, PECVD has become the most frequently-used technique for a-Si:H deposition. In 1975, Spear and LeComber found that a-Si:H can be substitutionally doped by adding doping gases like diborane or phosphine into the reactant gases [*Spear and LeComber 1975*]. Ever since then, the researches in the material properties and device applications of a-Si:H boomed rapidly. In the next year, the first thin film solar cell with a-Si:H as absorber came into being , showing an efficiency of 2.4 % [*Carlson and Wronski 1976*]. Other a-Si:H based material, such as a-SiGe:H and a-SiC:H, were also applied to thin film solar cells and other optoelectronic devices [*Hamakawa 2000 and references therein*]. Yang et al. achieved high efficiency of 14.6 % in an a-Si:H/a-SiGe:H/a-SiGe:H triple junction solar cell [*Yang 1997*].

The most important drawback of a-Si:H is that the material quality and solar cell performance deteriorate after long term sun light illumination. This is called the 'Staebler Wronski Effect' [*Staebler and Wronski 1977*]. This problem still exists after decades of efforts by many researchers and largely limits the application of a-Si:H solar cells.

1.2.2 Microcrystalline silicon thin films and solar cells

Opposite to the homogeneous nature of a-Si:H, μc-Si:H films can be considered as a mixture of crystallites, amorphous tissue, grain boundaries and voids. Parameters related to crystallites are crystalline volume fraction, grain size and crystal orientation, etc.

μc-Si:H was first deposited by Vepřek and Mareček in 1968, who used a hydrogen plasma and the chemical transport method at 600 °C [*Vepřek and Mareček 1968*]. Later on, PECVD was also used to deposit μc-Si:H films by high hydrogen dilution of silane [*Usui and Kikuchi 1979*]. It was found that varying the deposition parameters, such as hydrogen dilution and substrate temperature etc., shifted the films from amorphous to microcrystalline growth [*Mastuda 1983*].

In the early 1980s, Vepřek and co-workers published a series of important papers, which described in detail the structural, optical and electrical properties of the μc-Si:H films deposited by PECVD and chemical transport method [*Vepřek 1981, Iqbal and Vepřek 1982, Iqbal 1983, Vepřek 1983*]. However, probably due to the low material quality and/or low deposition rate (R_D, usually far below 0.1 nm/s by PECVD), it was difficult at that time to fabricate intrinsic μc-Si:H layers with sufficient quality and thickness as thin film silicon solar cell absorbers. In addition, because of the low optical absorption and high doping efficiency, doped μc-Si:H layer used in thin film silicon solar cells became the major research subject in the whole 1980s and in the early 1990s. PECVD working with very high plasma excitation frequency greatly increased R_D of silicon thin films [*Curtins 1987, Oda and Noda 1988, Prasad 1990, Howling 1992, Finger 1992, Finger 1994*]. This made it possible to deposit a thick μc-Si:H absorber layer in a reasonable short period of time. The first thin film silicon solar cell with μc-Si:H as absorber layer appeared in the early 1990s [*Wang and Lucovsky 1990, Flückiger 1992, Faraji 1992*]. Later on, Meier et al. found that such solar cells did not degrade after a long term light soaking [*Meier 1994*]. In addition, it was found that, together with an a-Si:H top cell, μc-Si:H cell could replace the a-SiGe:H cell to form an a-Si:H/μc-Si:H double-junction solar cell [*Meier 1994a*]. The first a-Si:H/μc-Si:H tandem cell showed a high efficiency of 9.1 % [*Meier 1994a*]. The success of μc-Si:H solar cells stimulated an intensive research on this type of material and devices.

The as-deposited μc-Si:H films are usually slightly n-type [*Vepřek 1983*], which was previously ascribed to the high defect density or oxygen contamination [*Vepřek 1983, Wang and Lucovsky 1990, Meier 1994a*]. Micro-doping with boron shifted the Fermi level back to the middle of the band-gap. As a result, it increased the long wavelength response of the solar cells [*Meier 1994a*]. Reducing the oxygen or water vapor in the reactant gases by using gas purifiers in the gas supplying system reduced the oxygen content in the films and enhanced the solar cell long wavelength response too [*Torres 1996*].

Structure properties have critical influences on the optical and electrical properties of μc-Si:H films and devices, and thus have long been intensively investigated by many researchers [*Vepřek 1983, Tsai 1989*]. Luysberg et al. investigated μc-Si:H films deposited with different plasma excitation frequencies and observed the columnar structure along the growth direction [*Luysberg 1997*]. While studying the microstructure of μc-Si:H films deposited with different silane concentrations (SC), Houben and Vallat-Sauvain et al. found that the crystalline volume fraction and grain size decreased with the increasing SC [*Houben 1998, Vallat-Sauvain 2000*]. Here, a very important observation was that the optimum

solar cells, in terms of the highest efficiency, were not made of the material with the highest crystalline volume fraction and the largest grain size, but of that deposited close to the transition from microcrystalline to amorphous growth [*Vetterl 2000, Roschek 2002, Klein 2004*]. It was found that μc-Si:H films with high crystallinity were usually highly defective [*Baia Neto 2000, Finger 2002*]. Such films were also very porous and subject to the in-diffusion of atmospheric molecules [*Finger 2003*].

Various models have been proposed for the description of μc-Si:H growth, such as the partial chemical equilibrium model [*Vepřek 1990*] or the related selective etching model [*Tsai 1989*], the surface diffusion model [*Matsuda 1983*], and the chemical annealing model [*Shirai 1991, Nakamura 1995*] etc. Although different from each other, these models have in common that a high hydrogen radical density in the plasma is indispensable for the formation of μc-Si:H. In good agreement with these models, μc-Si:H films and solar cells were usually deposited with high hydrogen dilution in the reactant gases.

At present, PECVD is the most commonly-used method for μc-Si:H deposition. Very high frequency plasma (VHF) excitation increased the deposition rate and improved the material quality of silicon thin films [*Oda and Noda 1988, Prasad 1990, Finger 1994*]. Guo and Kondo et al. proposed a high pressure depletion (HPD) regime for high quality μc-Si:H deposition [*Guo 1998, Kondo 2000*], and achieved high R_D in a conventional radio frequency (RF) regime [*Guo 1998, Kondo 2000, Roschek 2002, Repmann 2004*]. Recently, also combinations of VHF-PECVD and HPD have been investigated successfully [*Fukawa 2001, Lambertz 2001, Matsui 2002, Graf 2003, Gordijn 2005, Kilper 2005*]. However, there are still many questions left unanswered. Clarifying these questions is one of the main objects of this thesis. High rate growth of μc-Si:H with PECVD requires reasonably high discharge power for high dissociation of the reactant gases. High discharge power usually increases the peak-to-peak voltage over the electrodes and thus high ion energy, if the other deposition parameters are maintained constant [*Chapman 1980*]. However, high-energy ions impinging on the growth surface are considered to be detrimental to the quality of μc-Si:H, causing defect formation and retarding nucleation [*Matsuda 1983, Vepřek 1989, Kondo 2000*].This thesis reports further studies of the combination of VHF-PECVD at 94.7 MHz and high working pressure of 2-4 hPa to achieve high R_D and reduce the ion energy at the same time. As high pressure is employed together with high discharge power, we shall refer to this deposition regime as hphP (high pressure - high power) in contrast to the conventional low power, low pressure (lplP) conditions.

Ever since Mastumura and Mahan et al. proved that hot wire chemical vapor deposition (HWCVD) was also capable of providing high quality a-Si:H [*Matsumura 1986, Mahan 1991*], μc-Si:H deposited by HWCVD became a hot research topic [*Matsumura 1991, Rath 1997, Schropp 1997, Alpuim 1999*]. However, great progress was not made in solar cells with HWCVD μc-Si:H *i*-layers until Klein et al. employed a low substrate temperature (T_S) technique [*Klein 2001, Klein 2004*]. Low T_S usually required a low filament temperature and a long filament-substrate distance, which remarkably reduced the deposition rate [*Klein*

2004]. Microcrystalline silicon thin films and solar cells deposited by PECVD and HWCVD are similar from many aspects. For example, optimum solar cells always consist of i-layers obtained close to the transition from μc-Si:H to a-Si:H growth [*Vetterl 2000, Roschek 2002, Klein 2003*]. In addition, high efficiency over 9 % was obtained in μc-Si:H solar cells deposited by both methods [*Klein 2003, Feitknecht 2003, Matsui 2004, Gordijn 2005, Kilper 2005*]. However, these two types of solar cells also show distinct differences. For example, HWCVD cells have higher open voltage (V_{OC}) than the PECVD cells at the same i-layer crystallinity [*Klein 2005*]. In addition, V_{OC} of the HWCVD optimum solar cells is about 50 mV higher than that of the optimum cells deposited by PECVD [*Vetterl 2000, Roschek 2002, Klein 2003*]. As high V_{OC} is important to achieve high efficiency in the single junction or stacked cells, understanding the physics behind is of great scientific and technical interest. Furthermore, the growth rates of the HWCVD solar cells deposited at low substrate temperature were significantly reduced due to the low filament temperature. Thus, making use of the advantages of the HWCVD and PECVD processes, namely, high V_{OC} by HWCVD and high growth rate by PECVD, will be very promising for the industrial application. For these purposes, efforts were made in this thesis to compare the state of the art μc-Si:H thin films and solar cells deposited by these two methods.

1.3 Aims and outline

As mentioned above, high rate growth of μc-Si:H is one of the research topic of this work. Efforts will be made to solve the following questions,

- How to achieve stable and homogeneous deposition under VHF+hphP conditions?
- What are the influences of the deposition parameters?
- What is the relationship between the material properties and solar cell performance?
- Is it possible to further increase the deposition rate while maintaining high material and device quality?

μc-Si:H deposited by PECVD and HWCVD show both great similarity and distinct differences. Understanding the physics behind the differences may help to increase the solar cell performance further. Therefore, μc-Si:H thin films and solar cells deposited by PECVD and HWCVD will be systematically studied and compared. In this part of work, finding out answers for the following questions will be major tasks,

- In how far are μc-Si:H material and solar cell properties governed by the individual deposition processes (HWCVD vs. PECVD)?

- Can similar structure and electronic properties be achieved with both deposition techniques?
- What determines the open circuit voltages in μc-Si:H solar cells?
- In how far are the thin film silicon solar cell properties determined by interface effects?

The outline of the thesis is as below:

- Chapter 2 will briefly introduce the fundamental aspects of a-Si:H and μc-Si:H thin films and solar cells.
- In Chapter 3, the deposition techniques and characterization methods for μc-Si:H thin films and solar cells will be presented.
- The results of the high rate growth of μc-Si:H material and solar cells by PECVD are presented in Chapter 4. In this chapter, the structural, electrical and optical properties of μc-Si:H deposited at high rate at hphP will be first compared with those deposited with conventional lplP process. Second, the influences of deposition parameters, such as power and flow rate etc., on the solar cell performance will be studied. Third, the structural, electrical and optical properties of the solar cells and their influences on the solar cell performance will be investigated. Finally, the results will be discussed and summarized.
- In Chapter 5, it will be tried to find out the mechanisms determining the differences between the PECVD and HWCVD solar cells and to make use of the advantages of these two processes. μc-Si:H films and solar cells deposited by PECVD and HWCVD will be first compared. Second, the differences between the PECVD and HWCVD cells will be found to be nearly eliminated by inserting an intrinsic HWCVD p/i interface layer into the PECVD cells. Third, efforts will be made to find out how the HWCVD interface layers improve the solar cell performance. Finally, the results will be discussed and summarized.
- In Chapter 6, the most important results will be summarized. The outlook of future work is also given.

Chapter 2

Fundamentals of a-Si:H and μc-Si:H

2.1 Hydrogenated amorphous silicon

Since hydrogenated amorphous silicon (a-Si:H) has been intensively investigated in the past decades, and detailed description of properties of this material are available in many monographs [*Street 1991, Luft and Tsuo 1993*], just a brief overview will be given in this section.

Amorphous silicon consists of a covalent random network of Si-Si and Si-H bonds. Compared to the crystalline silicon with periodic atomic structure, the most distinct feature in a-Si:H material is the absence of the long range order and translation symmetry. Such disorder is caused by the deviations in the bond lengths and bond angles of the Si-Si bonds. However, the short range order is still present in the material. The two types of material have the same neighboring atoms and similar bond lengths and bond angles. The average deviation of bond angle and bond length in a-Si:H material are about 8 % and 1 %, respectively [*Street 1991*].

The presence of bond angle and length deviation creates a large amount of strained bonds or broken bonds and causes electron and hole localization. The energy levels associated with the strained bonds form the band tails, as compared to the sharp band edge in c-Si. If the broken bonds are not saturated by the other atoms, they generate defects in the mid-gap region (dangling bonds) and act as the recombination centers for free charge carriers. The termination of dangling bonds in a-Si:H is usually fulfilled by H atoms. For the amorphous silicon material without atomic hydrogen, the defect density is typically about 10^{19} cm^{-3}. The hydrogenation of amorphous silicon can significantly reduce the defect density down to a much lower level (for high quality a-Si:H about 10^{16} cm^{-3}).

Due to the absence of translation symmetry, the conservation of the quasi momentum $\vec{k}$ in the band-to-band transition is relaxed. As a result, a-Si:H material behaves like a direct band-gap semiconductor, resulting in a much higher absorption coefficient than c-Si at photon energy between 1.9 eV and 3.5 eV (Fig. 2.1). Therefore, the a-Si:H solar cells can be made much thinner than the c-Si cells.

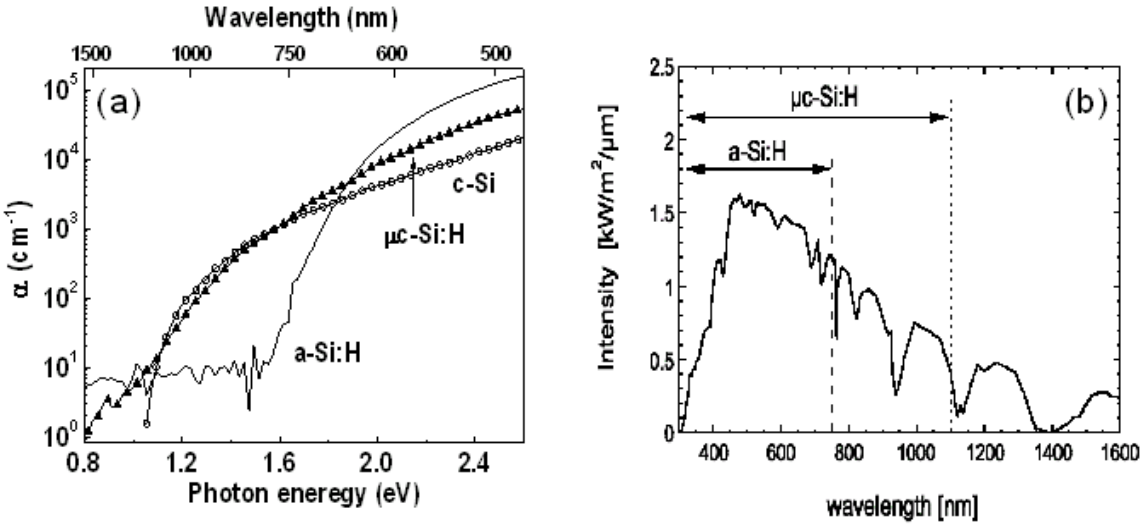

Figure 2.1: *(a) Optical absorption coefficient α of a-Si:H, μc-Si:H and c-Si. (b). Spectral intensity of AM1.5 solar spectrum reaching the Earth's surface. The spectral ranges which are absorbed by a-Si:H and μc-Si:H are also indicated.*

The most important drawback of a-Si:H is that the material quality and solar cell performance deteriorate after long term sun light illumination. It was found that the degradation was caused by the increased defect density after light soaking, which would reduce the life time of free charge carriers. The additional defects can be recovered after a few hours annealing at 150 °C. Such effect was first observed by *Staebler and Wronski* in 1977 and was afterward named as 'Staebler Wronski Effect'. Many researchers have been trying to find out the mechanism of defect generation for years. But it is still not clearly understood yet. For a recent review of this topic, see Ref. [*Shimizu 2004*].

2.2 Hydrogenated microcrystalline silicon

Opposite to the homogeneous nature of a-Si:H, μc-Si:H can be considered as a mixture of crystallites, amorphous tissue, grain boundaries and voids. Depending on the deposition conditions, the volume fraction and spatial distribution of crystallites and amorphous tissues can be significantly different. It was found that variation of many deposition parameters in the PECVD or HWCVD process, such as silane concentration, power, pressure

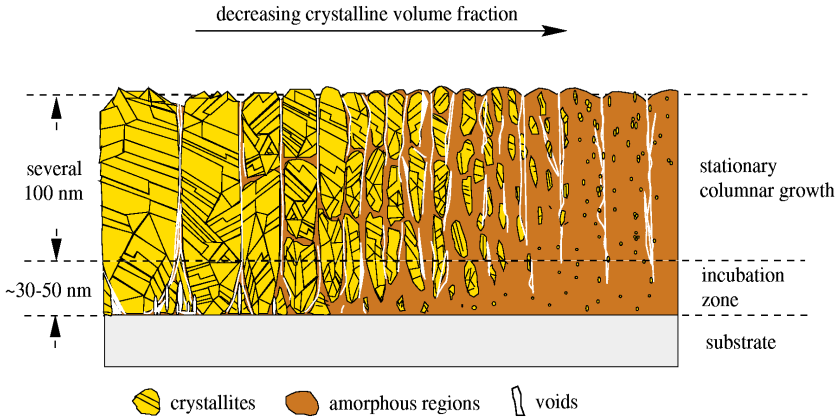

Figure 2.2: *Schematic diagram illustrating the microstructure properties of microcrystalline silicon films. From the left to the right, structure composition shifts from high crystallinity to amorphous growth. This figure is taken from [Vetterl 2000].*

and total flow rate, can adjust the structure composition from highly microcrystalline to fully amorphous growth. Fig. 2.2 is a schematic diagram illustrating structure properties of μc-Si:H deposited on foreign substrates. This diagram was based on the research results obtained by transmission electron microscopy, X-ray diffraction, Raman spectroscopy, IR spectroscopy and other characterization methods. From the left to the right, the figure indicates the microstructural properties of μc-Si:H films with structure composition from high crystallinity to the amorphous growth.

In the μc-Si:H material with high crystallinity, large columns with diameters up to 200 nm can be observed extending to the whole thickness. Note that such big columns do not correspond to single crystallites. On the contrary, they consist of a large number of coherent domains ($\approx$ 10nm), separated by stacking fault and twin boundaries [*Luysberg 1997, Houben 1998*]. Between the columns are voids or cracks, through which atmospheric molecules can easily diffuse into the films. In the films with medium crystallinity, a decrease in the size of columns and coherent domains can be observed. The columns are passivated by the residue amorphous tissues, preventing the post-deposition atmosphere in-diffusion. If the crystallinity decreases further, disrupted columns and small grains can be seen embedded in the amorphous network.

Another feature concerning the structure of μc-Si:H is the presence of an incubation layer at the interface between the film and the substrate. In the incubation layer, the nucleation starts and the crystallinity and column diameter typically increase with the thickness before the columns coalesce with each other and form a stationary growth. The incubation layer thickness at which the stationary growth starts depends on the substrates and

deposition conditions [*Collins and Yang 1989, Tzolov 1997, Collins 2003, Kondo 1996*]. The incubation layer in the films deposited on foreign substrates, like glass and Si wafer with native oxide, in some cases can be very thick. Thus, the *i*-layers in the solar cells, which are mostly deposited on μc-si:H *p*-layers, may not be the same as the films deposited on glass and c-Si substrates, although they were deposited with identical parameters. To reduce this mismatch, a highly microcrystalline seed layer concept simulating the solar cell *p*-layer on glass substrates was proposed by Ross et al. [*Ross 2005*].

As a mixed-phase material, μc-Si:H shows much more complicated transport mechanism than the single phase material like a-Si:H and c-Si. The electrical properties of μc-Si:H depends on the crystalline volume fraction and transport pathway. Some researchers proposed that, if the crystalline volume fraction is high enough, percolation might take place, and charge carriers might mainly transport through interconnected grains [*Carius 1997, Kocka 2003*].

The optical absorption coefficient (α) of a typical μc-Si:H film is shown in Fig. 2.1 (a) together with that of a-Si:H and c-Si as a function of photon energy. The absorption coefficients of μc-Si:H and c-Si overlap in a wide range of photon energy and show similar optical band gap [*Jun 2002*]. The higher α at photon energy above 1.6 eV in μc-Si:H can be partly attributed to the presence of the amorphous tissue with a higher α, to the internal scattering at the grain boundaries, or to the light scattering at the rough surface [*Iqbal 1983, Vaněček 1998, Diehl 1998, Poruba 2000*]. The higher absorption at photon energy below 1.2 eV comes from the presence of band tail states and the deep defects. Compared to a-Si:H, μc-Si:H shows higher absorption in the red and infrared region. Accordingly, μc-Si:H solar cells have higher spectral response in the wavelength range between $\sim$700 nm of a-Si:H solar cells to $\sim$1100nm [Fig. 2.1 (b)].

The light-induced meta-stability is a tricky issue in the amorphous silicon material and solar cells [*Staebler and Wronski 1977, Shimizu 2004*]. As to μc-Si:H, early studies found that the μc-Si:H solar cells, usually with high crystallinity, were very stable against the light soaking [*Meier 1994, Keppner 1999, Yamamoto 2000*]. However, the material close to the μc-Si:H/a-Si:H transition, which yields the highest solar cell efficiency, consists of a considerable amount of amorphous phase [*Vetterl 2000, Klein 2003, Roschek 2002*]. Consequently, such solar cells were found to have the same light induced performance degradation as found found in a-Si:H solar cells [*Vetterl 2001a, Klein 2004a, Roschek 2003, Yan 2004*]. The light induced degradation in μc-Si:H solar cells depends on the *i*-layer structural composition [*Klein 2004a*] and is also affected by the light spectra [*Yan 2004*]. In addition to the degradation caused by the light soaking, the atmospheric impurity in-diffusion after long term storage in air may also worsen material quality [*Vepřek 1983, Finger 2003*], and degrades the solar cell performance [*Yan 2002, Mastui 2004, Sendova-Vassileva 2004*]. It was found that material obtained at the transition region is stable in air, probably due to the grain boundary passivation from the residue a-Si:H tissue, while material with high crystallinity is susceptible to in-diffusion of atmospheric gases [*Finger*

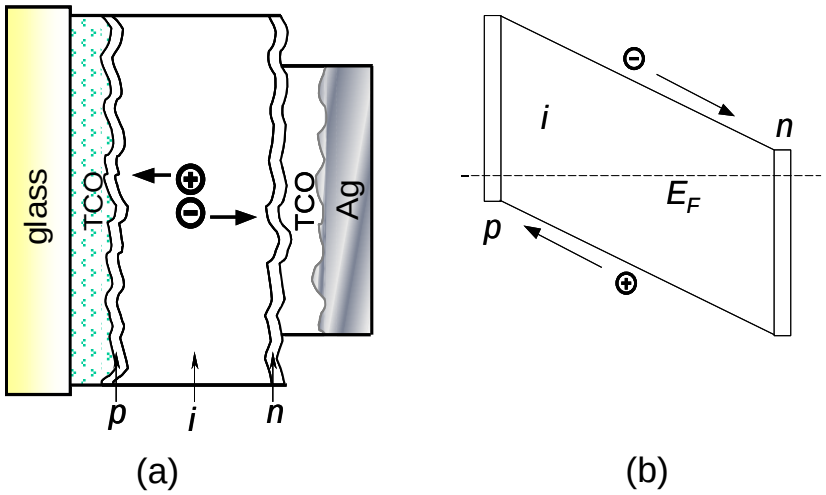

Figure 2.3: *(a), schematic diagram of a p-i-n structure thin film silicon solar cell. (b), band diagram of a ideal p-i-n solar cell under short circuit condition.*

2003].

2.3 Thin film silicon solar cells

2.3.1 Operating principle

Here the basic working principle of thin film silicon solar cells will be briefly summarized. Details of the physics of this type of devices are available in many works [*Sze 1981, Schropp and Zeman 1998*].

Due to the high defect density and thus the short diffusion length of charge carriers in the doped μc-Si:H and a-Si:H films, the p-n junction structure used in c-Si solar cells does not work in thin film silicon cells. For this reason, in thin film silicon solar cells, an intrinsic layer (i-layer) of about 1 μm thick is usually used as light absorber to generate the electron-hole pairs. The electron-hole pairs are separated by the electrical field created by the p- and n-doped layers deposited on both sides of the i-layer. Following the electric field, holes will be driven to the p-layer, and electrons to the n-layer. Consequently, the separation of charge carriers build up a voltage between p- and n-layers. This voltage is called photovoltage. If the p- and n-layers are connected through the electrodes by an external circuit, a photocurrent is produced. The p-i-n structure and the electron-hole pair generation and separation process are illustrated by the schematic diagram in Fig. 2.3 (a) and by the band diagram in (b). Note that diagram (b) is just a schematic picture for

an ideal single junction thin film silicon solar cell under short circuit conditions. In the real cells, the situation may be different. For example, the presence of charge defects at the p/i and i/n interfaces results in band bending at the two interfaces. The band bending reduces the electric field and thus worsens the interface quality. Furthermore, the solar cells under the operating condition have a forward bias voltage (about 0.5 V for μc-Si:H solar cell), which accordingly reduced the electric field in the i-layer. As the diffusion length of charge carrier in the intrinsic a-Si:H and μc-Si:H (typically about 200 nm for μc-Si:H) is much smaller than the i-layer thickness, the carrier extraction mainly results from the drift of the electric field. This type of solar cells are called drift cells, in contrast to the diffusion cells like c-Si solar cells.

Due to the smaller hole mobility in the thin film silicon material, illumination usually occurs from the p-layer side of the solar cell. As the result of p-side illumination, most of the sun light is absorbed in the region close to the p-layer, resulting a shorter distance for the low mobility holes to travel to the p-layer. It was recently found that, for the high quality μc-Si:H solar cells, hole mobility is high enough to make the n-side illumination possible [*Gross 2002, Dylla 2005*]. However, if a μc-Si:H cell is combined with an a-Si:H cell to form a a-Si:H/μc-Si:H stacked cell, illumination through the p-layers is required for the a-Si:H cell and thus mandatory for the whole device. According to the deposition sequence of the p-, i- and n-layers, thin film silicon cells can be classified as p-i-n or n-i-p cells. In a p-i-n solar cell, also called superstrate cell, a transparent substrate is serving as the window of the solar cell, and the p-layer is the first layer deposited on the substrate and then i- and n-layer. Fig. 2.3 (a) shows schematic diagram of a p-i-n solar cell. Note that all the solar cells presented in this work are deposited in a p-i-n sequence.

Substrate and back contact

An absorber layer with a reasonable thickness is important for sufficient light absorption. However, a too thick i-layer is not favorable for low cost production and high conversion efficiency, since it needs longer deposition time, increases the charge carrier recombination and enhances the light induced degradation. To increase the light absorption, especially for long wavelength light, without increasing the i-layer thickness, the so-called light trapping schemes are now widely used. The light trapping schemes increase the pathway of the incident lights by scattering effect at the rough surface, and thus increase the light absorption. There are two commonly-used light trapping schemes in thin film silicon solar cells with p-i-n structure: one is rough front electrode, another is rough back reflector. Fig. 2.4 visualizes the light scattering at the surface of front electrode and back reflector in the p-i-n thin film silicon solar cells.

Application as front electrodes requires high transparency and high conductivity. Aluminum doped ZnO (ZnO:Al) films are good candidates fulfilling the above requirements, and all solar cells presented in this thesis were deposited on ZnO:Al covered Corning 1737 glass. Detailed information about the preparation and optimization of ZnO:Al substrate

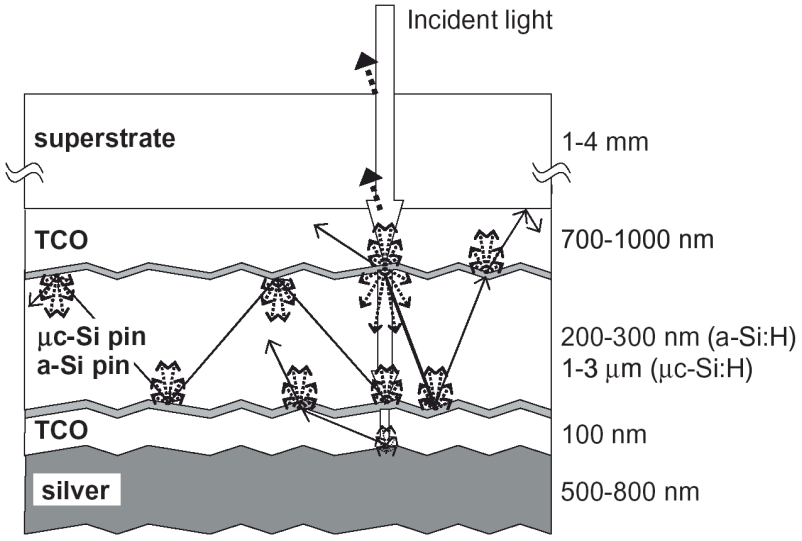

Figure 2.4: *Schematic sketch of the cross section of a silicon thin film p-i-n solar cell (a-Si:H and/or µc-Si:H) with rough interfaces. Thicknesses of the individual layers are typical values. The concept of light trapping is illustrated by the arrows representing incoming and scattered sun light. Different light paths and scattering events are sketched. Figure is taken from Ref. (Müller 2004).*

can be found in the publications of O. Kluth [*Kluth 2001, Kluth 1999*]. For better light trapping, a high surface roughness was achieved by wet etching in a 0.5 % hydrochloric acid solution. Fig. 2.5 illustrates the surface morphology of such a film before and after the etching process. The application of such textured-etched ZnO:Al enhances the light utilization in the long wavelength region, which is reflected by the increased quantum efficiency and reduced total reflectance (see Fig. 2.4 in Ref. [*Müller 2004*]).

If the average photon is not absorbed in the first pass, a highly reflective back contact is necessary for effective light trapping. To satisfy the optical requirements and sufficient electrical conductivity of the back contact, aluminum and silver are commonly used as back reflector. Silver is used as the back reflector material in most of the solar cells presented in this work due to its higher reflectivity and simple preparation. In our cases, the silver back contacts are prepared by thermal evaporation. It was found that introducing a TCO layer between the silicon and metal contact increase the reflectivity [*Morris 1990*], and enhance the light absorption in the solar cells [*Müller 2004*]. For this reason, ZnO/Ag back reflectors are employed in some optimized solar cells to obtain high efficiency. In addition, ZnO/Ag contacts show better adhesion to the silicon surface than the Ag ones,

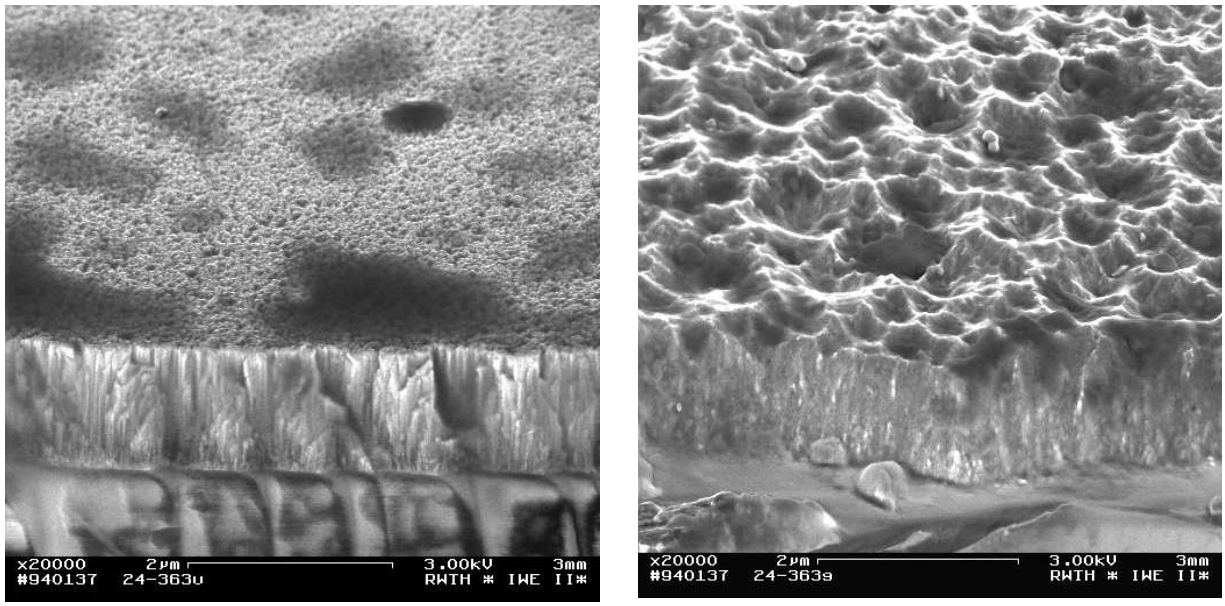

Figure 2.5: *Scanning electron microscope images of a ZnO:Al film before (left) and after (right) textured etching in HCl solution. Figure is taken from Ref. (Kluth 1997).*

and thus are usually used in the solar cells for long-term light soaking experiments.

Chapter 3

Experimental methods

In this chapter, the two deposition techniques for μc-Si:H used in this thesis, plasma-enhanced chemical vapor deposition (PECVD) and hot wire chemical vapor deposition (HWCVD) will be described, followed by the details of the deposition system. In addition, the characterization methods, such as Raman scattering spectroscopy, and transmission electron microscopy, will be introduced.

3.1 Plasma-enhanced chemical vapor deposition

This section will briefly introduce the deposition process of thin film silicon by PECVD. For detailed information, see Ref.[*Luft and Tsuo 1993, Bruno 1995*].

In the PECVD process, the silicon containing gases, such as silane (SiH_4), and other gases for doping or alloying are usually used as reactant gases in the deposition for thin film silicon. After the introduction of the deposition gases, a low temperature glow discharge is ignited and sustained by an electric field between the two parallel electrodes (Fig. 3.1 (a)). The electrons are accelerated in the electric field and gain enough energy to decompose the gas molecules into neutral radicals and ions. In the bulk of plasma, complicated gas phase reactions happen between the radicals, ions and molecules. Such secondary reactions are so important that they predominantly control the electronic and structural properties of the resulting films. The radicals, ions and their reaction resultants may contribute to the film growth, and thus are usually refereed to be growth precursors. One part of the precursors reaching the growth surface will be physically adsorbed on the growth surface. Through the interactions between the adsorbed precursor and growth surface, such as hydrogen abstraction, radical diffusion and chemical bonding, one part of the precursors will be incorporated into the film and fulfill the growth. Ref. [*Bruno 1995*] describes in detail the possible reactions in the plasma and on the growth surface.

The potential distribution between the electrodes, averaged over one RF period, is depicted in Fig. 3.1 (b). The potential maintains almost constant in the bulk plasma due to the charge equivalence. Compared to the electrodes, the bulk plasma is at a higher poten-

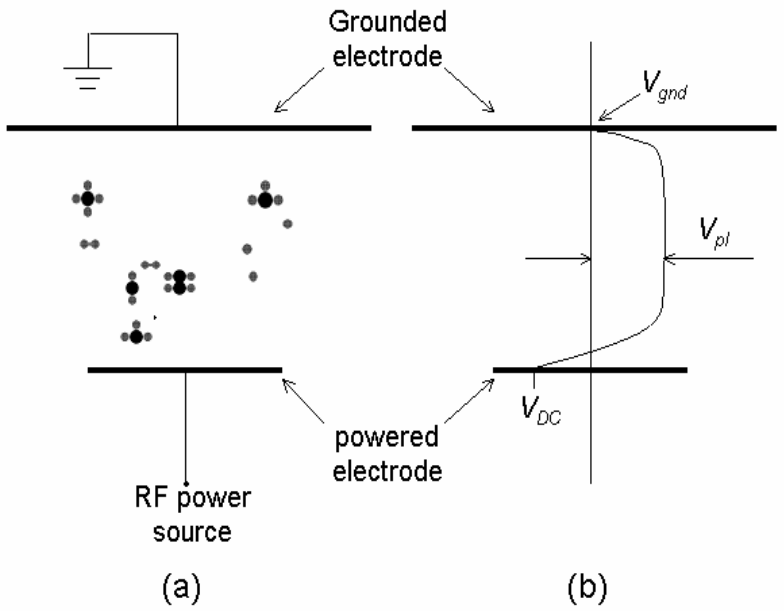

Figure 3.1: *(a), A schematic picture of a capacitatively coupled PECVD reactor. (b), Time average potential distribution between the powered and grounded electrodes.*

tial level. The region between the plasma and electrodes, where the potential differences are presented, are the plasma sheaths. In the sheath, the positive ions will be accelerated towards the electrodes. If the sheath potential is higher enough, ions may gain enough energy to damage the growth surface [*Matsuda 1983, Vepřek 1989, Kondo 2000*]. Therefore, a low ion energy is a key issue to obtain high quality thin film silicon by PECVD. The use of VHF plasma excitation is a good way to decrease the sheath potential and thus ion energy, through reducing the peak-to-peak voltage [*Köhler 1985, Finger 1992, Howling 1992, Bruno 1995*]. High gas pressure, which enhances the collision probability in the plasma, is also believed to be an effective to reduce the ion energy [*Guo 1998, Kondo 2000*].

3.2 Hot-wire chemical vapor deposition

Different from the PECVD process, the hot-wire chemical vapor deposition (HWCVD) is based on the decomposition of reactant gases at the hot surface of a catalyst. The decomposition of the reactant gases was proven to be a catalytic effect [*Sault and Goodman*

1990, Heintze 1996, Matsumura 1998, Tange 2001]. This is the reason that such a process is also referred to be cat-CVD in some cases. Various material, such as tungsten, tantalum and graphite etc., can be used as catalyst. The dissociation of gas molecules on the catalyst has been investigated by many groups [*Matsumura 1998, Nozaki 2000, Tange 2001, Duan 2001*]. Depending on the experiment conditions and evaluation methods, the results from different group may have minor differences. Most researchers showed that silane molecules are fully decomposed into Si and H atoms at high filament temperature (T_f) above 1430 °C [*Matsumura 1998*]. Products like SiH_3 and SiH_2 are only available at low T_f. As proposed by Tange et al. [*Tange 2001*], the silane dissociation process at the surface of catalyst is based on a hydrogen abstraction mechanism via

$$SiH_4 \rightarrow SiH_3 + H \rightarrow SiH_2 + 2H \rightarrow SiH + 3H \rightarrow Si + 4H. \tag{3.1}$$

$$H_2 \rightarrow 2H. \tag{3.2}$$

At low p_{depo}, where the radical mean free path length is sufficiently long,the radicals can diffuse to the substrate without further gas phase reaction. However, material deposited under such conditions show poor quality [*Molenbroek 1997*]. A certain amount of gas phase reaction is needed for the high quality material deposition. Thus, a relatively high p_{depo} and larger substrate-filament distance is necessary. Too high p_{depo} and too long substrate-filament distance, however, result in gas polymerization and deteriorate the material quality and solar cell performance.

In the HWCVD process, the substrates are always exposed to the thermal radiation from the hot catalyst. If high T_f and small filament-substrate distance are used, the substrate heating from the hot filaments should be taken into account [*Klein 2002a, Matsumura 1998*]. Too high substrate temperature (T_S) may thermally desorb the atomic hydrogen from the material and results in a poor grain boundary passivation [*Finger 2002*]. To avoid the detrimental radiative substrate heating, a low T_S HWCVD process was developed [*Klein 2002a, Klein 2005*]. The low T_S was achieved by the low heater temperature, low T_f and enlarged substrate-filament distance. With such process, high quality material with low defect density and solar cells with high efficiency were obtained. A drawback of this low T_S process is the reduced deposition rate resulting from the low gas decomposition at low T_f. By optimizing the filament configuration, R_D can be increased up to about 0.4 nm/s without a significant increase in T_S [*Lossen 2004*].

The HWCVD process does not need the plasma to decompose the reactant gases. Thus, there is no plasma sheath present. In addition, the electrons emitting from the filaments have too low energy (0.25 eV) to ionize the radicals [*Matsumura 1998*]. Therefore, ions and the consequent ion bombardment are absent in the HWCVD process. This is regarded as one of the advantages of HWCVD over the PECVD process.

Figure 3.2: *Photograph of the deposition system used for μc-Si:H films and solar cells deposition by PECVD and HWCVD.*

3.3 Deposition system

All μc-Si:H films and solar cells presented in this thesis were deposited in a cluster system, a multi-chamber system consisting of three PECVD chambers, one HWCVD chamber, one transfer chamber and one load lock chamber. The photograph of this deposition system is shown in Fig. 3.2. Two PECVD chambers are assigned to the *p*- or *n*-doped layer depositions, and another one to the intrinsic layer depositions. The HWCVD chamber was only used for intrinsic μc-Si:H layer deposition in this thesis. All deposition chambers and the load lock chamber are connected to the transfer chamber located in the middle of the system. The robot arm in the transfer chamber can handily transfer the substrates from one chamber to another. All chambers are equipped with a two-stage pumping system, which consists of a turbo-molecular pump and a rotary pump. This allows a base-pressure lower than 2×10^{-8} hPa. The substrates, with maximum area of 10×10 cm^2, are supported by a stainless steel carrier with 3 mm thick stainless steel backing plate. The substrate transfer, valve operation and deposition parameter variation can be controlled

by a computer.

In the following, details of the deposition chambers will be presented. The schematic diagrams of the PECVD chambers and that of the HWCVD chamber are shown in Fig. 3.3 (a) and (b), respectively. In all PECVD and HWCVD chambers, the substrates supported by the carrier holder are heated by the heater 3 cm above. The substrate temperature can not be directly measured during the deposition and is estimated from the calibration conducted in advance. However, the calibration in the PECVD chambers was usually made without plasma or under conventional low pressure, low power conditions. Using the same calibration under high pressure and high power conditions may underestimate the real substrate temperature since higher pressure leads to stronger convection and thus enhances the heat transfer from the heater to the substrate. In addition, the plasma heating to the substrate may be no longer negligible as high power is coupled into the plasma [*van den Donker 2005a, Niikura 2004*].

In the PECVD chambers, the electrode configuration consists of a 13.5 cm-diameter powered electrode and a 12×12 cm^2 substrate carrier in a carrier supporter as the grounded electrode. Substrate size is 10×10 cm^2. The electrode distance is easily variable in-situ between 60 mm and 12 mm. A metal shield around the electrodes to prevent deposition on the chamber walls, as indicated in Fig. 3.3, can be removed for discharge adjustment. The gas supply is a simple cross-flow geometry, i.e. no gas showerhead arrangement. During deposition, the pressure is controlled by a throttle valve, which is located before the turbo-molecular pump. Under some conditions, it is necessary to change the power, p_{depo} or electrode distance to ignite the discharge. To avoid the resulting irreproducibility, a shutter is placed in front of the substrate while starting the plasma. All PECVD chambers are equipped with a wide-range high frequency generator with a frequency range between 100 KHz and 125 MHz and separate matching networks for the radio-frequency (RF) and very-high-frequency (VHF) regime. In this thesis, 13.56 MHz excitation frequency is used in the RF regime, and 95 MHz is used in the VHF regime. The input and reflected powers are nominal values measured by a directional power meter (Rhode & Schwartz NAP meter, power head: NZ-4) between the VHF generator and the matching network. To guarantee a good power coupling into the discharge, care was taken by large diameter cables and corresponding electric vacuum feed through, short cable lengths and individually adjusted matching networks. The measured reflected power was typically below 1 % of the input power.

Without the RF or VHF generator and matching networks, the configuration of the HWCVD chamber is more simple as compared to that of PECVD chambers. In this thesis, two tantalum filaments with diameter of 0.5 mm were used as catalyst. The filaments, which are usually coiled to increase the surface area, are fixed between two filament holders. The distance between the two holders are 13 cm. The distance between the substrate and filaments can be adjusted between 5 and 10 cm. The filaments are resistively heated by a DC-power supply, and the filament temperature is measured by a dual beam pyrometer

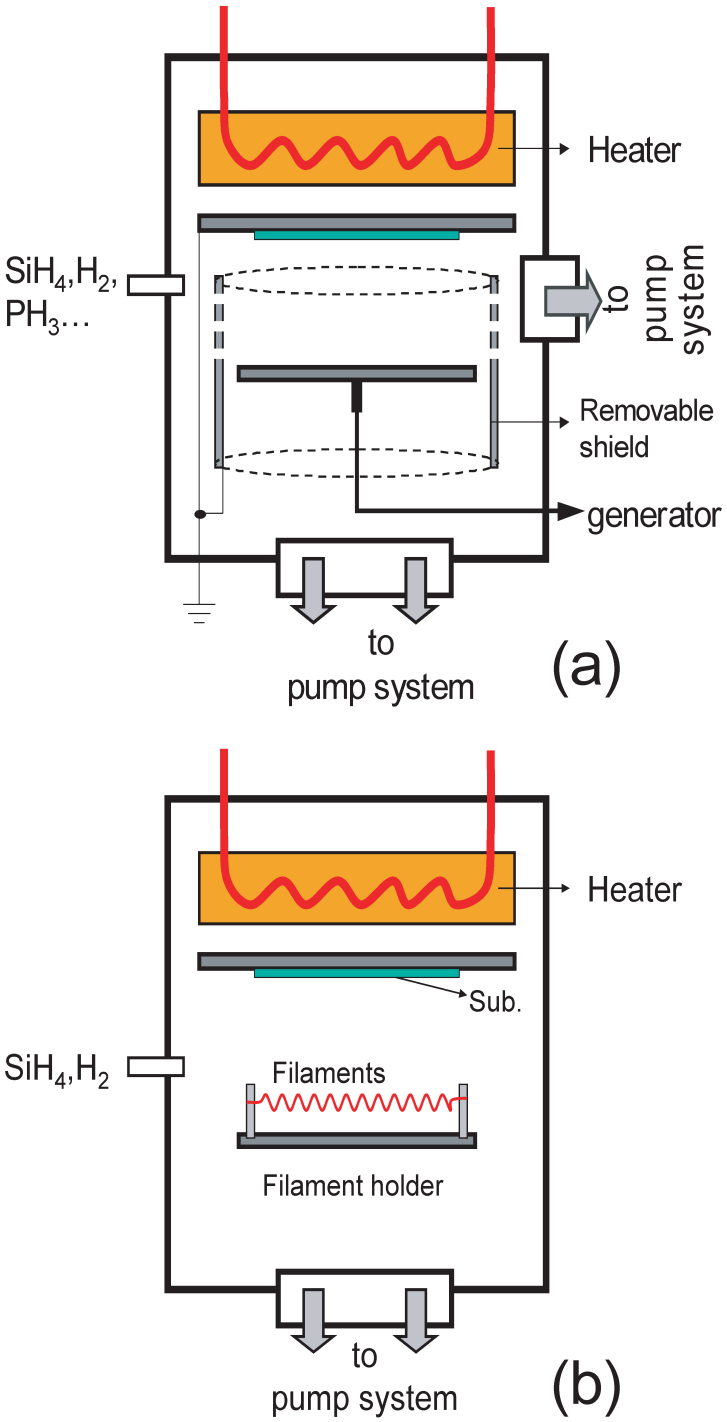

Figure 3.3: *Schematic diagrams of deposition chambers. (a), PECVD chamber, (b), HWCVD chamber.*

(Raytek Marathon) through an inspection window on the side of the chamber. A shutter is also used in the HWCVD chamber to prevent the deposition on the substrate before a stable deposition is reached.

3.4 Preparation of material and solar cells

Microcrystalline silicon films were deposited on 1 mm thick sodium-free glass substrates (Corning 1737) for thickness, conductivity, Raman scattering spectroscopy and optical absorption measurement. IR-measurements were carried on the films deposited on double-side polished c-Si wafers. Aluminum doped zinc oxide (ZnO:Al) coated glass was used as superstrates for all solar cells presented in this thesis. The ZnO:Al was prepared by the RF-magnetron sputtering from a ceramic target. The initial thickness is about one micrometer. The rough surface was created by the textured-etching in 0.5 % HCl solution for 30 seconds. For details of the ZnO:Al preparation, see Ref. [*Kluth 2001*]. Before the silicon layer deposition, the substrates were preheated for more than two hours to desorb the moisture and gases from substrate surface and to reach the temperature equilibrium.

Silane concentration, SC = $[SiH_4]$ / ($[SiH_4]$ +$[H_2]$), defined by the gas flow ratio of silane and hydrogen, was kept constant during the individual deposition for the intrinsic films and the *i*-layers in solar cells.

The *p*- and *n*-doped layers in the solar cells were prepared in separate chambers by PECVD. Very high frequency of 95 MHz was used to excite the plasma for the *p*-layer deposition. Trimethylboron [TMB, $B(CH_3)_3$] was the doping gas to achieve boron doping in the *p*-layers. As the μc-Si:H cells are usually illuminated from the *p*-layer sides, a *p*-layer of about 15 nm is used to achieve a high blue light response and an adequate built-in potential. At the same time, serving as the seed layer for the *i*-layer growth, a *p*-layer requires a considerable crystalline volume fraction. However, high crystallinity is difficult to obtain in the thin layers. In addition, the boron doping in such layers also deteriorate the crystalline growth [*Dasgupta 2001*]. To achieve high crystallinity, we employed a two-step method for the *p*-layer deposition. Firstly, a very thin nucleation layer was deposited with low silane and TMB concentration. A 15 nm thick layer was then deposited on top of the nucleation with higher silane concentration and doping level. The 20 nm thick amorphous *n*-layers were deposited from the gas mixture of SiH_4, phosphine and H_2. An amorphous *n*-layer is important to reduce the current collection effect during the *J*-*V* parameter measurement.

After the deposition of the *p*-*i*-*n* structure of solar cells, silver pads and grids, serving as solar cell electrodes, were made by thermal evaporation. The solar cell area is simply defined by the area of silver pads. It was previously found that the current collect effect is negligible in our 1×1 cm^2 cells with amorphous *n*-layers [*Feng 2003*]. For some selected cells, highly reflective ZnO/Ag instead of the normal Ag back contacts were used to enhance the light absorption.

3.5 Material and solar cell characterization

3.5.1 Thickness measurement

The thickness of the films and solar cells were determined mechanically by a step profiler (Sloan DEKTAK 3030). The μc-Si:H films were usually made to be about 500 nm thick by adjusting the deposition time according to their deposition rates. For the films with such thickness, it was easy to make a step by peeling off part of the film with adhesive tape after a slight scratching with a stylus. For the very thin films to which the above simple method could not be applied, the steps were obtained by KOH etching. To measure the solar cell thickness, the thickness of all ZnO:Al substrates were measured before the deposition. After the deposition of silicon layers, the total thickness of the ZnO:Al substrate and silicon layers were measured by the step profiler. Neglecting the doped layers, one can estimate the i-layer thickness by subtracting the ZnO thickness from the total thickness.

3.5.2 Electrical conductivity

Electrical conductivity measurement was carried on μc-Si:H films deposited on glass substrates. Two coplanar silver contacts with 0.5 mm gap in between were deposited on the samples by thermal evaporation. Conductivity was measured at room temperature in vacuum after two hours annealing at 170 °C. The illumination with intensity of 100 mW/cm^2 from a halogen lamp was applied to the samples during the photo-conductivity measurement. The photo-conductivity (σ_{photo}) and dark-conductivity (σ_{dark}) are calculated from

$$\sigma_{photo}, \sigma_{dark} = \frac{Il}{Vwd} \tag{3.3}$$

in which I is the current measured in the dark or under illumination with an applied voltage V. l is the gap between the silver contacts of 0.5 mm. w is the width of the contacts (5 mm in our cases). And d is the film thickness.

3.5.3 Raman spectroscopy

Raman spectroscopy is a convenient method to determine the crystalline volume fraction of thin film silicon material [*Houben 1998*]. The Raman effect results from the interaction between photons and phonons in material. This leads to an inelastic scattering of the incident photons. The photon loses or gains energy by generating or absorbing a phonon during the inelastic scattering, leading to a frequency shift of the incident light. The conservation of phonon momentum in crystalline silicon gives rise to a single line at 520 cm^{-1} (Transverse optical, TO, phonon peak) with a natural line width of about 3.5 cm^{-1} at room temperature. In amorphous silicon, the momentum selection rule does not

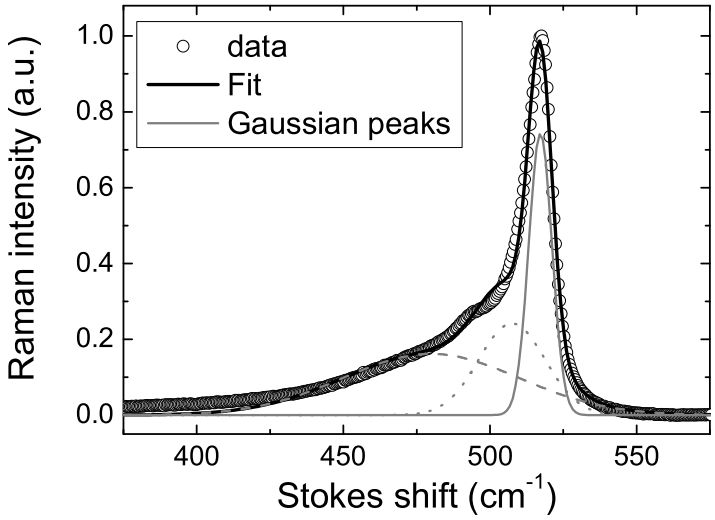

Figure 3.4: *Raman spectrum of a typical μc-Si:H film and the Gaussian peaks fitted to the spectrum according to the procedure described in the text.*

apply due to the loss in long range order. Thus, all phonons are optically allowed and the Raman spectrum resembles the phonon density of states with a broad prominent hump at 480 cm^{-1}. Consisting of amorphous tissue and crystallites, μc-Si:H simultaneously shows a crystalline peak and an amorphous peak in the Raman spectrum. In addition, a third peak at around 500 cm^{-1} is often observed in the Raman spectra of μc-Si:H. This peak was previously attributed to the stacking faults or hexagonal silicon (*Kobliska and Solin 1973, Houben 1998*).

Fitting three Gaussian peaks the Raman spectra is an easy way to determine the integrated intensities of crystalline and amorphous peaks. The Raman spectrum of a typical μc-Si:H film and the Gaussian fitting to this spectrum are exemplarily shown in Fig. 3.4. The integrated intensity ratio of the Gaussian peaks at ~520 and ~505 cm^{-1} to the summation of the crystalline and amorphous peaks can be used as a semi-quantitative value for crystalline volume fraction. This ratio, referred to be integrated Raman intensity ratio (I_C^{RS}) in this work, is written as:

$$I_C^{RS} = \frac{I_{520} + I_{505}}{I_{520} + I_{505} + I_{480}} \tag{3.4}$$

Note that I_C^{RS} are only semi-quantitative values, since the Raman cross sections are different for crystalline and amorphous phase, and may depend on the excitation wavelength. Furthermore, the absorption coefficient difference in the crystallites and in the amorphous

phase makes it more difficult to determine the real crystalline volume fraction from Raman spectra. Still, Raman spectroscopy is a simple and useful method to provide the structure information of the material, and thus is widely used in many researches.

Laser with long wavelength can probe deeper into the samples than the short wavelength laser does. Thus, Raman scattering measurements performed with different wavelength can be used to trace the thickness dependent structure effect [*Vetterl 2001a, Droz 2003*]. For an incident light with initial intensity I_0, after penetrating a layer with thickness of d, its intensity is attenuated to $I(d) = I_0\ \mathrm{e}^{-\alpha(\lambda)\cdot d}$, in which α is the absorption coefficient, a function of wavelength λ. Thus, the Raman signal at the depth of d is proportional to $\mathrm{e}^{-\alpha(\lambda)\cdot d}$. As the scattered light has to travel out of the film before it can be detected, its contribution to the probed Raman signal at the surface can be written as:

$$I_{Raman} \propto e^{-2\alpha(\lambda)\cdot d} \tag{3.5}$$

With this equation, one can roughly estimate the contribution of an individual layer with certain thickness in a μc-Si:H film to the whole Raman signal. The contributions from the layers on the top of a film with different thickness are listed in Table 3.1. In the calculation, three laser wavelength of 415, 488 and 647 nm are used, and the absorption coefficient α is taken from a μc-Si:H films with high crystallinity. From this table, it can be clearly seen that the scattering from the top region of the film dominates the Raman signal if a short wavelength laser is used in the Raman scattering measurement.

wavelength	415nm	488nm	647nm
top 0.1μm	97%	69%	12%
top 0.2μm	100%	90%	23%
top 0.3μm	100%	97%	32%
top 0.5μm	100%	100%	48%
top 1.0μm	100%	100%	73%

Table 3.1: *Contribution of the top layer with different thickness in the total Raman signal. The contribution values are calculated for three different probing laser wavelengths.*

Although one can use the Raman scattering measurement with different wavelengths to study the structure development in μc-Si:H, this method has it own limitation. It is difficult for this method to obtain the crystallinities of the film at different stages of growth. To solve this problem, a 'Raman structure depth profile' method is developed here. Craters with

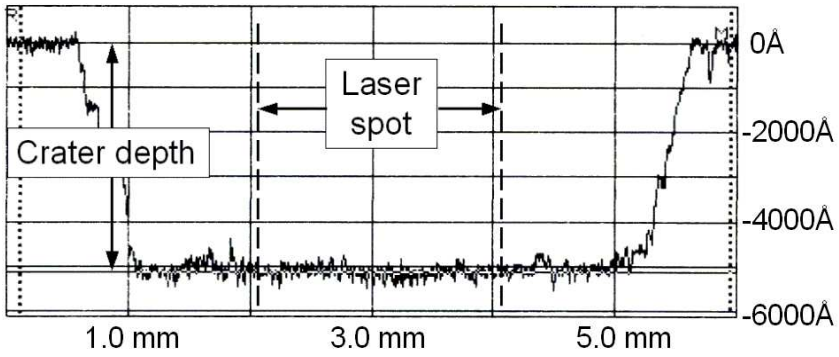

Figure 3.5: *Depth profile of a crater etched with KOH solution into a p-i-n solar cell structure. The dimension of the laser spot in the Raman scattering measurement is also indicated.*

different depth created by KOH etching make it possible to obtain the structure information at different stages of growth directly by Raman scattering measurement. Choosing the appropriate KOH solution concentration, etching temperature and etching time, different crater depth with sufficient smoothness at the bottom can be achieved, which can be monitored by the step profiler. With this method, a depth resolution of ±50nm can be obtained. Fig. 3.5 shows an exemplary picture of a crater measured by the step profiler. The 4 mm long and 2 mm wide flat bottom allows an accurate Raman measurement with the 2×0.3 mm^2 large laser point. In this depth profile experiment, a 488 nm line of an argon laser is used for excitation. According to Table 3.1, 90 % of the Raman signal is from the top 200 nm of the μc-Si:H film.

3.5.4 Transmission electron microscopy (TEM)

Transmission electron microscopy (TEM) provides information on the microstructure of μc-Si:H. It is based on the diffraction contrast generated by electrons, which have passed through a very thin sample. Detail of this technique can be found in literature [Reimer 1993]. The application to μc-Si:H based material has been shown in Ref. [*Houben 1998, Luysberg and Houben 2005, and references therein*]. In conventional diffraction contrast imaging TEM, the contrast is realized by placing an aperture in the back focal plane of the objective lens. By selecting the transmitted or scattered electron in the sample to pass the aperture, bright-field images or dark-field images can be obtained. In the bright-field images, the dark areas corresponds to the crystallites. While in the dark-field images, crystallites appear as white regions.

A quantification of the crystalline fractions in selected areas of the samples can be

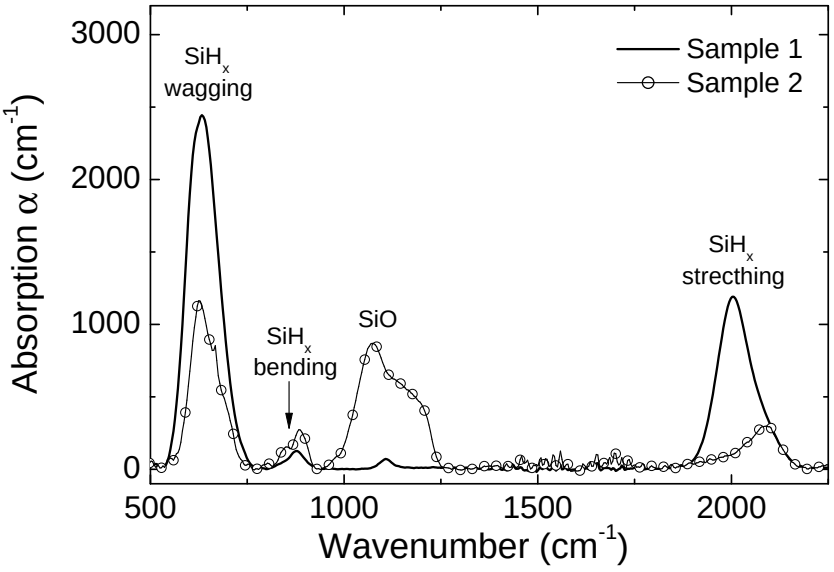

Figure 3.6: *Infrared absorption spectra o f two typical thin film silicon samples.*

obtained from the analysis of the selected area diffraction patterns (SADP). The process of the crystalline volume fraction calculation from SADP spectra is explained in detail in Ref. [*Luysberg and Houben 2005*]. The TEM experiments were carried out in a Philips CM20FEG microscope in Institut für Festkörperforschung (IFF), Forschungszentrum Jülich.

3.5.5 Fourier transform infrared spectroscopy

The hydrogen content (C_H) and hydrogen bonding structure in the thin film silicon can be investigated by Fourier transform infrared (FTIR) spectroscopy. In addition, information about the bonded oxygen and carbon in the silicon films can also be obtained from the infrared spectra. Fig. 3.6 shows the infrared absorption spectra of two typical thin film silicon samples. The SiH_x wagging mode at about 640 cm^{-1}, bending mode at ~870 cm^{-1}, stretching mode between 2000 and 2100 cm^{-1}, and SiO vibration modes at ~1100 cm^{-1} can be distinguished from the spectra. Detailed information of the vibration modes in amorphous silicon and germanium was summarized in Ref. [*Cardona 1983*].

The bonded hydrogen content in material can be calculated from the SiH_x wagging mode intensity at 640 cm^{-1} or from the stretching mode between 2000 and 2100 cm^{-1} [*Brodsky 1977, Fang 1980, Beyer and Abo Ghazala 1998, Langford 1992*]. In this thesis, C_H of μc-Si:H films were determined from the wagging mode intensities, assuming that

the SiH absorption intensity is proportional to the density of bonded hydrogen. Thus the bonded hydrogen density can be expressed as:

$$N_H = A_{640} \cdot \int_\nu \frac{\alpha(\nu)}{\nu} d\nu \tag{3.6}$$

A_{640} in Eq. 3.6 is the proportionality constant between the infrared absorption and the bonded hydrogen. It has different values in literature, depending on the methods used to determine the total hydrogen and even on the hydrogen content itself [*Fang 1980, Langford 1992, Beyer and Abo Ghazala 1998*]. Since this work doesn't intend to verify different proportionality values, a value of 1.6×10^{19} cm^{-2} is used for A_{640} here [*Fang 1980*]. Thus, the hydrogen content can be written as:

$$C_H^* = \frac{N_H}{N_H + N_{Si}}, \tag{3.7}$$

in which $N_{Si} = 5\times10^{22}$ cm^{-3} is the Si atom density in the material. As multiple reflections of the infrared light beam at the film/vacuum interface lead to higher absorption in thin films, a correction of the calculated hydrogen content from Eq. 3.7 is necessary for the films with thickness smaller than 1 μm. The correction can be made according to the formula derived by *Maley 1992*:

$$C_H = \frac{C_H^*}{1.72 - 0.7 \cdot d \cdot \mu m^{-1}}, \tag{3.8}$$

in which d is the film thickness in μm. Note that besides the bonded hydrogen atoms, which can be detected by the infrared spectroscopy, there are indications for the presence of molecular hydrogen in the μc-Si:H material [*Kroll 1996, Beyer and Abo Ghazala 1998*].

The SiH stretching modes at 2000-2100 cm^{-1} depend on the bonding environment of the hydrogen atoms. The hydrogen atoms bonded in compact material result in a peak at 2000 cm^{-1}, while atoms bonded on the internal surfaces or grain boundaries give rise to the peak at 2100 cm^{-1} [*Wagner and Beyer 1983, Cardona 1983, Richter 1983*]. Therefore, the fraction of vibrational intensity at 2100 cm^{-1} in the total stretching mode absorption intensity, microstructure factor R,

$$R = \frac{I_{2100}}{I_{2000} + I_{2100}}, \tag{3.9}$$

can be regarded as the measure for material porosity.

SiO bonds can also be detected by FTIR spectroscopy. However, the sensitivity of this method is so low in a way that only O content higher than 0.5 at.% (corresponding to about several 10^{20} cm^{-3} in the μc-Si:H material) can be detected [*Paesler 1978*]. The oxygen content in the material can be "roughly" estimated from the absorption intensity of SiO mode between 960 - 1200 cm^{-1} in the same way as used for the H content calculation,

Bonded oxygen density, N_O:

$$N_O = A_O \cdot \int_\nu \frac{\alpha(\nu)}{\nu} d\nu,$$

Bonded oxygen content, C_O:

$$C_O = \frac{N_O}{N_O + N_{Si}}, \tag{3.10}$$

in which A_O is the proportionality constant. The oscillator strength of the SiO bonds in the amorphous silicon and crystalline silicon has been intensively studied. However, very different results were obtained for the A_O values [*Lucovsky 1983, Yacobi 1981, He 2000 and references therein*]. Due to the same reason as for A_{640}, a proportionality constant of 7.8×10^{18} cm^{-2} [*Lucovsky 1983*] is used in this thesis.

A FTIR spectrometer (Nicolet 740) was employed in the measurements for thin silicon films deposited on double-side-polished silicon wafers. The system was purged with dry N_2 before and after measurement to minimize the signal of H_2O and CO_2.

3.5.6 Optical absorption

The optical absorptions of μc-Si:H material presented in this thesis were measured by photothermal deflection spectroscopy (PDS) on glass substrates. The technique of PDS was first used for optical absorption measurement of thin film silicon by Jackson et al. in 1981 [*Jackson 1981*]. In the PDS measurement, the samples is placed in the liquid (usually CCl_4 as used in our experiments). A monochromatic light absorbed by the sample generates heat in the films, and lead to a refractive index gradient in the surrounding liquid. By probing the gradient of the varying refractive index with a second beam (probe beam), one can relate its deflection to the optical absorption of the sample [*Jackson 1981*].

PDS is a powerful method measuring the optical absorption directly and boasting high sensitivity at low absorption coefficient. Therefore, it is capable of providing high accuracy in the so-called sub-gap absorption measurement. In a-Si:H, sub-gap absorption is believed to be associated with deep defects [*Jackson and Amer 1982, Wyrsch et al. 1991*]. Such correlation is also proposed for μc-Si:H material [*Bronner 2000, Vaněček 2000*]. As the interface has great effect on sub-gap absorption, especially in the thin samples, great care has to be made during the PDS measurement. In our cases, a phase correction procedure is used to reduce the interface effect.

3.5.7 Solar cell *J-V* characteristics

Dark *J-V* characteristics

The measurement and analysis of the dark J-V characteristics provide the information about the charge carrier transport in the solar cells. Following the description in literature

[*Sakai et al. 1990, Rech et al. 1997, Brammer and stiebig 2005*], the forward dark current in thin film silicon solar cells can be divided into the interface recombination current (j_{int}(V)) at the interfaces or in the i-layer close to the interfaces and the bulk recombination current (j_{bulk}(V)) in the bulk i-layer. That is,

$$j_{dark}(V) = j_{bulk}(V) + j_{int}(V) \tag{3.11}$$

The bulk recombination current plays an important role in the total current density under the high level injection (HLI) conditions with $\Delta n = \Delta p \gg n_0$. According to the depletion region approximation for p-n junctions which corresponds to the i-layer in the p-i-n diodes [*Sah et al. 1957, Sze 1981*], the bulk recombination current, describing the current-voltage characteristics caused by recombination via deep traps in the i-layer, can be written as:

$$j_{bulk}(V) = j_1 \cdot [e^{(qV/2kT)} - 1] \tag{3.12}$$

in which

$$j_1 \propto \frac{n_i W_i}{\tau} \frac{1}{V_{bi} - V}, \qquad with \qquad V_{bi} > V \tag{3.13}$$

where n_i is the intrinsic current density, W_i the i-layer thickness, τ the carrier recombination lifetime, and V_{bi} the built in potential.

Under the low level injection conditions, the recombination in p-i-n solar cells mainly happens in the doped layers and at the interface. The interface recombination current can be written as:

$$j_{int}(V) = j_2 \cdot [e^{(qV/kT)} - 1] \tag{3.14}$$

in which

$$j_2 \propto \frac{n_i^2 \mu_e}{N_A W_p} \tag{3.15}$$

where n_i is the intrinsic current density, μ_e the electron mobility, N_A acceptor density, and W_p the p-layer thickness.

The two terms in Eq. 3.11 can be combined into one term by introducing the diode factor n and the dark current density j_0.

$$j_{dark}(V) = j_0 \cdot [e^{(qV/nkT)} - 1] \tag{3.16}$$

Depending on the ratio between j_{bulk}(V) and j_{int}(V), the diode factor n has values between 1 and 2. An n value close to 1 suggests that the interface recombination dominates the dark current density, and values close to 2 suggest an bulk recombination dominance.

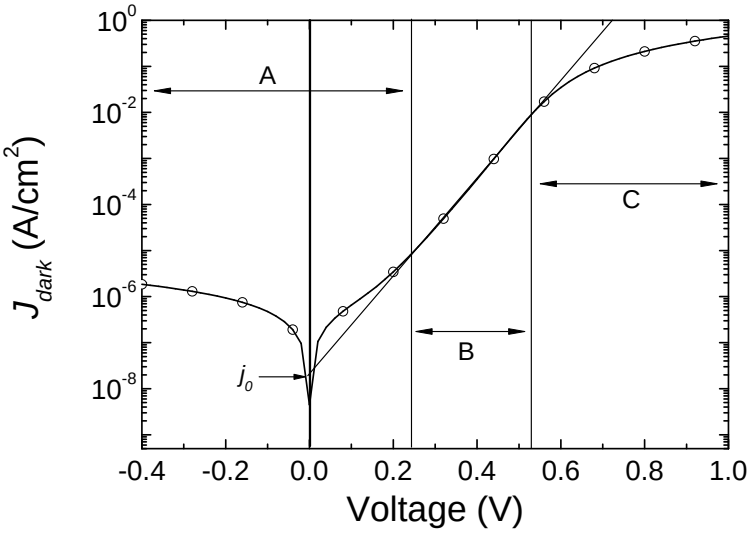

Figure 3.7: *An experimentally obtained dark J-V curve. The regions, A, B and C indicate the voltage range where shunts, exponential diode behavior and series resistance dominate the dark current density, respectively.*

If the series resistance (R_S) and shunt resistance (R_{sh}) can not be neglected, Eq. 3.16 shall be rewritten as:

$$j_{dark}(V) = j_0 \cdot [exp\frac{q(V - j_{dark}(V)R_S)}{nkT} - 1] + \frac{V - j_{dark}(V)R_S}{R_{sh}} \tag{3.17}$$

An experimentally obtained dark J-V curve is indicated in Fig. 3.7. The shunt resistance and series resistance show strong effect on the dark current density in the region A and C, respectively. In region B, the dark current density is dominated by the diode behavior. Thus, the diode factor n and j_0 are determined from a fit to the dark J-V curve in this region.

AM1.5 J-V characteristics

Measuring μc-Si:H solar cells under AM1.5 illumination is the commonly-used method to determine the solar cell conversion efficiency. Detailed introduction to the measurement principle can be found in Ref. [*Ashok and Pande 1985*]. Fig. 3.8 shows the J-V curve of a μc-Si:H solar cells measured in the dark and under AM1.5 illumination. The efficiency is defined as the ratio of the output power at the maximum power point (P_{MPP}) to the incident solar radiation solar power (P_{in}).

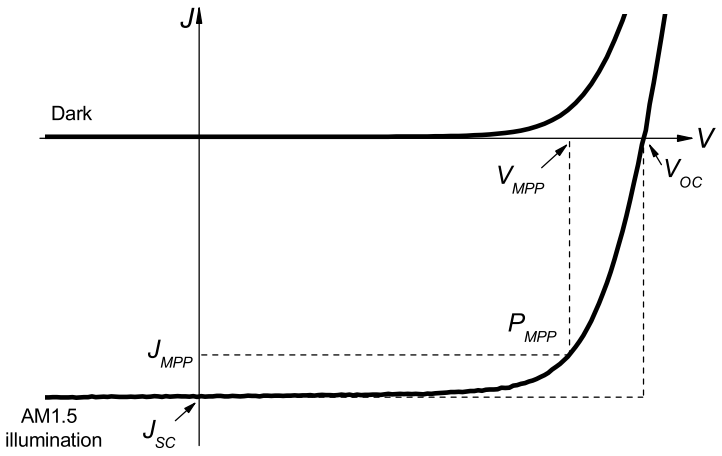

Figure 3.8: *J-V curves of a μc-Si:H solar cell measured in the dark and under illumination. J-V parameters, such as V_{OC}, J_{SC} and maximum power point, are indicated.*

$$\eta = \frac{P_{MPP}}{P_{in}} \tag{3.18}$$

The short circuit current (J_{SC}) is the highest current generated by the solar cells, usually under short circuit conditions with voltage equal to zero. Open circuit voltage (V_{OC}) is the maximum voltage generated by the solar cells. Fill factor (FF), usually used as the measure of the collection efficiency at the maximum power point, is defined as:

$$FF = \frac{P_{MPP}}{V_{OC} \cdot J_{SC}} = \frac{V_{MPP} \cdot J_{MPP}}{V_{OC} \cdot J_{SC}} \tag{3.19}$$

If the superposition principle is valid for μc-Si:H silicon solar cells, the output current *j(V)* can be regarded as the summation of dark current and the photo-generated current $j_{photo}(\mathrm{V})$,

$$j(V) = j_{dark}(V) - j_{photo}(V) = j_0 \cdot [e^{(qV/nkT)} - 1] - j_{photo}(V) \tag{3.20}$$

Thus, $J_{SC} = j(\mathrm{V}{=}0) = -j_{photo}(\mathrm{V}{=}0)$. For solar cells with high quality *i*-layer material, J_{SC} is mainly determined by the absorption of the incident light, due to effective extraction of the photo-generated charge carriers. Measured with no external current flow, V_{OC} can also be deduced from the Eq. 3.20 as below,

$$V_{OC} = \frac{nkT}{q} \cdot ln(\frac{J_{SC}}{j_0} + 1) \tag{3.21}$$

If not otherwise stated, all solar cells were annealed in air for 30 minutes at 160 °C before the J-V measurements. The J-V measurements were performed under standard test conditions, using an AM1.5 spectrum with an intensity of 100 mW/cm^2 at a temperature of 25 °C. A class A double source solar simulator (WACOM-WXS-140S-Super) was used for the illumination. The solar simulator was calibrated before each measurement with a Hamamatsu photodiode S1336-8BQ (spectral range: 190-1100 nm). The run-to-run reproducibility is better than 2 %. A band-pass filter (bg7, centered at the wavelength of 480 nm) and a cut-on filter (og590, at 590 nm) were used to characterize the p/i interface and the bulk i-layer quality, respectively.

Quantum efficiency

Through the quantum efficiency measurement, deeper insight into the spectral response and charge carrier extraction can be obtained. The quantum efficiency QE(λ) is defined as,

$$QE(\lambda) = \frac{j_{ph}(\lambda, V)}{e \cdot \Phi(\lambda)} \tag{3.22}$$

in which j_{ph}(λ,V) is the photo-generated current collected at the electrodes, and $\Phi(\lambda)$ is the incident light quanta per wavelength interval.

As the short wavelength light (for example for $\lambda \leq 520$ nm) is strongly absorbed in the p-layer and at the p/i interface, the quantum efficiency in the short wavelength region can be regarded as a measure for the p-layer and p/i interface quality. The long wavelength light above 600 nm, on the other hand, is nearly homogeneously absorbed in the i-layer. Thus, the long wavelength QE reflects the i-layer quality. In addition, voltage dependent QE measurement provide further information about the charge carrier collection efficiency.

In our QE measurement setup, the light beam is generated by a xenon lamp and a monochromator. The setup covers the range between 300 and 1100 nm with a spectral resolution better than 10 nm. The QE measurements were carried out at 25 ∘C. Detailed introduction to the experimental principle can be found in Ref. [*Ashok and Pande 1985, Metzdorf 1987*].

Light soaking

The light soaking experiments were carrier out on selected samples to investigate the stability against the light illumination. All the investigated cells were placed under the AM1.5 illumination at a temperature of 50 ∘C under open circuit conditions. Details of the experimental setup can be found elsewhere [*Rech 1997a, Amvene-Edjongolo 2000*].

Chapter 4

High rate growth of μc-Si:H by PECVD

The low deposition rate (usually < 0.1 nm/s) in the conventional RF-PECVD restricts the application of intrinsic microcrystalline silicon (μc-Si:H) in thin film solar cells as absorber layer, which is usually thicker than 1.5 μm. Therefore, high rate deposition is desired in the industry to reduce the processing time. In this chapter, it will be shown that high deposition rate (R_D) over 1 nm/s can be prepared by VHF-PECVD working at high pressure and high power (hphP). It will be tried in this chapter to find out answers for the questions like, (1), compared to the conventional low pressure, low power (lplP) condition, what are the advantages and disadvantages of hphP? (2), is it possible to keep the same material quality at high R_D? (3), what are the effects of R_D on material quality and solar cell performance? ...

4.1 Stable and homogenous deposition under high pressure

Deposition processes in the hphP-regime deliver a considerable increase in the growth rate [*Guo 1998, Kondo 2000*], but the low electron energy, caused by a reduced mean free path under high pressure conditions and by a low peak-to-peak voltage at high plasma excitation frequency, makes it difficult to start and sustain stable discharges. For this reason, an adequately high discharge power and/or a small electrode distance, leading to a stronger electric field between electrodes, are necessary for the combination of VHF and high pressure. Fig. 4.1 shows the minimum power, which is required for a given working pressure (p_{depo}) in order to maintain a stable plasma at different electrode distances (d). Note that only H_2 plasma is used in this experiment, thus the required power and electrode distance might be different when a SiH_4 and H_2 plasma is used for the real i-layer deposition. The necessary discharge power (P_{VHF}) sharply increases with p_{depo} at a constant electrode distance. At smaller distance, lower P_{VHF} is sufficient at a given p_{depo} due to the stronger electric field and the lower collision probability. All combinations of

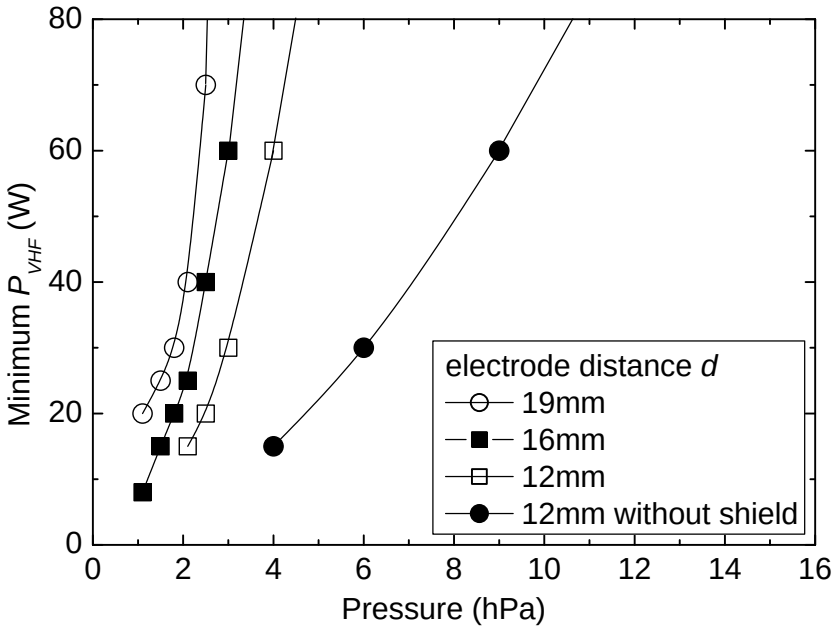

Figure 4.1: *Minimum discharge powers (P_{VHF}) to sustain a stable discharge as a function of p_{depo} for different electrode distances. Lines are guides for the eye.*

P_{VHF} and p_{depo} yielding stable plasma conditions should be located above the corresponding line for a given electrode distance. Leading to high R_D and simultaneously providing a wide deposition parameters space within the system's technical limit, the pressure of 2.1 hPa is the one generally used under the hphP condition in this chapter. The removal of the metallic shield resulted in less parasitic losses of the power between electrode and shield, requiring a considerable lower minimum power to sustain a stable plasma. Also, less powder accumulated at the electrode edges, which in turn led to a better stability of the individual discharge as well as run-to-run reproducibility. The high working pressure made sure that the plasma was well confined between the electrodes after the removal of the shield. Therefore, depositions in the later stage of the present research work were carried out without shield. The comparison of the solar cell performance, to be presented later on, showed that the removal of the shield had no major influence on the deposition rate or the solar cell properties, apart from the improved process stability. In addition, it is found that a reduction of the electrode distance improved the homogeneity of the discharge across the substrate.

It needs to be mentioned that p_{depo} of 0.25 hPa, P_{VHF} of 10 W and an electrode distance of 19 mm were used under the lplP conditions. Keeping the electrode distance unchanged, an increase of p_{depo} up to 2.1 hPa and P_{VHF} up to 60 W greatly increases

R_D from 0.2 nm/s at lplP to 1.23 nm/s. However, such samples suffered from strong structural inhomogeneities on a substrate size of 10×10 cm^2. In addition, they show poor efficiency. By reducing the electrode distance to 12 mm, the homogeneity greatly improved. Therefore, the majority of the investigations in this chapter were performed with an electrode distance d of 12 mm and p_{depo} of 2.1 hPa. The thickness and structure homogeneity in the samples deposited in the hphP regime with different parameters will be shown in section 4.3.1.

4.2 μc-Si:H films deposited with lplP and hphP

VHF-PECVD working at hphP was used to deposit μc-Si:H films at high growth rate (R_D) in this section. The deposition parameters are listed here: P_{VHF} = 60W, p_{depo} = 2.1 hPa, electrode distance = 12 mm, excitation frequency = 94.7 MHz and total flow rate (Fl_{total}) = 100 sccm. A series of samples were deposited with different silane concentration (SC) to obtain different structural composition from highly crystalline to amorphous growth. Another series of samples were deposited under the conventional lplP condition for comparison. The deposition parameters at lplP were the same as those of the hphP series except P_{VHF}, p_{depo} and the electrode distance mentioned in former section. Raman spectroscopy, IR spectroscopy, photothermal deflection spectroscopy and conductivity measurements were used to investigate structural, electrical and optical properties of these μc-Si:H samples. The film thickness was kept at about 500 nm by adapting the deposition time according to the estimated R_D.

4.2.1 Deposition rate

Fig. 4.2 shows R_D of the two series deposited with hphP and lplP, plotted as a function of SC. The deposition rate R_D was calculated from the thickness measured in the middle of the 10×10 cm^2 substrates. A linear increase of R_D with increasing SC can be found in both series in the investigated SC region. The lplP samples show an R_D of 0.1 - 0.3 nm/s at SC between 2 and 7.5 %. Upon the variation of SC from 6 % to 12 % , R_D for the hphP samples increases from about 0.8 to 1.5 nm/s. The hphP series shows much higher R_D than lplP samples at the same SC. This is probably due to the high dissociation rate of reactant gases at hphP. The thickness difference across the substrate area is typically about 15 % for all solar cells. In general, samples deposited under lplP conditions have better homogeneity than hphP ones. For more detailed discussion of the homogeneity problem under hphP conditions, see section 4.3.1, where hphP solar cells deposited with different parameters are summarized.

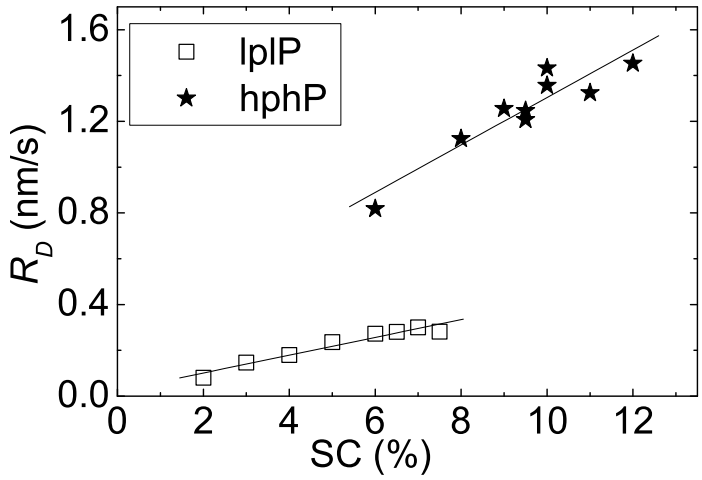

Figure 4.2: *R_D of hphP and lplP films plotted as a function of SC. A linear increase of R_D with increasing SC can be observed in both series. Lines are linearly fitted to the data.*

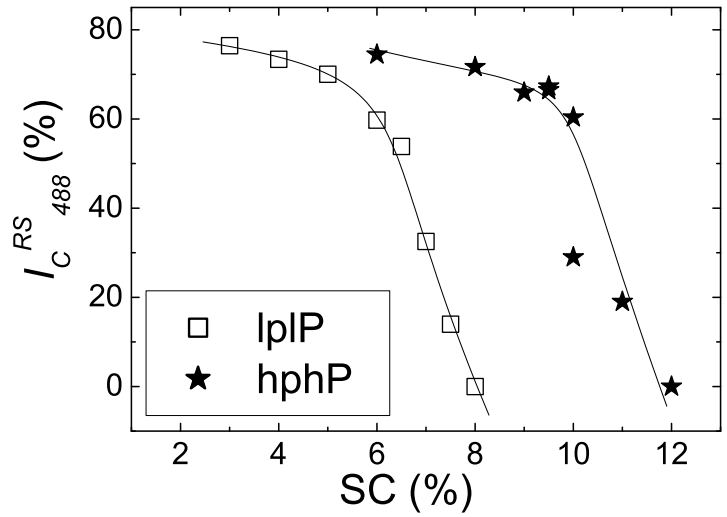

Figure 4.3: *I_{C488}^{RS} of hphP and lplP films as a function of SC. A sharp decrease of crystallinity can be observed in both series, indicating the transition from μc-Si:H to a-Si:H growth. Lines are guides for the eye.*

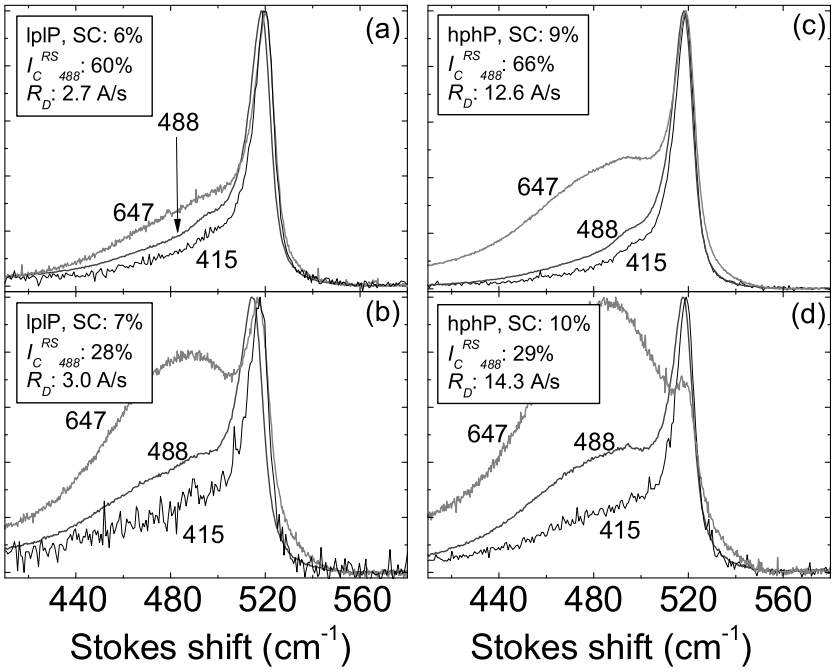

Figure 4.4: *Raman spectra of selected hphP and lplP samples measured with different laser wavelengths. Numbers indicated at the spectra refer to the excitation wavelengths used in the measurements (in unit of nm).*

4.2.2 Structure properties

As the properties of μc-Si:H depend critically on the material structure composition, crystalline volume fraction is a more suitable parameter for the comparisons of different material rather than SC for deposition. Fig. 4.3 shows I_{C488}^{RS} of the two sample series. As can be seen, I_{C488}^{RS} decreases with increasing SC in both series. The hphP samples with the same I_{C488}^{RS} as lplP films were usually obtained at higher SC.

The presence of an amorphous incubation layer and an increasing crystallinity upon the growth have been widely observed in μc-Si:H material, especially in the samples on foreign substrates like glass or c-Si covered with native oxide [*Koh 1998, Houben 1998, Ross 2000, Collins 2003*]. In order to study the structure development along the growth axis, Raman scattering measurements were performed from the film side with three different excitation wavelengths, 415, 488 and 647 nm. Four selected samples, two from the lplP series and another two from the hphP series, with similar crystallinity of either ~60 % or ~30 %, were used in this experiment. The Raman spectra normalized to the highest intensities are shown in Fig. 4.4. An increase in the amorphous peak with increasing wavelength

can be observed in all samples. As the bottom of the film shows stronger contribution to the Raman signal measured with longer excitation wavelength (see section 2.5.3), a more amorphous initial stage of growth can be deduced from these observations. Among these samples, the highly crystalline lplP sample [with I_{C488}^{RS}=60% in diagram (a)] shows best homogeneity in the growth direction. Material with lower total crystallinity shows less homogeneous structure [diagram (b)], although R_D of the two lplP samples are very similar (0.27 and 0.30 nm/s at low and high SC, respectively). Deposited at higher R_D, the hphP samples show stronger structure development, compared to the lplP samples with similar I_{C488}^{RS}. The hphP sample deposited at SC = 10 % appears to be almost fully amorphous in the Raman spectrum measured with the 647 nm laser, while the spectrum with 488 nm line still indicates a sizeable crystalline fraction (I_{C488}^{RS}=29 %). Therefore, one must keep in mind that the actual average crystallinity may be considerably overestimated in some samples grown on glass substrates, especially in the hphP samples with low crystallinity, if I_{C488}^{RS} is used as nominal crystallinity for the material comparison.

4.2.3 Infrared absorption

FTIR measurements were conducted on μc-Si:H films from time to time after the deposition. FTIR spectra for the samples prepared under hphP conditions, measured after one year storage in air to saturate the atmospheric in-diffusion, are shown in Fig. 4.5. For clarity, some samples are omitted with respect to the full set referred to in Fig. 4.2 and 4.3. The percentage numbers in this figure are the I_{C488}^{RS} values of the corresponding samples. Three absorption bands related to the SiH bond can be identified in all spectra (see section 2.5.5). The absorption intensities of the SiH wagging mode centered at ∼630 cm^{-1} and stretching mode at around 2000 cm^{-1} increase steadily with the decreasing crystalline volume fraction, indicating the increasing bonded H content. The wagging mode absorption peak position is almost independent of the crystallinity. In the two samples with $I_{C488}^{RS} >$ 70 %, absorption at 2100 cm^{-1}, related to SiH bonds at the internal surface, dominates the stretching mode absorption. The absorption at 2000 cm^{-1} increases with the SC (i.e. with decreasing I_{C488}^{RS}) and become dominant in the stretching absorption band in the two samples with low crystallinity. The SiO absorption between 960 and 1200 cm^{-1} can be seen in the samples with $I_{C488}^{RS} \geq 60$ %.

The infrared absorption spectra of selected samples in the lplP series, measured after one year storage in air, are displayed in Fig. 4.6. The evolution of absorption due to SiH bond vibrations with decreasing crystallinity shows a similar trend as the hphP samples. Noticeable absorption associated with O incorporation between 960 and 1200 cm^{-1} can only be found in one sample with the highest crystallinity (78 %).

Fig. 4.7 (a) and (b) show the bonded hydrogen content (C_H) and microstructure factor R of the hphP and lplP samples as a function of I_{C488}^{RS}. C_H is estimated from the SiH wagging mode absorption intensities. As I_{C488}^{RS} decreases from about 80 % to 0 %, C_H increases from ∼4 at.% to ∼11 at.% in both series. At the same time, the microstructure

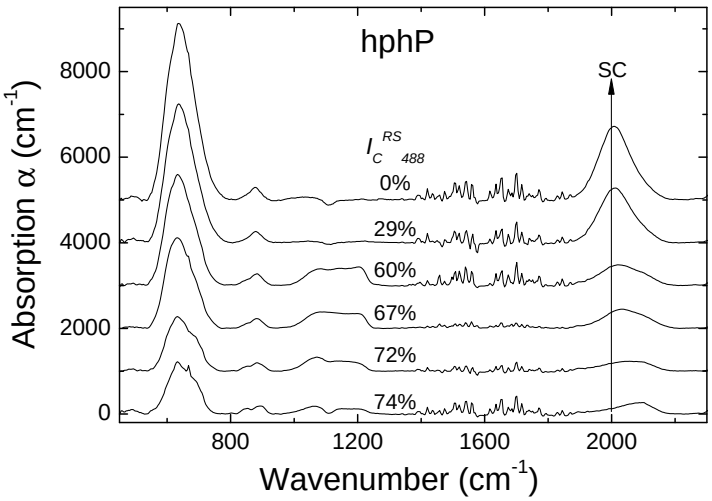

Figure 4.5: *Infrared absorption spectra of the samples deposited under hphP conditions. Percentage numbers in the figure are I_{C488}^{RS} value of the samples. Some spectra were shifted upward for clarity.*

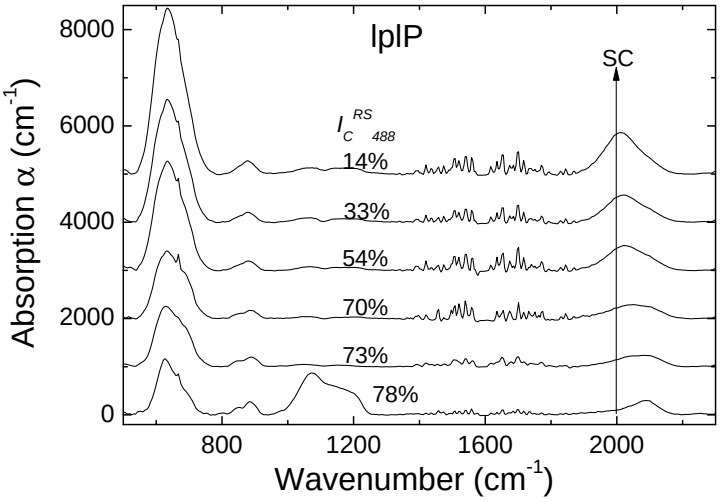

Figure 4.6: *Infrared absorption spectra of the samples deposited under lplP conditions. Percentage numbers in the figure are I_{C488}^{RS} value of the samples. Some spectra were shifted upward for clarity.*

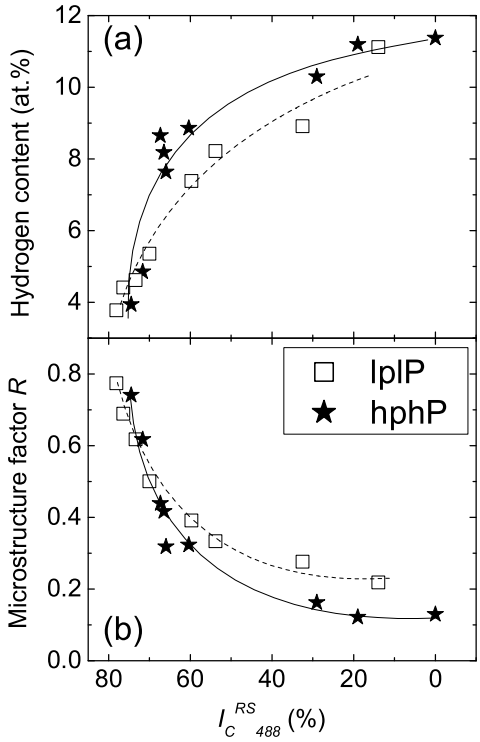

Figure 4.7: *(a) Bonded hydrogen content (C_H) and (b) microstructure factor* R *of the μc-Si:H material deposited under hphP and lplP conditions, plotted as a function of I_{C488}^{RS}. Lines are guides for the eye.*

factor R decrease from ∼0.8 to ∼0.15. At I_{C488}^{RS} of 60 %, where high efficiency solar cells are typically found, C_H is ∼8 at.% and R is ∼0.35 in both series. A systematically lower R values and higher C_H can be found in the hphP samples with I_{C488}^{RS} below 65 %. A thicker and/or less crystalline incubation layer in the hphP films might be the reason for this difference.

To investigate the atmospheric impurity in-diffusion process, FTIR measurements were carried out on these samples after different air exposure time, i.e. within 0.5 hour, after 7 days, 30 days, 60 days and more than one year. The SiO absorption bands of three selected hphP samples with different I_{C488}^{RS} are exemplarily shown in Fig. 4.8. In diagram (a) and (b), the two vertical arrows indicate the progressive developing of the SiO absorption peaks in two highly crystalline samples with the prolonged exposure time from within 0.5 hour to over 1 year. The post-oxidation process starts to saturate in the two samples after 30 days storage in the air and only slow development happens with further air exposure. Such remarkable enhanced oxygen incorporation can hardly be found in the amorphous

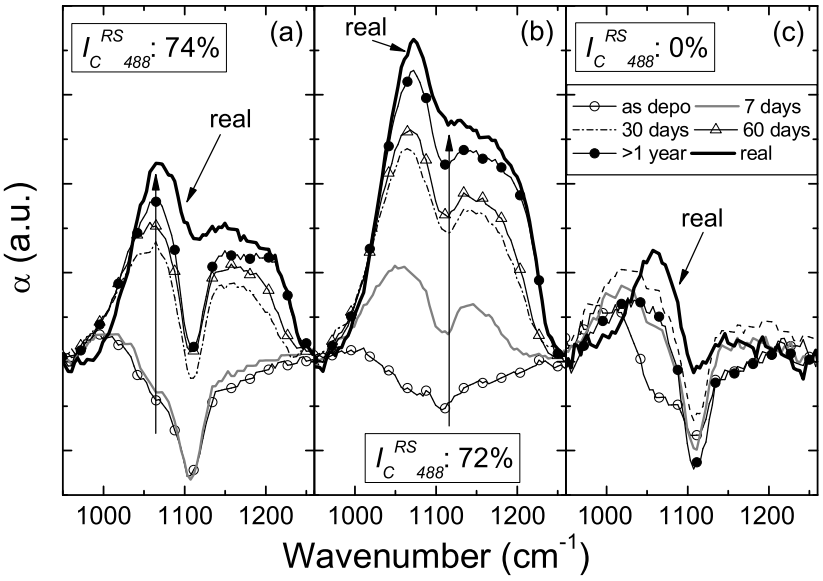

Figure 4.8: *FTIR spectra of three hphP sample with different I_{C488}^{RS} values measured within 0.5 hour, after 7 days, 30 days, 60 days and more than one year. The two vertical arrows in diagram (a) and (b) indicate the increasing air exposure time. The post-deposition oxygen uptake, which can be deduced from the differences between SiO absorption intensities in the spectra measured as-deposited and after one year, are also shown in the figure, labelled with "real".*

sample [diagram (c)]. However, the spectra measured directly after deposition were not flat in the frequency region between 1000 and 1200 cm^{-1}. Instead, a valley with minimum at ∼1100 cm^{-1} were found in almost all the spectra. The inhomogeneous distribution of the native oxide layer on an individual c-Si wafer were believed to be the origin of this phenomenon [*Klein 2004, Lossen 2003*]. To exclude the influence from the substrates and obtain the real post-deposition oxygen incorporation, the as-deposited spectra were used as the references to subtract the latest measured spectra. The differences between them are also indicated in the figure marked by labels of "real". Note that the SiO absorption in some samples, such as the one in diagram (c), doesn't change much after one year in air. Under such conditions, the measurement accuracy is easily affected by the data processing, such as baseline subtraction etc.

The O incorporation during deposition is typically determined by the background pressure, feed gas purity, leakage rate and out-gas of the deposition chamber. For the high quality a-Si:H and μc-Si:H films deposited in ultra-high vacuum systems equipped with

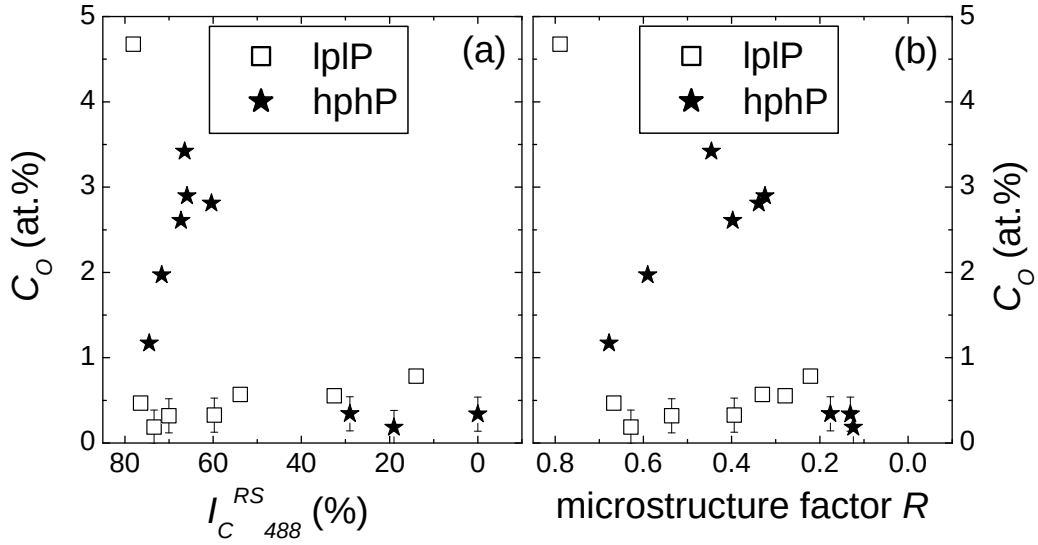

Figure 4.9: *Oxygen content (C_O) of hphP and lplP samples plotted as a function of I_{C488}^{RS} in diagram (a) and of microstructure factor* R *in diagram (b). C_O are determined from the SiO absorption intensities measured after more than one year's storage in the air.*

gas purifiers, O contents of below 10^{16} cm^{-3} can be obtained [*Kamei 1996*]. The device quality material deposited by PECVD and HWCVD in our institute usually contains O contents of about 10^{18} cm^{-3} [*Mück 2000, Klein 2001*]. This concentration is much lower than 10^{20} cm^{-3}, the measurement limit of SiO bond density by FTIR [*Paesler 1978*]. A pronounced SiO mode absorption can be seen in some samples in Figures 4.5 and 4.6, indicating remarkable O uptake after the deposition. Fig. 4.9 shows the O contents of the hphP and lplP material calculated through Eq. 3.10, plotted as a function of I_{C488}^{RS} in diagram (a) and of microstructure factor R in diagram (b). The SiO absorption intensity is determined from the spectra measured after more than one year's storage in the air. Three samples peeled off from the substrates after one or two months, thus in these cases, the O content were estimated from the final measurement results. Almost all samples in the lplP series maintain a low O content close to the measurement limit after prolonged air exposure, except the one deposited at SC = 2 % with high I_{C488}^{RS} = 78 %. A high C_O of 4.7 at.% was found in this sample. The hphP samples with high crystallinity above 60 % or microstructure factor $R > 0.3$ show high O content of 1 - 3.5 at.%, compared to the lplP samples with the same I_{C488}^{RS} or R. These results are consistent with the former finding that μc-Si:H films deposited at high rates (achieved by applying higher power) are generally more porous than the μc-Si:H material at low rate [*Mück 2000*]. Three hphP

samples with $I_{C488}^{RS} < 30$ % were very stable against the ambient air. Although strong post-deposition oxygen incorporation happens in the highly crystalline samples in both series, a clear correlation between O content and I_{C488}^{RS} can not be found in Fig. 4.9 (a). The hphP samples with medium I_{C488}^{RS} of about 65 % have the highest O content, while C_O values are almost constant in the lplP films with I_{C488}^{RS} below 76 %. The lack of O content dependence on the material crystallinity and R was also previously observed in μc-Si:H deposited by HWCVD at high deposition rate [*Lossen 2004*]. This contradicts the previous hypothesis which regarded microstructure factor R as a measure for structure porosity in the a-Si:H material [*Wagner and Beyer 1983, Richter 1983*]. Possible explanations for this discrepancy will be discussed later.

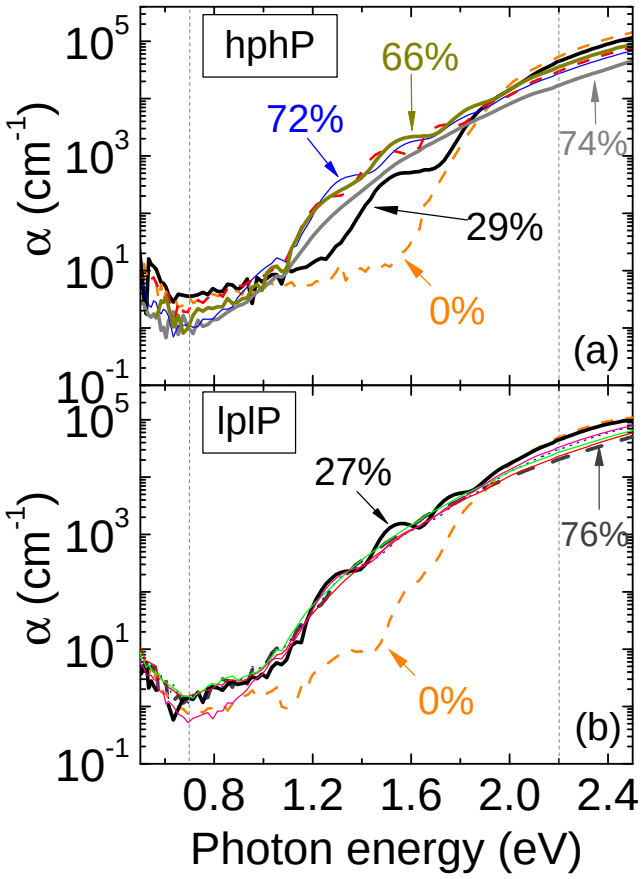

Figure 4.10: *Optical absorption coefficient of hphP and lplP films at different photon energies measured by PDS. Percentage numbers in the figure are* I_{C488}^{RS} *values of corresponding samples.*

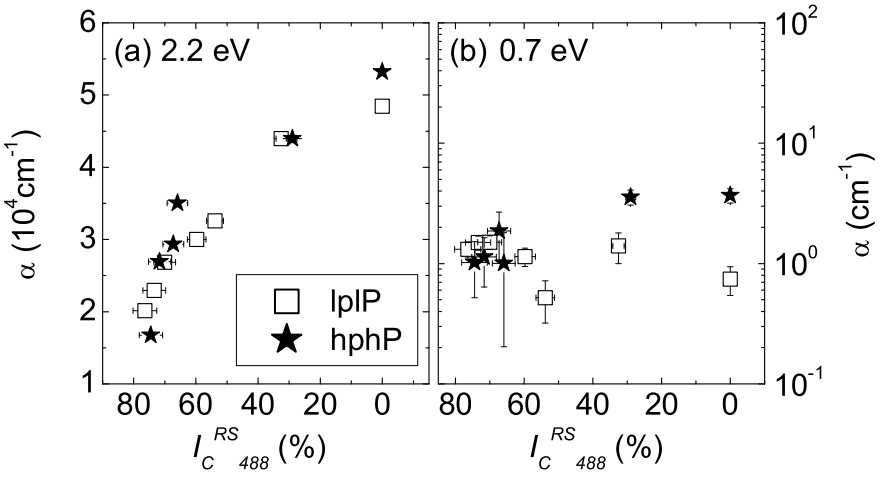

Figure 4.11: *Optical absorption coefficient of hphP and lplP films at the photon energy of 2.2 eV (a) and 0.7 eV (b), plotted as a function of* I_{C488}^{RS}.

4.2.4 Optical absorption

Fig. 4.10 (a) and (b) show the optical absorption of the hphP and lplP series at photon energies between 0.5 eV and 2.5 eV measured by photothermal deflection spectroscopy (PDS). Some hphP samples of which data are presented in figure 4.2 peeled off during the PDS measurements, therefore no absorption coefficient data are shown in this figure. The percentage values in the figure are the I_{C488}^{RS} values of the corresponding samples. A systematic increase in the above-gap (at 2.2 eV for example) absorption can be observed with decreasing crystallinity in both series. This can be attributed to the high optical absorption of the increasing amorphous phase in the material. Compared to the amorphous material with $I_{C488}^{RS} = 0$ %, μc-Si:H material shows an enhanced absorption in the photon energy range between 1.2 and 1.8 eV, which can be attributed to the narrower optical band-gap in the crystalline phase. In the same photon energy region, remarkable interference fringes are present in most of the hphP samples with I_{C488}^{RS} between 72 % and 29 %, but can only be found in one single lplP material at I_{C488}^{RS} of 27 %. Note that primary interference oscillations rising from reflection at the interfaces of the film, were corrected in the evaluation procedure using the transmittance data [*Carius 2005*]. The reason for residual interference fringes is believed to be the structure in-homogeneity along the growth axis [*Carius 2005, Ross 2005*]. The presence of the more pronounced structure in-homogeneity in the hphP material of high crystallinity is confirmed by Raman depth profile measurements (Fig. 4.4).

Fig. 4.11 compares the above-gap and sub-gap optical absorption of the hphP and lplP material at similar I_{C488}^{RS}. The absorption coefficient at photon energy of 2.2 eV increases

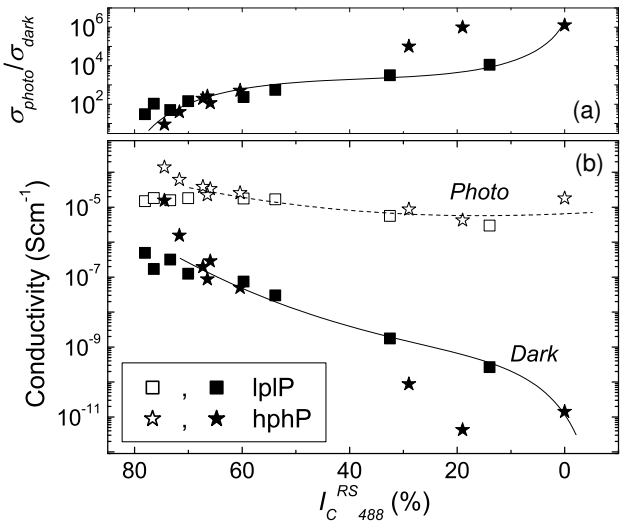

Figure 4.12: *(a): Photosensitivity ($\sigma_{photo}/\sigma_{dark}$) of these samples. (b): Photo- and dark-conductivity (σ_{photo}, indicated by open symbols, and σ_{dark}, indicated by full symbols) of hphP and lplP μc-Si:H material as a function of I_{C488}^{RS}.*

with the increasing amorphous volume fraction in both series, and no significant difference can be found for the two types of material at similar I_{C488}^{RS} (diagram a). The sub-gap absorptions at 0.7 eV remains at a low level of about 1 cm^{-1} except in two hphP samples with low I_{C488}^{RS} of 30 % and 0 %. If the sub-gap absorption is proportional to the deep defect density [*Klein 2004, Wyrsch 1991, Jackson and Amer 1982*], these results imply high material quality in the samples deposited at high R_D with hphP.

4.2.5 Conductivity

σ_{photo} and σ_{dark} of the hphP and lplP films are shown in the bottom diagram of Fig. 4.12. The σ_{photo} data are presented by open symbols and σ_{dark} by full symbols. An almost constant σ_{photo} at 10^5 Scm^{-1} with the decreasing I_{C488}^{RS} can be observed for lplP and hphP material, except the hphP samples with very high crystallinity. σ_{dark} strongly decreases by several orders of magnitude down to below 10^{-10} Scm^{-1}, as the structure composition shifts from highly crystallinity to amorphous dominance. Together with the small variation of σ_{photo}, the decreased σ_{dark} leads to an increased photosensitivity with decreasing crystalline volume fraction, which is shown in the top diagram. A photosensitivity values between 200 and 500 were obtained for both series with I_{C488}^{RS} between 50 and 65 %. Vetterl et al. suggested that such material could be applied as absorber layer in thin film silicon solar cells [*Vetterl 2002*].

Although σ_{photo} and σ_{dark} in both series are quite similar, especially at I_{C488}^{RS} of about 60 %, differences can still be found between them. Both σ_{photo} and σ_{dark} of the hphP series

show a sharp increase with increasing I_{C488}^{RS} in the highly crystalline region. The impurity incorporation in these samples could be the reason. The post-deposition oxygen uptake may shift fermi level towards the conduction band and thus increase charge carrier lifetime [*Beyer and B. Hoheisel 1983, Finger 2002, Brüggemann and Main 1998*]. This leads to higher σ_{photo} and σ_{dark}. Two hphP samples with low crystalline volume faction of 29 % and 19 % show lower σ_{dark} than the lplP samples with similar I_{C488}^{RS}, which leads to a higher photo-sensitivity in these two sample. The remarkable structure development in the hphP films, forming a thick amorphous incubation layer and thus reducing the total intrinsic carrier density, can be a possible reason.

4.3 μc-Si:H solar cells deposited at high rates

4.3.1 Influences of deposition parameters on solar cell deposition rate and performance

In this section, investigations on the influences of the deposition parameters, such as p_{depo}, P_{VHF}, Fl_{total} and electrode distance d on solar cell deposition rate and performance will be first presented. For the individual change of deposition parameters, variations of the silane concentration SC series were performed to cover the range from highly crystalline to amorphous growth and to obtain the optimum solar cells. For detailed information about the deposition parameters in each SC series, see Table 4.1. The first column shows the names assigned to the SC series, which will be used hereafter for the presentation and discussion of the results. Data for one series of solar cells deposited under low-pressure, low-power (lplP) conditions at R_D between 0.1 and 0.3 nm/s, are also presented for comparison. R_D and the conversion efficiency for the optimum solar cell in the lplP series are about 0.2 nm/s and 8 %, respectively. The results for this lplP series are in excellent agreement with earlier work and the solar cell parameters show the well-known trend upon the variation of SC [*Vetterl 2000*].

In the hphP series deposited with different Fl_{total} and in the lplP series, an improved, thinner p-layer, yielding higher blue light response, is used. In the i-layer deposition of these solar cells, the metallic shield around the powered electrode was removed to obtain more reproducible and stable deposition.

Effect of power on the deposition rate and solar cell performance

Five different discharge powers, P_{VHF} of 20 W, 30 W, 40 W, 60 W and 90 W, were applied to investigate the influence on deposition rate (R_D) and on the properties of μc-Si:H solar cells at high deposition pressure. The R_D of these SC series with different P_{VHF} are shown in Fig. 4.13 as functions of SC. In addition, two series of solar cells prepared with larger electrode distance (hphP 19 mm) or higher p_{depo} (hphP 4 hPa) at P_{VHF} = 60 W are also plotted in Fig. 4.13. A linear increase of R_D with increasing SC is

Series name	p_{depo} (hPa)	P_{VHF} (W)	Fl_{total} (sccm)	d (mm)	shield	p-layer
hphP 20 W	2.1	20	100	12	with	Normal
hphP 30 W	2.1	30	100	12	with	Normal
hphP 40 W	2.1	40	100	12	with	Normal
hphP 60 W	2.1	60	100	12	with	Normal
hphP 90 W	2.1	90	100	12	with	Normal
hphP 19 mm	2.1	60	100	19	with	Normal
hphP 4 hPa	4.0	60	100	12	with	Normal
hphP 100 sccm	2.1	60	100	12	w/o	Improved
hphP 200 sccm	2.1	60	200	12	w/o	Improved
hphP 400 sccm	2.1	60	400	12	w/o	Improved
lplP	0.25	10	100	19	w/o	Improved

Table 4.1: *Deposition parameters of the silane concentration (SC) series.*

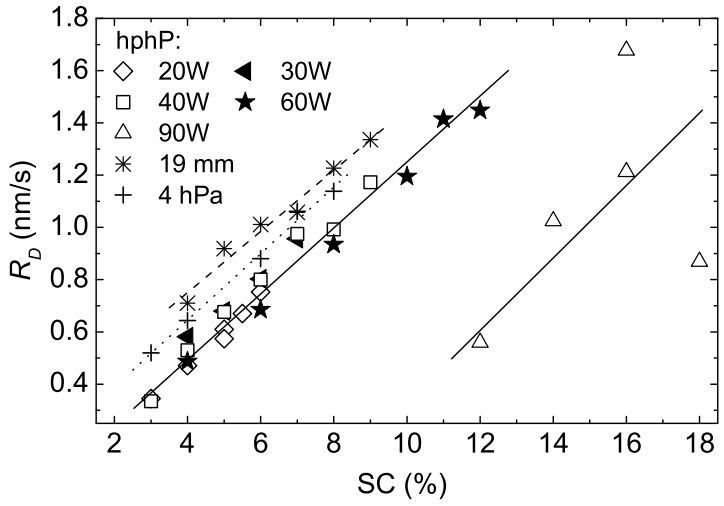

Figure 4.13: *R_D of solar cells deposited with different P_{VHF} plotted against SC. p_{depo} = 2.1 hPa and* d *= 12 mm were used for most of the series, except for the two series with higher p_{depo} or larger electrode distance (4 hPa and 19 mm, respectively). Lines are linearly fitted to the data.*

observed in all cases. At P_{VHF} = 90 W, the plasma became unstable and inhomogeneous, and considerable scatter of R_D was observed. Further geometry rearrangement, such as employing a gas showerhead and bigger cable feed-through etc., is necessary for such high

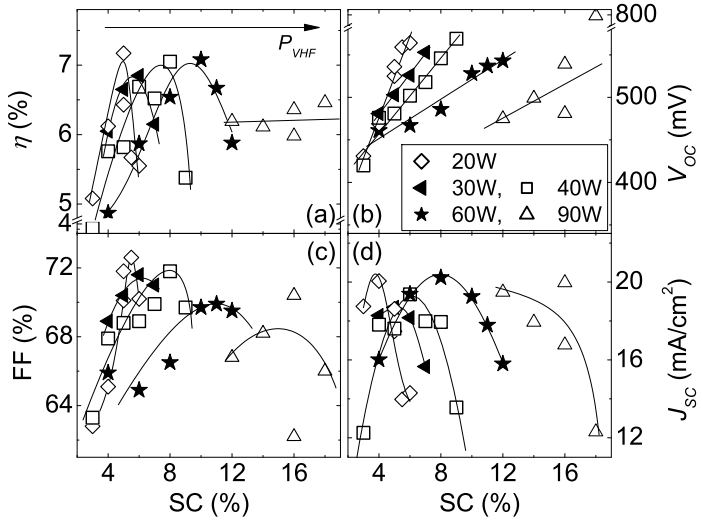

Figure 4.14: J-V *characteristics (a) η, (b) V_{OC}, (c) FF, (d) J_{SC} under AM1.5 illumination of solar cells deposited under hphP conditions with different P_{VHF}. Samples are the same as those shown in Fig. 4.13 with p_{depo} of 2.1 hPa and d of 12 mm. Lines are guides for the eyes.*

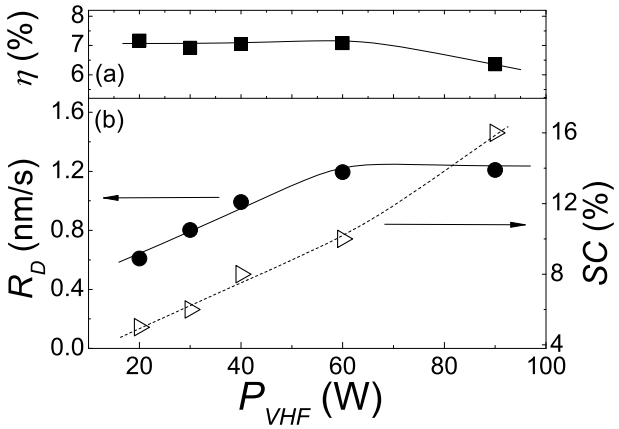

Figure 4.15: *(a) Efficiencies of the optimum solar cells in the SC series deposited with different P_{VHF}. (b) Corresponding deposition rates R_D and SC of these cells. Lines are guides for the eyes.*

P_{VHF} for the present reactor design. The increase of P_{VHF} does not result in any significant increase of R_D at fixed SC and above certain P_{VHF}, R_D even decreases. Assuming that up to 60 W the "real" power dissipated in the discharge at least increases to some extent, the saturated R_D suggests that the amount of silane molecules in the plasma are near to the silane depletion condition. If almost all silane molecules are dissociated into radicals under the depletion condition, higher discharge power can not increase the deposition further. The above deduction is based on R_D calculated from the thickness in the middle of the 10×10 cm^2 substrates. The good homogeneity of the four series samples with P_{VHF} below 90 W guarantees the validity of this conclusion. On the other hand, it can be seen that increasing p_{depo} or the electrode distance d at a given discharge power of 60 W results in higher R_D for all SC compared with the other series deposited at 2.1 hPa and 12 mm electrode distance. The origin will be discussed later.

Fig. 4.14 shows the J-V characteristics for the series of solar cells deposited with different P_{VHF} at 2.1 hPa. The electrode distance is 12 mm for all series. For each P_{VHF}, similar behavior of J-V parameters for μc-Si:H solar cells was observed when varying SC, except the scattered results of the hphP 90 W series. FF and J_{SC} increase with SC at first and drop after the maximum. V_{OC} increases almost linearly in the investigated SC range. The solar cells with maximum efficiency show a V_{OC} of about 540 mV. Note that the J-V parameters are taken from the best 1×1 cm^2 cell of each 10×10 cm^2 substrate. The low J_{SC} at high SC is attributed to the red and infrared response loss in these solar cells. This is confirmed by the quantum efficiency measurement (to be shown in Fig. 4.26 in section 4.3.2). The highest FF in each SC series decreases systematically upon increasing P_{VHF}, but a significant drop of the optimum cell efficiency was only observed at P_{VHF} = 90 W. The most important observation is the shift of the maximum values in efficiency, FF and J_{SC} to higher SC upon the increase of the discharge power. As a consequence, optimum cells deposited with higher P_{VHF} have higher R_D, as indicated in Fig. 4.15, in which efficiency, R_D and required SC of the optimum cells of these series are plotted vs. P_{VHF}. The required SC for optimum solar cells increases linearly with P_{VHF}. The increase of the silane supply leads to a linear increase of R_D up to 60 W.

The optimum cells of hphP 19 mm and hphP 4 hPa series show lower conversion efficiency of about 6 % and strong structural inhomogeneity over the 10×10 cm^2 substrates. The J-V characteristics of these samples are not shown here.

Effect of total flow rate on deposition rate and solar cell performance

As was shown in Fig. 4.13, an increase of the discharge power at hphP conditions from 20 to 60 W does not lead to an increase in the deposition rate at constant SC. At the same time, the deposition rate increases linearly with silane concentration, i.e. the source gas supply. This points to silane depletion under these conditions. It means that, at a given SC, the precursor density cannot be increased much by higher discharge power. A possible solution to this problem would be to increase the volume of reaction zone between the two

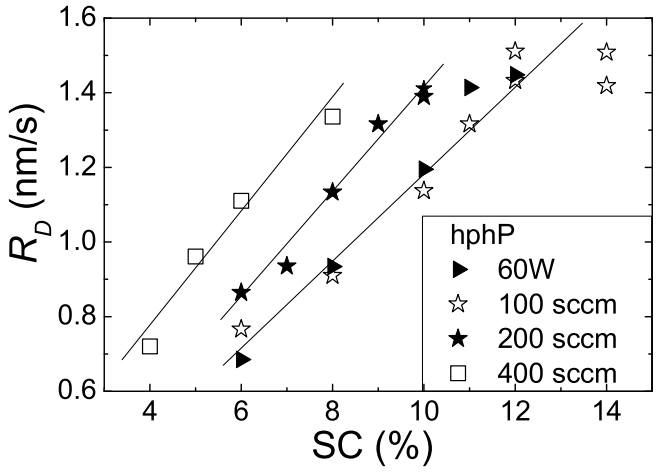

Figure 4.16: *R_D of solar cell i-layers deposited with different Fl_{total} plotted as a function of SC. Series hphP 60W was deposited with the same parameters as series hphP 100 sccm except that the plasma shield was removed for the latter's deposition*

electrodes or to increase the silane supply by increasing the gas flow. As an additional beneficial effect of higher gas flow, powder formation, which is frequently observed in high deposition rate processes, could possibly be suppressed [*van den Donker 2005, Matsuoka 1999*].

Three different Fl_{total}, 100 sccm, 200 sccm and 400 sccm, were used to prepare μc-Si:H solar cells at a discharge power of 60 W and a pressure of 2.1 hPa. Again, SC series were done to cover the range from highly crystalline to amorphous material structure. Furthermore, the metallic steel shield around the powered electrode was removed for the *i*-layer deposition. Fig. 4.16 shows the R_D of the solar cells deposited at different flow rates, plotted against SC. A linear increase of R_D with increasing SC is observed at different Fl_{total}. At constant SC, doubling Fl_{total} increases, but far from doubles, the R_D, resulting in lower gas utilization at higher Fl_{total}. Compared to the hphP 60 W series in Fig. 4.13, the hphP 100 sccm series was deposited with identical parameters except that the metallic shield was removed during the deposition. R_D of the hphP 60 W series are also shown in Fig. 4.16. One can see that the removal of the shield makes no difference in the R_D.

The *J-V* characteristics of these series of solar cells deposited at different Fl_{total} are shown in Fig. 4.17. The dependence of η, V_{OC}, J_{SC} and FF with the variation of SC is similar to that with different P_{VHF}. Compared to the solar cells in Fig. 4.14 deposited with different P_{VHF}, thinner *p*-layers in the three series in this figure increase the blue light response and thus J_{SC}, leading to higher efficiencies. At constant SC, solar cells deposited with higher Fl_{total} exhibit higher V_{OC}, suggesting a lower crystallinity in the

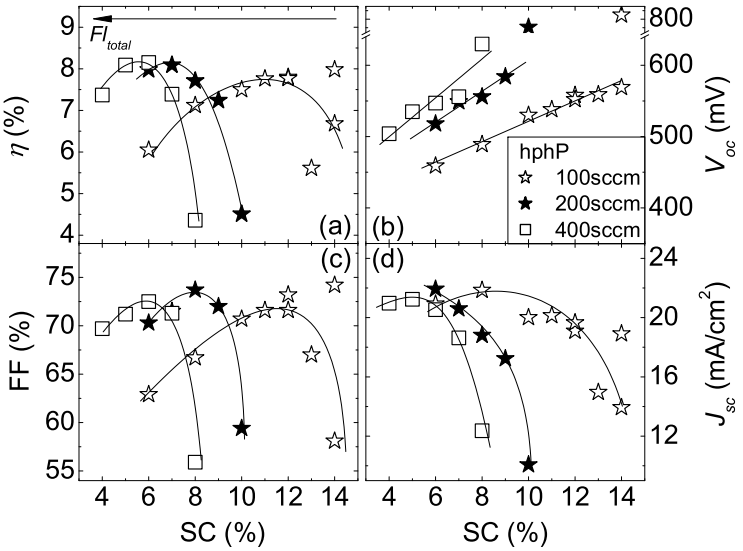

Figure 4.17: *J-V characteristics (a) η, (b) V_{OC}, (c) FF, (d) J_{SC} under AM1.5 illumination of solar cells deposited under hphP conditions with different Fl_{total}.*

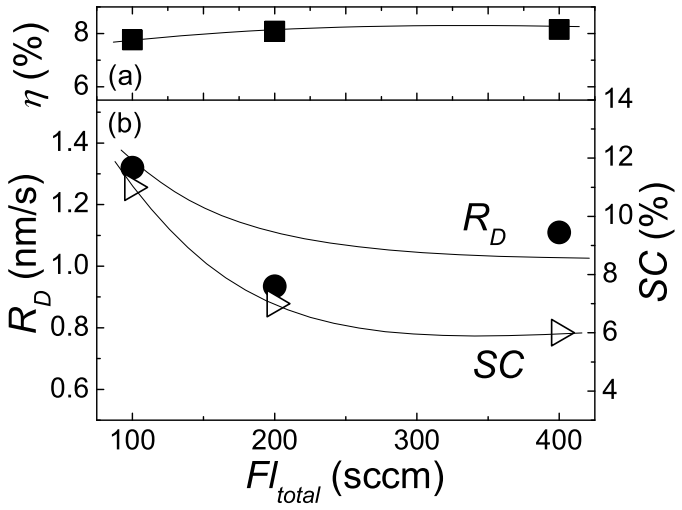

Figure 4.18: *(a) Efficiencies of the optimum solar cells in the SC series with different Fl_{total}. (b) Corresponding deposition rates R_D and SC of these cells.*

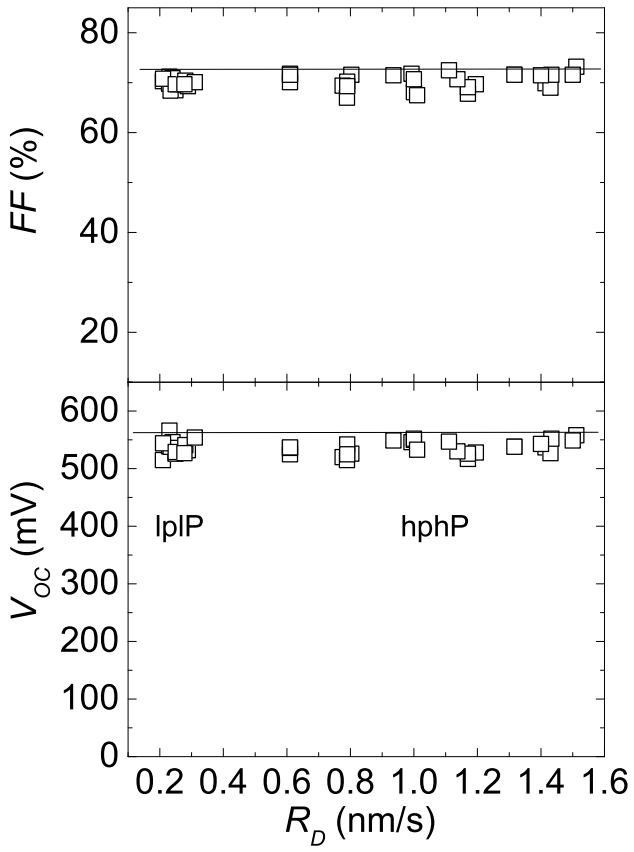

Figure 4.19: *FF and V_{OC} of the optimum μc-Si:H solar cells deposited under lplP and hphP conditions, plotted against R_D. Samples with R_D above 0.6 nm/s are deposited with hphP and those below 0.35 nm/s with lplP. Lines in the figure are guides to the eyes as the upper limit of the two* J-V *parameters.*

i-layers. In Fig. 4.18, R_D, η and SC of the optimum cells, deposited with different Fl_{total}, are shown. An increase of Fl_{total} from 100 sccm to 400 sccm results in a slight increase of the efficiencies of the optimum cells. At higher Fl_{total}, the required SC for optimum solar cells is shifted to lower SC, leading to lower R_D for the optimum cells and suggesting a corresponding shift of the μc-Si:H/a-Si:H transition.

Solar cell performance versus R_D

Applying the VHF-PECVD in the lplP and hphP regime, μc-Si:H solar cells can be deposited over a wide range of R_D between 0.2 nm/s and 1.5 nm/s without detrimental influence of the high deposition rate on the solar cell performance. In Fig. 4.19, V_{OC} and

FF of μc-Si:H solar cells with high conversion efficiency are plotted against their R_D. FF and V_{OC} maintain constant high values of 72 % and 550 mV, respectively, independent of R_D and the deposition regime. J_{SC} is not taken into account here because it is more sensitive than FF and V_{OC} to factors other than the i-layer properties, such as the type of TCO, the p-layer quality and thickness and the i-layer thickness.

Powder formation and homogeneity problem

Powder formation in the PECVD process has been investigated for a long time [*Perrin 1991, Bouchoule 1991, Howling 1993, Watanabe 1996*]. Besides leading to strenuous chamber cleaning work, micrometer-size particles also deteriorate the material quality [*Matsuda 2003, Ross 1984*]. Such a problem is more severe in the high pressure regime, in which the gas phase radicals and molecules have longer residence time in the plasma and thus have more chance to agglomerate [*van den Donker 2005*]. Other deposition parameters also show influence on the powder formation. It was found that the increase in the excitation frequency and Fl_{total} can suppress the powder generation [*Howling 1992, Matsuoka 1999*]. Closer electrode distance was also found to have the same effect, and this was attributed to gas heating from the electrodes [*Guo 1998*]. Although it is very critical for the hphP deposition regime, it is not intended to make a systematic and quantitative research on the powder generation mechanism. In the following, the observation in the powder formation is just briefly described under hphP conditions.

Under the hphP conditions, powder can be evidently seen on the chamber wall just after several runs of i-layer depositions, while this happens later in the conventional lplP regime. With the metal shield installed, powder was visible between the shield and electrode. This would influence the plasma and lead to deteriorated run-to-run reproducibility. After the removal of the shield, the powder was mainly visible on the chamber wall. The two electrodes were usually powder free. As a result, although pronounced, powder formation did not 'significantly' affect the deposition reproducibility and material quality. Typically, high performance solar cells could be prepared up to a accumulative layer thickness of at least 20 μm in the reaction chamber before chamber cleaning was needed. Similar result was also found by Rech et al. [*Rech 2005*], who reported that even up to 80 μm accumulative deposition did not deteriorate the module performance. In addition, without a precise quantitative investigation, the clear evidence for the powder reduction at higher Fl_{total} or smaller electrode distance was not observed.

Compared to the lplP deposition regime, our PECVD process working with very high frequency and hphP caused non-uniformity across the substrates in some cases. Here, a summary of the thickness and structure homogeneity of the solar cells on 10×10 cm^2 substrates will be made, when different deposition parameters were used. Fig. 4.20 shows the ratios between the thickness at the corner and in the middle (D_{corn}/D_{mid}) on individual substrates, plotted as a function of P_{VHF}. The corner thickness is measured close to the solar cells at the corner, which is illustrated by the inset in the figure. A thickness ratio close

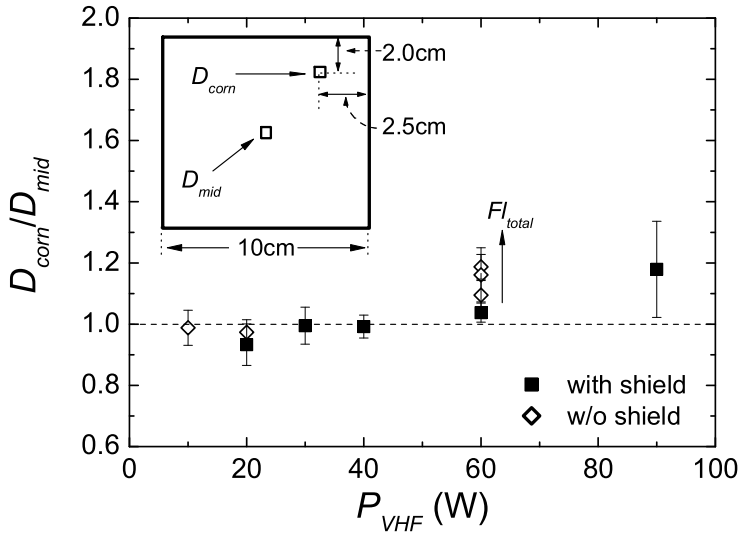

Figure 4.20: *The ratios between the thickness measured at the corner and in the middle on individual 10×10 cm^2 substrates as a function of P_{VHF}. The inset in the figure shows the positions of measuring points on the substrates. Data are averaged from the samples in each silane concentration series in Table 1.1. The standard deviations are indicated by error bars. The hphP samples were deposited with $P_{VHF} \geqslant 20$ W. Depositions with or without the plasma shield around the powered electrode are presented by full squares and open diamonds, respectively.*

to 1 suggests a uniform growth in the sample. Data are averaged from the samples in each silane concentration series in Table 4.1. The error bars indicate the standard deviations in each series. The hphP samples were deposited with $P_{VHF} \geqslant 20$ W. Depositions with or without the plasma shield around the powered electrode are presented by full squares and open diamonds, respectively. From this figure, almost no difference between the thickness at the corner and in the middle can be seen in the samples deposited at P_{VHF} equal to or below 40 W, except the 20 W samples deposited with the plasma shield. Removing the plasma shield slightly improves the homogeneity at $P_{VHF} = 20$ W. In the solar cells deposited at $P_{VHF} \geqslant 60$ W, larger corner thickness values are typically found. Removal of the plasma shield slightly enlarged the thickness ratio (D_{corn}/D_{mid}), and the increased Fl_{total} from 100 to 400 sccm led to further homogeneity deterioration. But a D_{corn}/D_{mid} below 1.2 at 400 sccm indicates that the thickness uniformity under such condition is still reasonable. Therefore, the deduction of silane depletion from R_D at different P_{VHF} (see section 4.3.1) was not affected because of the sufficient uniformity in the four series with P_{VHF} below 90 W. The unstable deposition at P_{VHF} of 90 W is reflected by a high average

D_{corn}/D_{mid} value and huge scatter of D_{corn}/D_{mid} in individual cells.

Generally, the solar cells showing thickness inhomogeneity also suffer from the inhomogeneity in the structural composition, namely, different parts on the 10×10 cm^2 have different crystallinities. The variation of open circuit voltages of solar cells on one substrate evidently reflects the change in the crystallinity, which was confirmed by Raman scattering measurements. In the samples presented in this chapter which show structural inhomogeneity, the area close to the border of the 10×10 cm^2 substrates are typically more microcrystalline than the middle region. The variation in the crystallinity leads to a fluctuation of solar cell performance on the same substrate.

4.3.2 Structural, optical and electrical properties of solar cells

To compare the properties of the μc-Si:H solar cell absorber layers grown at different deposition conditions with different growth rates, it is essential to know the structural composition of the i-layer. As has been suggested above considering the results of the solar cell J-V parameters (Figs. 4.14 & 4.17), the variation of power and flow under hphP conditions shifts the μc-Si:H/a-Si:H transition considerably to different silane concentration SC. This shall be confirmed in the following through Raman scattering experiments performed directly on the solar cells. Knowing the I^{RS}_{C488} values allows a comparison between solar cells prepared at similar crystalline volume fraction but under different conditions and at different deposition rates.

A further point of concern for solar cell materials prepared at high deposition rate is that the i-layer absorber material might exhibit a structure evolution along the growth axis. The frequently observed interface or incubation layer with pronounced porosity and amorphous phase could be expected to be more developed, i.e. thicker, at higher growth rates. This was investigated in the present research by Raman depth profile methods.

Finally, the influence of different deposition rates on the electronic and optical properties of the i-layer absorber material in the μc-Si:H solar cell is of interest. The dark J-V characteristic and quantum efficiency measurements can be used to evaluate the absorber quality.

Raman scattering experiments and structure depth profiles

The I^{RS}_{C488} values of the solar cells presented in Fig.s 4.14&4.17 are shown in Fig. 4.21 as a function of SC. Note that Raman measurements were carried out on solar cells with amorphous n-layers removed by KOH etching. For the hphP 20 W and hphP 40 W series, only the optimum cells were measured. A decreasing i-layer crystallinity with increasing SC can be observed in each series. Depositions with or without shield around the cathode made no remarkable difference in the structure properties, when comparing the hphP 60 W to the hphP 100 sccm series. Although the μc-Si:H/a-Si:H transition occurs at different SC when different deposition conditions are applied, optimum cells, which can be found

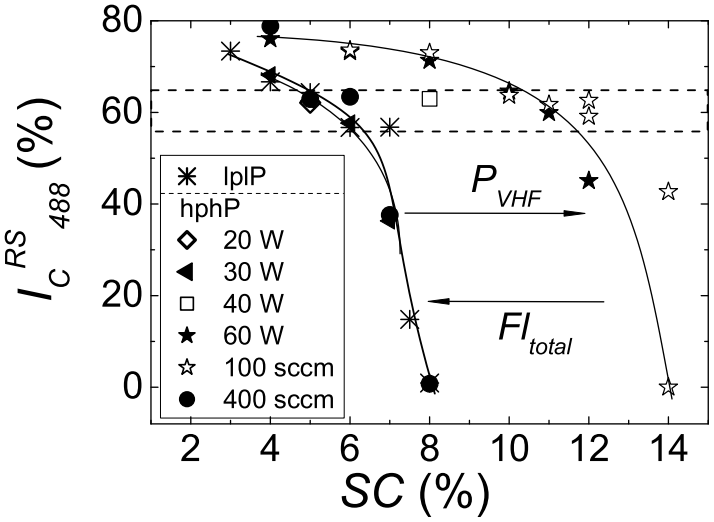

Figure 4.21: *Raman scattering intensity ratio with 488 nm excitation, I_{C488}^{RS}, of the lplP and hphP solar cells. Optimum solar cells in the SC series are found between the two dashed lines shown in the figure. Arrows in the figure indicate the shift of I_{C488}^{RS} by applying higher P_{VHF} or Fl_{total}. Lines are guides to the eyes.*

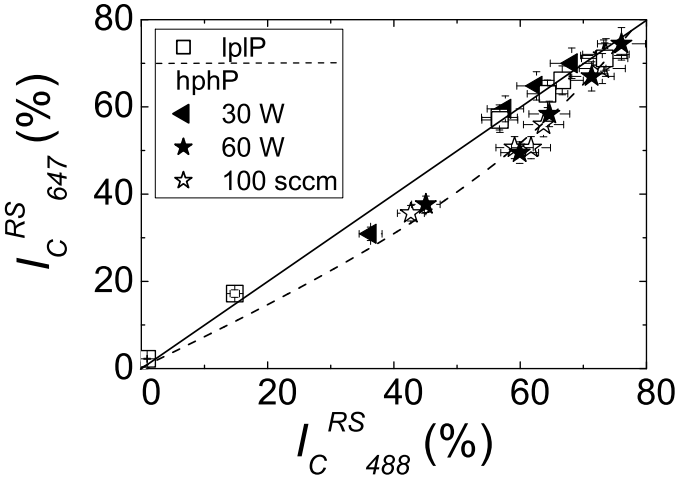

Figure 4.22: *I_{C647}^{RS} of the lplP and hphP solar cells plotted as a function of I_{C488}^{RS}. Lines are guides to the eyes.*

between the two dashed lines in this figure, are always obtained at similar crystallinity around 60 %. The results confirm the conclusions made from the J-V parameters: An increase of P_{VHF} shifts the μc-Si:H/a-Si:H transition to higher SC values; an increase of Fl_{total} shifts this transition to lower SC values. As R_D in all cases increase with SC, such shifts in the transition result in a shift of the deposition rates for optimum solar cells.

The structural development of three series of μc-Si:H solar cells, hphP 30 W, hphP 60W and hphP 100 sccm, prepared at medium and high deposition rate have been investigated by Raman scattering measurements with different excitation wavelengths. The results are compared with similar studies on solar cells with standard lplP absorber layers. Fig. 4.22 shows the I_C^{RS} values calculated from Raman spectra with 647 nm excitation (I_{C647}^{RS}), plotted against those with 488 nm (I_{C488}^{RS}). The deviation from the diagonal reflects the structure difference between the back of the i-layer near the etched-away n-layer and close to the p/i interface. The lplP samples deposited at low R_D show a very homogeneous distribution of the crystalline fraction along the growth direction, no matter if highly crystalline or almost amorphous. On the other hand, for the hphP solar cells close to the transition, the I_{C647}^{RS} values are significantly smaller than I_{C488}^{RS}, indicating a structural evolution during the i-layer growth. However, the resolution in growth direction of this method with different wavelengths is of course not very high. The I_{C647}^{RS} values, considered here to emphasize more

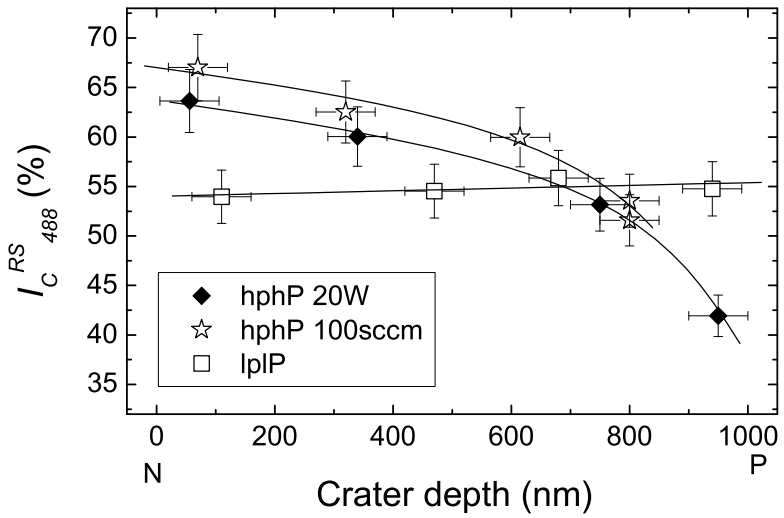

Figure 4.23: *The I_{C488}^{RS} at different depths in the* i*-layer show the structure development along the growth axis. Solar cells are optimum cells of three SC series deposited by lplP and hphP. For the 1 μm thick solar cells, crater depth of 0 and 1000 nm correspond to the* n *and* p*-layer position, respectively. Lines are guides to the eyes.*

the contribution close to the p/i interface, are still strongly affected by the top region.

In order to evaluate the crystallinity at different stages of the i-layer growth, Raman measurements with 488 nm excitation were done on craters with different depths which were etched into the solar cells by KOH. Fig. 4.23 shows the I^{RS}_{C488} at different depths measured on the optimum solar cells of selected series. As the solar cells are all about 1 μm thick, position 0 and 1000 on the x-axis corresponds to the position of the n and p-layer, respectively. Consistent with the "different wavelength" method, the lplP solar cell exhibits very similar I^{RS}_{C488} at different stages of growth, i.e. no structure evolution. For the hphP optimum solar cells, the structure development, already indicated in Fig. 4.22, is confirmed by this method. I^{RS}_{C488} differences of up to 20 % between the top and the bottom of the i-layer was observed. Deposited at relatively lower R_D, the hphP 20

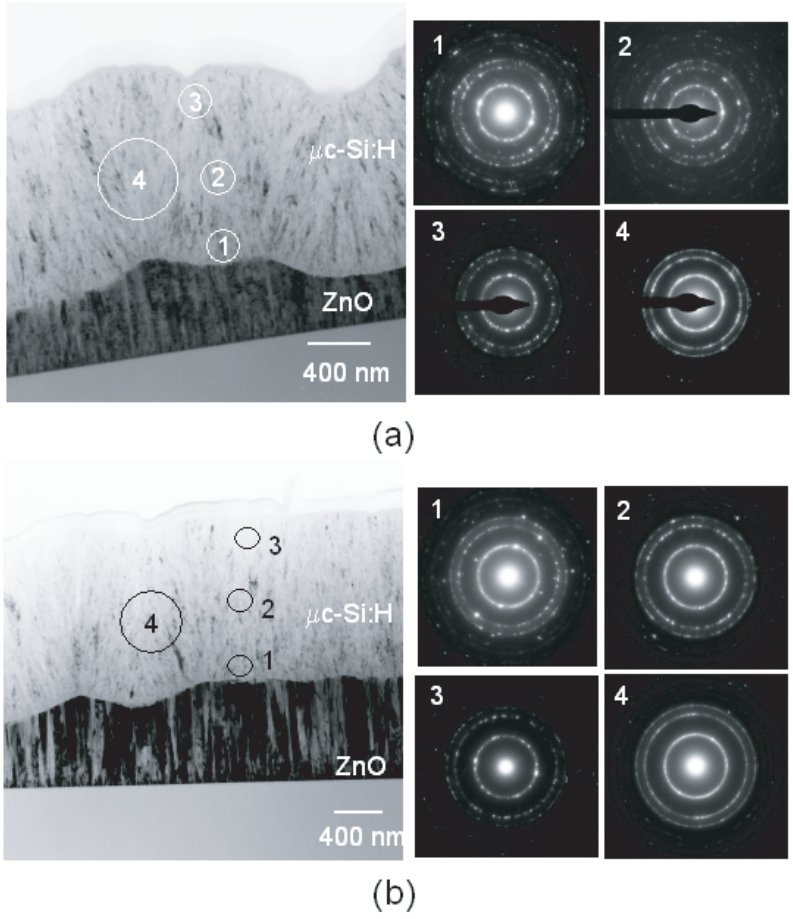

Figure 4.24: *The bright-field TEM images and selective electron diffraction patterns measured on two hphP solar cells. The numbered SAED patterns are taken from the corresponding regions in the TEM images. (a), hphP 20W, (b), hphP 100sccm.*

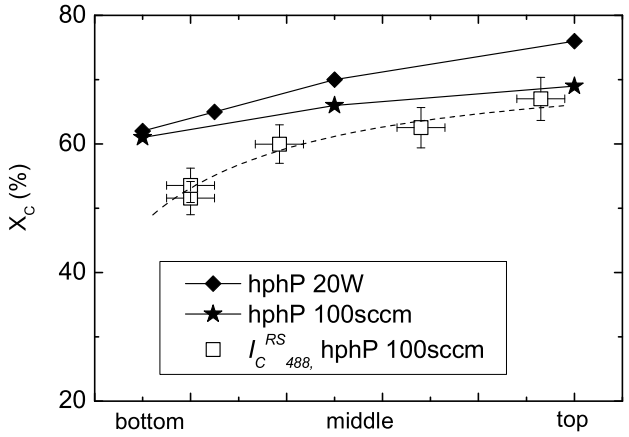

Figure 4.25: *X_c of the hphP 20 W and hphP 100sccm cells in the regions close to the bottom, middle and top. X_c are estimated from the ED patterns taken from the circular region with diameter of 200 nm. The I_{C488}^{RS} values of the hphP 100sccm series are also indicated here for comparison.*

W optimum cell indicates similar or even more pronounced structure development in the i-layer, probably due to the less microcrystalline p-layer.

Transmission electron microscopy

Transmission electron microscopy (TEM) were measured on the two solar cells showing pronounced structure development by the 'Raman structure depth profile' method Fig. 4.23. Selective area electron diffraction was also used to quantitatively investigate the structure development in the i-layer. Fig. 4.24 shows the bright-field images and the electron diffraction patterns of the two samples. The bright-field images are very similar to each other and no structure development can be directly observed. The crystallinity can be calculated from the ratio of the integrated power of the crystalline and amorphous contributions in azimuthally averaged Debye-Scherrer diffraction patterns [*see section 3.5.4 or Luysberg and Houben 2005*]. Fig. 4.25 indicates the crystallinity (X_c) of the three solar cells. Note that X_c is the average crystallinity of the region with diameter of 200 nm. Structure development can be seen in both samples from hphP 20W and hphP 100sccm series. The I_{C488}^{RS} values of the hphP 100sccm sample are also indicated in this figure for comparison. Although the X_c and I_{C488}^{RS} values are not the same in the whole range of depth, they have the same trends and confirm the structural development along the growth axis.

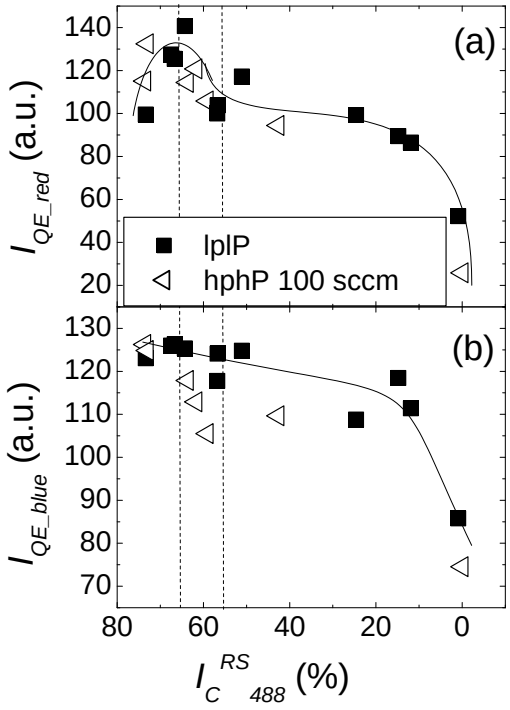

Figure 4.26: *The integrated intensities of the quantum efficiency, (a) I_{QE_red} and (b) I_{QE_blue}, in long and short wavelength region, respectively, of the lplP and hphP 100 sccm solar cells, plotted vs. the I_{C488}^{RS}. Lines are guides for the eyes.*

Quantum efficiency

In an attempt to study the influence of structure development on the carrier generation and transport, quantum efficiency measurements were performed on two solar cell series, lplP and hphP 100 sccm. As the short wavelength light will be fully absorbed in the p-layer and the i-layer close to the p/i interface, the short wavelength response can be in general considered as a criterion for the p-layer and p/i interface quality. Long wavelength light, with lower absorption coefficient for microcrystalline silicon, will be homogeneously absorbed in the whole 1 μm thick i-layer. The integrated intensity of QE between 300 and 520 nm, I_{QE_blue}, is used to evaluate the short wavelength response of solar cells, and that between 650 and 1100 nm, I_{QE_red}, for the long wavelength response. In Fig. 4.26 (a) and (b) are I_{QE_blue} and I_{QE_red} of the lplP and hphP 100 sccm series, plotted against I_{C488}^{RS}. Consistent with the highest J_{SC} in the region with intermediate crystallinity (Fig. 4.14 & 4.17), the long wavelength responses of both series show maximum values in this range (Fig. 4.26 (a)). At $I_{C488}^{RS} < 65\%$, the long wavelength response decreases to lower values with the increasing amorphous phase in the i-layer.

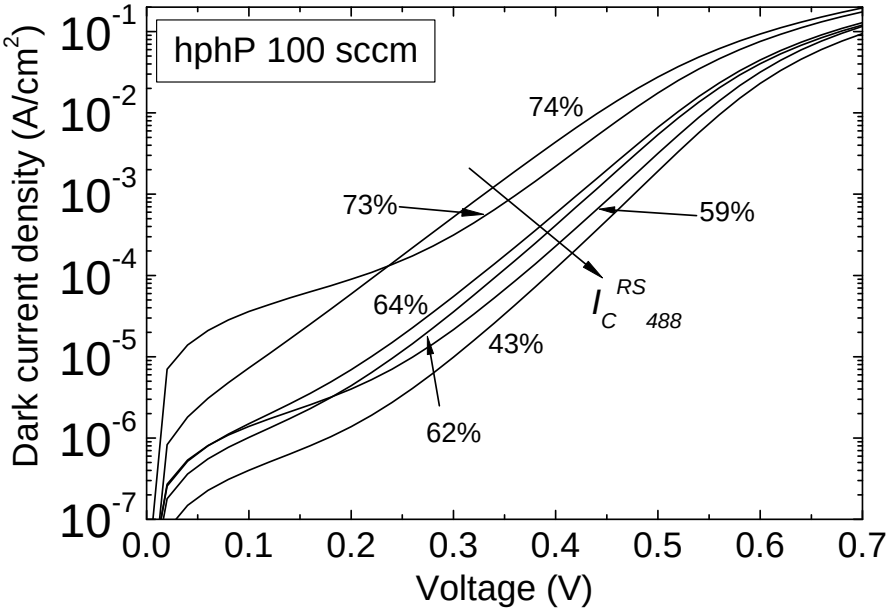

Figure 4.27: *The dark* J-V *curves of the solar cells in the hphP 100 sccm SC series. Numbers in the figure indicate* I_{C488}^{RS} *values of the corresponding samples.*

On the other hand, the blue light response shows pronounced difference between lplP and hphP solar cells. In lplP series, with the exception of the blue response at the highest I_{C488}^{RS} values, a higher I_{QE_blue} can be seen in almost the entire I_{C488}^{RS} range. This is also confirmed by the J-V measurements with blue light filter bg7 (not shown in this work). The differences in the short wavelength response could be attributed to a deteriorated p/i interface in high deposition rate material. The presence of a more amorphous or thicker incubation layer, as concluded from the depth profile methods, could lead to extraction problems for carriers generated near the p/i interface. However, the high FF and high V_{OC} values in these hphP optimum cells indicate that a moderate structure development in growth direction is not a sufficient reason for bad solar cell performance. Still, a further improvement of the solar cells by an adjustment of the crystallinity at the p/i interface could be possible.

Dark J-V measurements

A further possibility to obtain information about transport and recombination in the i-layers and at the interfaces of the p-i-n μc-Si:H solar cells are measurements of the dark J-V curves. In Fig. 4.27, the dark J-V curves of the solar cells of the hphP 100 sccm

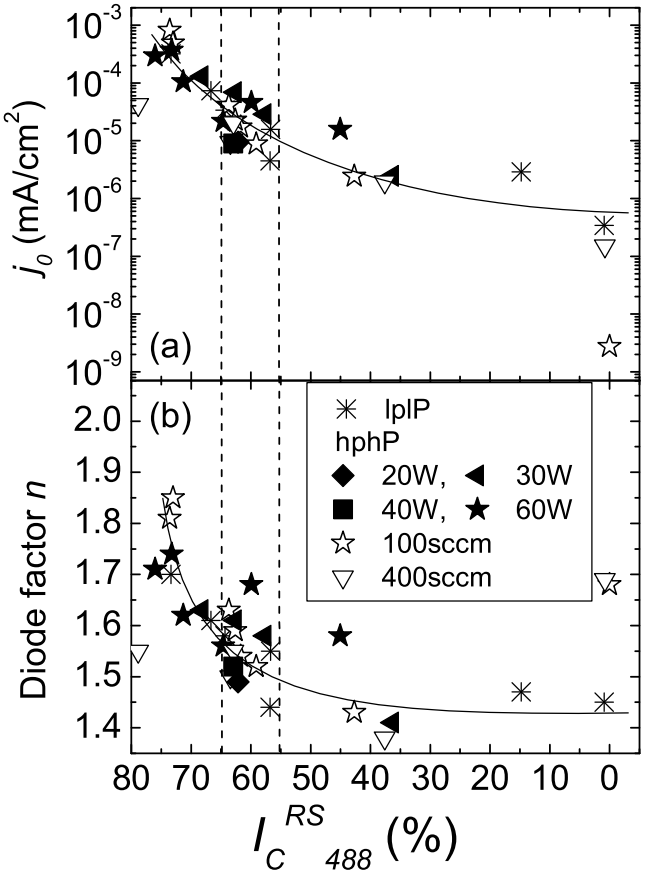

Figure 4.28: *(a) Saturation current density j_0 and (b) diode factor* n *of the solar cells deposited by lplP and hphP, plotted as a function of I_{C488}^{RS}. Optimum cells in different series are generally found between the two dashed lines in the figure. Lines are guides to the eyes.*

series are shown exemplarily. With the decrease of I_{C488}^{RS}, a systematic shift of the curves to lower current densities can be observed, which can also be found in all other SC series of Table 4.1. According to the simple p-n diode theory, if the validity of its application to μc-Si:H solar cells is assumed, the decrease in the current density with decreasing I_{C488}^{RS} qualitatively explains the increase of V_{OC}. Besides the shift of the curves, a change of the slope in the exponential range is also observed. The diode factor n and saturation current density j_0 are calculated from the fitting of exponential part of the dark J-V curves to the diode equation $j_{dark} = j_0 \cdot [\exp(\mathrm{eV}/n\mathrm{kT})\text{-}1]$, where shunt and series resistances have minor influence on the dark current density. The results are plotted for various solar cell series

prepared at different deposition conditions vs. I_{C488}^{RS} in Fig. 4.28. With the decrease of the i-layer crystallinity, the diode factor n decreases from a value of about 1.85 at high I_{C488}^{RS} to about 1.4 at low crystalline volume fraction. However, the values of n and j_0 at constant I_{C488}^{RS} show no systematic dependence on the deposition conditions or R_D and show no clear trend with the change of deposition parameters. This is consistent with the previous observation that the optimum cell performance is almost independent of R_D and deposition conditions.

4.3.3 Thickness dependence

Solar cell performance depends greatly on the i-layer thickness. An i-layer thickness series can help to find out the optimum cells with highest efficiency. In addition, the study of thickness dependent cell performance can help to understand the charge carrier transport. The illuminated and dark J-V characteristics of solar cells with optimum i-layer will be shown in the following section as a function of their i-layer thickness.

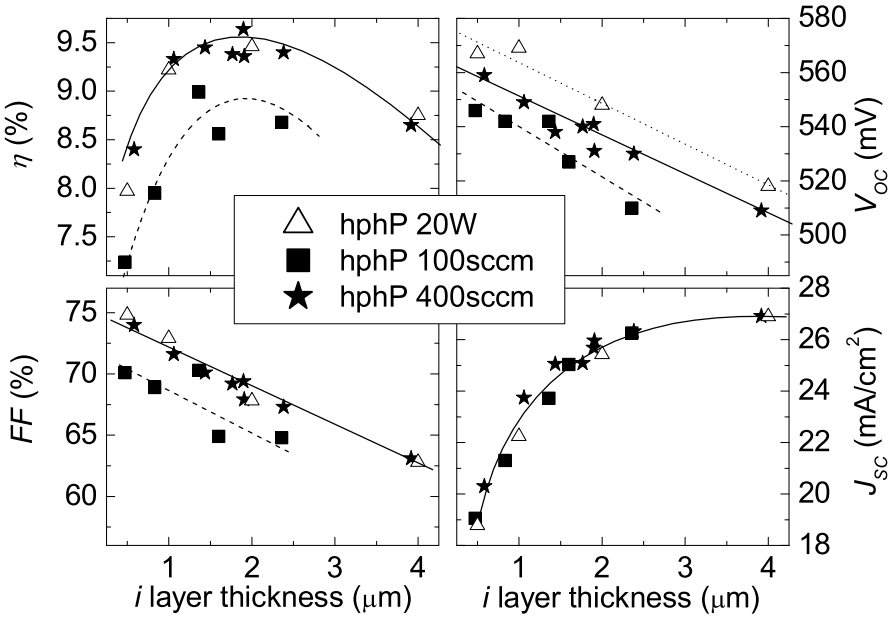

Figure 4.29: J-V *parameters of solar cells with optimum* i*-layer material deposited with different* P_{VHF} *and* Fl_{total} *are compared at different thickness. High efficiency solar cell can be obtained at a wide range of thickness between 1 and 2.5* μ*m. Lower* P_{VHF} *and high* Fl_{total} *result in better performance. Lines are guides to the eyes.*

J-V parameters and quantum efficiency

Microcrystalline silicon material deposited under hphP 20W, hphP 100sccm and hphP 400sccm conditions with optimized SC were used in this experiment. Fig. 4.29 shows the *J-V* parameters, η, V_{OC}, FF and J_{SC}, of the solar cells with *i*-layer thickness between 0.5 and 4 μm. In good agreement with previous results [*Vetterl 2001, Klein 2002*], V_{OC} and FF decrease almost linearly in all three series, suggesting reduced carrier extraction efficiency in the thick devices, probably due to the reduced electric field in the *i*-layer and longer carrier travel length. Thicker *i*-layers increases the light absorption and thus leads to a higher J_{SC}. At *i*-layer thickness below 2.5 μm, J_{SC} increase sharply with increasing *i*-layer thickness and start to saturate at about 2.5 μm. Due to the combinative effect of these three parameters, the efficiencies reach a plateau between 1 and 2.5 μm in all three series. Note that highly reflective ZnO/Ag back contacts were used in all solar cells in this figure. J_{SC} depends mainly on the *i*-layer thickness and no difference can be found between the solar cells with different *i*-layer material. Compared with the series with hphP 100 sccm optimum material, hphP 20 W series deposited with lower P_{VHF} and hphP 400 sccm with higher Fl_{total} show higher V_{OC} and FF at the same thickness, leading to higher efficiency in the two series. These results are not consistent with our previous observations that solar cell performance is independence of the deposition conditions. The reason for

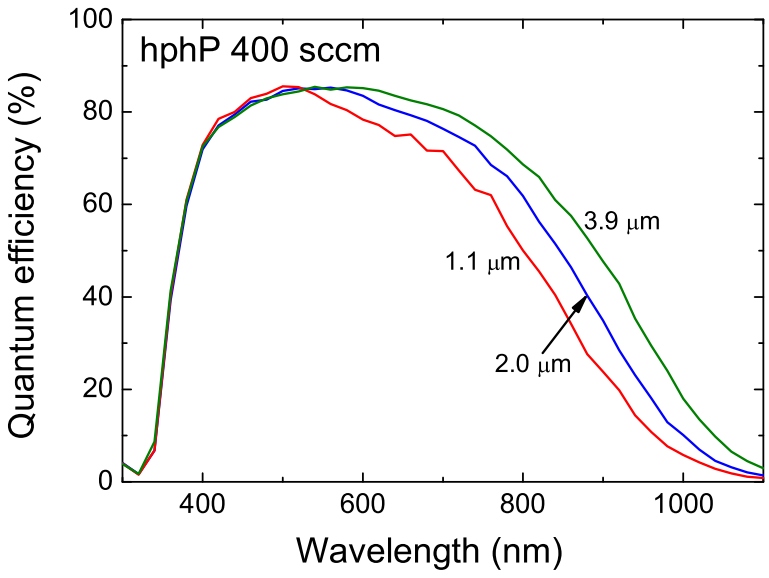

Figure 4.30: *Quantum efficiency of three solar cells with different* i*-layers thickness of 1.1, 1.9 and 3.9 μm. The* i*-layers were deposited by hphP 400 sccm with optimized SC of 6 %.*

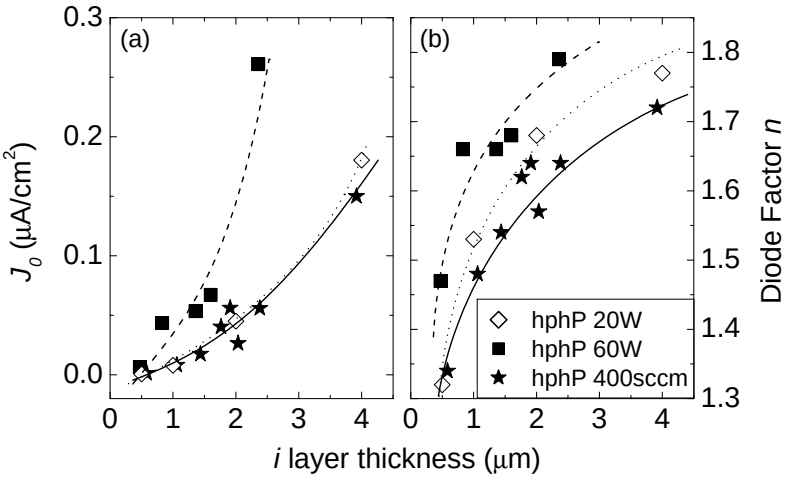

Figure 4.31: *(a), saturation current density j_0 and (b), diode factor* n *of the solar cells with different i-layer thickness (same as in Fig. 4.29). Lines are guides to the eye.*

this discrepancy is not clear. These three series were not fabricated at the same period of time. The run-to-run reproducibility of the deposition system can be a possible reason.

To give more detailed information on the increased J_{SC} with the thickness, quantum efficiency (QE) measurements were conducted on three cells from the hphP 400 sccm series with i-layer thickness of 1.1, 1.9 and 3.9 μm. QE measurements were carried out under short-circuit conditions. The QE curves are shown in Fig. 4.30. The improved p-layers result in exceptionally good short wavelength light response. These three cells show very high quantum efficiency of ~73 % at the wavelength of 400 nm. Increased i-layer thickness from 1.1 to 3.9 μm slightly decreases the QE between 400 and 520 nm, but strongly enhances the long wavelength light response, leading to higher J_{SC} in thicker solar cells. The simultaneous decrease of V_{OC} and FF suggests that part of the enhancement in J_{SC} may be compensated by the reduced carrier extraction, and therefore, there exists an upper limit for the improvement of J_{SC} by increasing the thickness [*Vetterl 2001a*].

Dark *J-V* measurements

Similar to the previously researches [*Vetterl 2001, Klein 2002*], dark J-V curves shift to higher current level with the increasing thickness, accompanied by a steady decrease in the curve slope. To make an quantitative comparison between the solar cells with different i-layer material, the diode factor n and saturation current density j_0 is compared in Fig. 4.31 (a) and (b), respectively. The saturation current density j_0 increases by about two orders magnitude as the i-layer thickness increases from about 0.5 μm to 2.4 μm in the

hphP 100 sccm series and to 4 μm in the other two. These results quantitatively explain the reduced V_{OC} in the thick solar cells. The solar cells in the hphP 20 W and hphP 400 sccm series show similar j_0 at similar i-layer thickness. Consistent with the lower V_{OC} at constant thickness, higher j_0 values are found in the hphP 100 sccm series. Similar to j_0, diode factor n also increases with the i-layer thickness in all three series. At similar thickness, diode factor R are higher in solar cells in hphP 100 sccm than in the other two series.

According to the diode theory [*Brammer and Stiebig 2003, Brammer and stiebig 2005*], j_0 of a μc-Si:H p-i-n solar cells depends strongly on the i-layer thickness and deep defect density. The higher j_0 values in the hphP 100 sccm series cells indicate inferior i-layer quality, in good agreement with the illuminated J-V measurement results. In addition, higher diode factor n value in a p-i-n diode suggests that the recombination in the bulk i-layer play a more important role in the total recombination in the device. Thicker i-layer reduces the electric field strength across the i-layer and and increases the mean travel length of the charge carriers, and thus enhances the bulk recombination. This is reflected by the higher diode factor values. Higher defect density in the hphP 100 sccm series can be deduced from the higher j_0, with respect to the other two series with similar crystallinity and the same thickness. Higher diode factor n values in hphP 100 sccm series, suggesting stronger bulk recombination, are consistent with relatively low i-layer quality. The reason for the higher n values in the hphP 20 W series, as compared to the hphP 400 sccm series, is not well understood. The less high-energy ion bombardment on the p-layers and p/i interface as a result of the lower P_{VHF} may be a possible reason [*Mai 2006*].

4.3.4 High efficiency solar cells and modules

Annealing the solar cells up to 2 hours increased efficiencies further for the samples in Fig. 4.29. The J-V curves of the optimum solar cell from the hphP 100 sccm and hphP 400 sccm series are shown in Fig. 4.32. The hphP 100 sccm cell is 1.4 μm thick and deposited at R_D of 1.2 nm/s, showing an efficiency of 9.2 %. Probably due to the good quality i-layer, the hphP 400 sccm cell maintains high performance at the thickness of 1.9 μm, leading to a higher J_{SC} of 25.7 mA/cm^{-2}. As the two solar cells have very similar V_{OC} and FF, the higher J_{SC} in the hphP 400 sccm cell results in higher efficiency of 9.8 %. The hphP 400 sccm cell was deposited at a slightly lower R_D of 1.1 nm/s.

This high growth rate material was also incorporated into modules. A single junction mini-module with an aperture area of 8×8 cm^2 was made with the hphP 400 sccm optimum i-layer material and achieved an efficiency of 7.9 %. A module with the optimum material of hphP 20 W series shows a higher efficiency of 8.8 % due to the better homogeneity. Fig. 4.33 shows the J-V and quantum efficiency curves of this module. The 1.6 μm i-layer was deposited by hphP 20 W at about 0.6 nm/s.

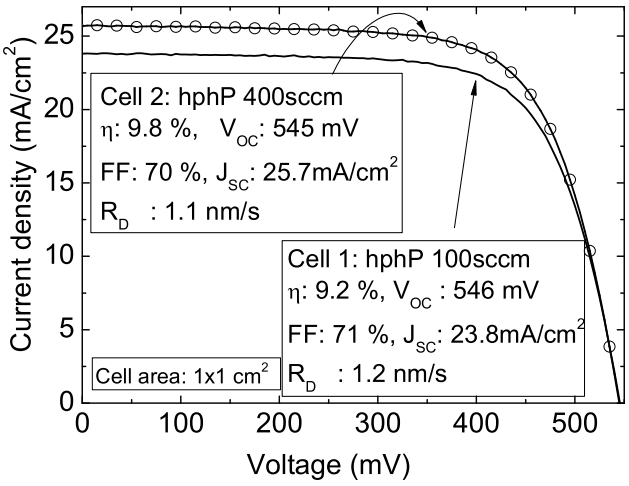

Figure 4.32: *High efficiency solar cells deposited under hphP conditions with optimized* i-*layer thickness and ZnO/Ag back contacts. Cell 1: hphP 100 sccm, SC = 11 %, thickness = 1.4 μm. Cell 2: hphP 400 sccm, SC = 6 %, thickness = 1.9 μm.*

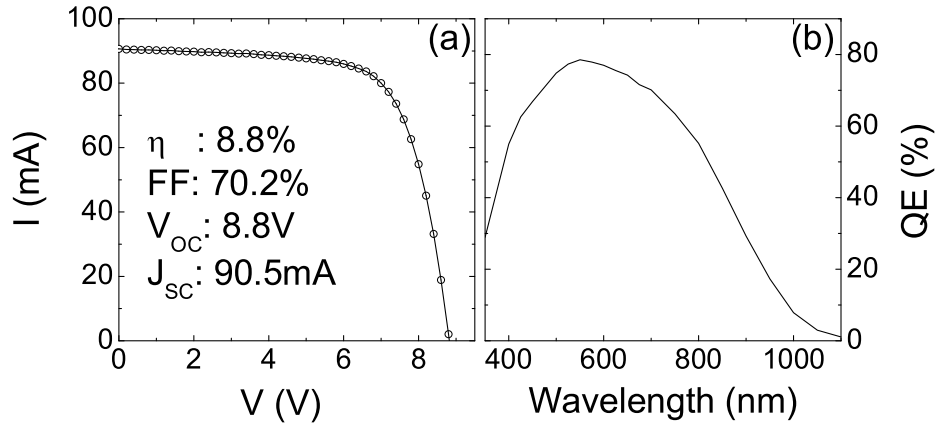

Figure 4.33: *(a),* J-V *curve of a μc-Si:H single junction module with 1.6 μm* i-*layer deposited by hphP 20 W. (b), Quantum efficiency at different wavelength of this sample. Aperture area: 8×8 cm^2.*

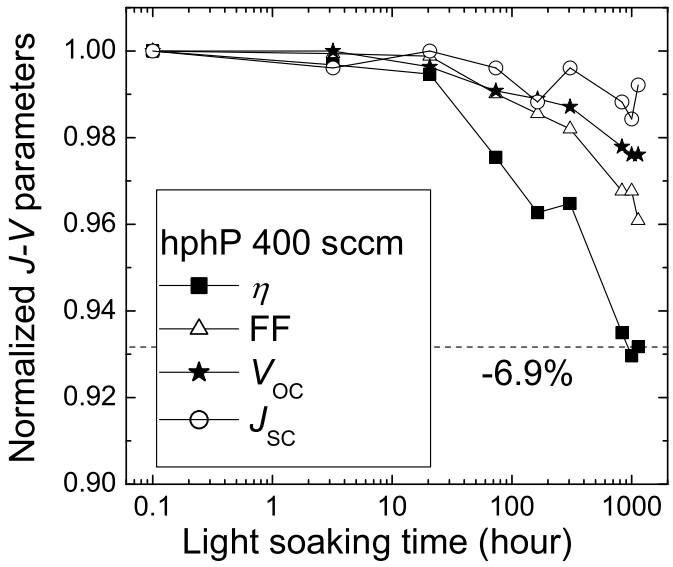

Figure 4.34: J-V *characteristics, η, V_{OC}, FF and J_{SC}, of the hphP 400 sccm optimum cell (the same as in Fig. 4.32) as a function of light soaking time. Data are normalized to the initial values.*

4.3.5 Stability

Post-deposition oxygen incorporation up to several at.% was observed in our hphP films with I^{RS}_{C488} above 60 % (see section 4.2.3). In addition, instability has been observed in the solar cells with high crystallinity after storage or treatments in air and water [*Yan 2002, Matsui 2004, Sendova-Vassileva 2004*]. Thus, it is necessary to investigate the ambient stability in the solar cells with such hphP material. The lplP and hphP cells deposited with different parameters were re-measured after at least 6 months exposure to air without illumination. Opposite to the noticeable oxygen incorporation in many hphP films, just one single sample in the hphP 60 W series with high I^{RS}_{C488} of 75 % degraded in this time period. The protection from the amorphous *n*-layers and silver back contact may help to reduce the atmospheric in-diffusion.

Prolonged AM1.5 light soaking was conducted on the hphP 400 sccm optimum cell (the same as in Fig. 4.32), which showed an initial efficiency of 9.8 % and an I^{RS}_{CR488} of 58 %. Fig. 4.34 shows its normalized *J-V* parameters as a function of the increasing light soaking time. *J-V* parameters were almost unchanged in the first 100 hours. The FF and V_{OC} started to decrease afterwards and after 1136 hours they reached 96 % and 98 % of the initial (annealed) values, respectively. Compared to FF and V_{OC}, J_{SC} is more stable upon the light soaking and only decrease by about 1 % in the end. With the reduced V_{OC}, FF

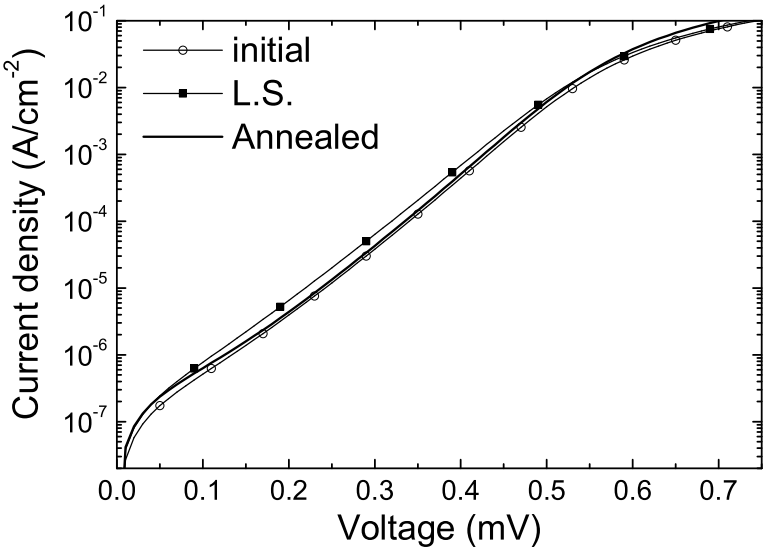

Figure 4.35: *Dark* J-V *curves before degradation, after 1136 hours light soaking and after annealing.*

and J_{SC}, solar cell efficiency decreases to 93.1 % of the initial value.

The relatively stable J_{SC} in this sample suggests that the overall performance degradation can not be fully attributed to deterioration of solar cell back contact after the prolonged illumination. Furthermore, 1 hour annealing at 160 °C after light soaking recovered the efficiency to some extent. This in return suggests that the efficiency degradation at least partly resulted from the light-induced defect formation. Dark J-V measurements were carried out on this sample before degradation, after 1136 hours of light soaking and after annealing. Compared to the initial state, the dark current density increased slightly after light soaking (Fig. 4.35). This quantitatively explains the decreased V_{OC}. One hour annealing almost recovered the enhanced dark current density. These results suggest that the degradation in the solar cell performance is related to the light-induced meta-stability.

4.4 Discussion

High quality material and high efficiency solar cells have been deposited at high deposition rate by the combination of VHF discharge excitation with high process pressure and power. Presumably, this achievement was made possible by effective dissociation of the process gases while keeping damage through high-energy ion bombardment at a low level. In the following, the influences of deposition parameters on the deposition precess,

material and device quality will be discussed.

4.4.1 Microcrystalline silicon films deposited at high rate

Compared to the samples deposited under conventional lplP conditions, μc-Si:H films deposited with hphP at high R_D show similar high material quality. High photosensitivity and low sub-gap absorption were found in films close to the transition from μc-Si:H to a-Si:H growth, indicating good applicability to thin film silicon solar cells. This was confirmed by the high efficiency in the solar cells with hphP absorbers.

Although similar in a number of aspects, μc-Si:H films deposited with hphP and lplP also have distinct differences. Above all, a more pronounced structure evolution along the growth axis was found in hphP films. This was confirmed by the Raman and TEM measurements. For a laser line of 488 nm wavelength, ~90 % of the Raman signal originates from the top 20 nm of the sample (see Table 3.1). That is to say, I^{RS}_{CR488} may largely overestimate the average crystallinity in the films, if a thick incubation layer is present in the films or solar cells. This makes the data evaluation and comparison somewhat problematic, especially for the parameters determined from the whole thickness. Let's take the microstructure factor for example. Microcrystalline silicon films deposited with hphP show slightly higher C_H and smaller R at $I^{RS}_{C488} < 65$ % (see Fig. 4.7). Microstructure factor R is regarded as the criterion for the porosity of a-Si:H [*Wagner and Beyer 1983*]. If this hypothesis is also valid for μc-Si:H, it is not in good agreement with the post-deposition Oxygen uptake in our samples. As can be seen, hphP samples with $I^{RS}_{C488} > 60$ % exhibit strong post-deposition oxygen uptake, compared to the lplP films with similar R values (Fig. 4.9). If the the pronounced structure development in the hphP films can be the possible explanation for this discrepancy: due to the high R_D, μc-Si:H top layer in the hphP film is porous and thus results in oxygen molecules and humidity adsorption after prolonged air exposure. As most of the Raman signal are contributed from the top layer of our 500 nm thick films, I^{RS}_{C488} values are mainly determined by the top layer crystallinity. While at the same time, the amorphous incubation layer, which is thicker in hphP films but still almost invisible in the Raman measurements with a short excitation wavelength of 488 nm, leads to a smaller average microstructure factor R and higher C_H. Similarly, the difference in the structure development in the hphP and lplP material also impairs the fine comparison of other parameters, such as conductivity etc.

Grown on microcrystalline p-layers, μc-Si:H i-layers in solar cells show less pronounced structure development as compared to the μc-Si:H films on glass substrates. Although structure evolution along the growth axis still occurs in some cells (Fig. 4.22), the i-layer growth is much more homogeneous than the films with similar I^{RS}_{C488}. Knowledge acquired from the investigations in μc-Si:H films may not be easily applied to their counterparts in the solar cells. Therefore, for fabricating a thin microcrystalline seed layer on glass, simulating the p-layers in solar cells, is important for the material characterizations on various substrates [*Vetterl 2003, Ross 2005*].

4.4.2 High rate deposition process and solar cell quality

Like in previous reports[*Vetterl 2000, Klein 2002, Roschek 2002*], it was found that optimum solar cells, no matter if deposited with hphP or lplP, were always obtained close to the transition from highly crystalline to the amorphous growth. These results demonstrate the importance to investigate the entire structure composition range from highly crystalline to amorphous to find the deposition parameters for the optimum phase mixture (OPM) absorber material while exploring a new deposition regime.

In the following, the influence of the deposition parameters under VHF-hphP conditions on the shift of the crystalline-to-amorphous growth conditions shall be discussed. An illustrative diagram, which considers the ratio of hydrogen over silane radicals as major parameter, explains the shift of the region for growth of OPM material. Further, the influence of the high deposition rate processes on the material structure and the resulting solar cell performance shall be discussed.

Structure adjustment for optimum phase mixture μc-Si:H materials

As a possible solution for high growth conditions of μc-Si:H without damage to the surface layer, the high pressure depletion method was proposed. [*Kondo 2000, Guo 1998*] In this approach, the application of high discharge power is used to decompose most of the silane in initial reactions of type,

$$SiH_4 \rightarrow SiH_x + (4-x)H. \tag{4.1}$$

Under silane depletion condition, the reaction

$$SiH_4 + H \rightarrow SiH_3 + H_2 \tag{4.2}$$

where silane molecules annihilate atomic hydrogen, will be suppressed and a high atomic hydrogen density is maintained. High working pressure, which is much higher than the several ten Pa, typically used in the conventional RF- or VHF-PECVD techniques for μc-Si:H growth, provides sufficient silane molecules and prevents detrimental ion damage. One of the consequences, when working under silane depletion conditions, is that one would expect little increase in the deposition rate with an increase in discharge power.

With the results of the present report the success of this approach can be confirmed. The results indicate "silane depletion", at least to some extent, although the term "depletion" is somewhat ambiguous. The upper limit of silane utilization can be varied by other deposition parameters, such as electrode distance and pressure. Thus, the increases of R_D with an increase of electrode distance and the pressure (Fig. 4.13) agree with the assumption of silane depletion. With higher pressure, the total amount of silane in the reaction zone is increased. With higher electrode distance, the volume of the reaction zone between the electrodes is increased. In both cases more silane precursor gas is available to overcome the depletion and obtain a higher silane utilization upper limit.

From the shift of the microcrystalline to amorphous growth conditions upon a variation of the process parameters, the author proposes that a proper ratio of atomic H over SiH_x (x = 0, 1, 2 or 3) should be maintained for the OPM material growth. Note that the contribution to the growth from individual kind of radicals and ions, such as SiH, SiH_2 or SiH_3, has long been discussed [*Perrin 1991, Bruno 1995, and references therein*] and will not be elaborated on here. Let us first look at the influence of P_{VHF}, which is visualized in the schematic diagram in Fig. 4.36 (a). At low P_{VHF}, a certain H/SiH_x ratio for the OPM material growth is established by the choice of SC. Higher P_{VHF} cannot produce more silicon-related precursors, due to the silane depletion in the whole investigated SC range (Fig. 4.13). But it will increase the atomic H density further, resulting in higher H/SiH_x ratio. This effect does not lead to higher R_D, but higher crystallinity in the i-layer (confirmed by the results of Fig. 4.13 and Fig. 4.21). In order to compensate the increased hydrogen radical density and maintain the required H/SiH_x ratio for the OPM material growth, more silane has to be added to the plasma, leading to higher R_D for the optimum solar cell.

Fig. 4.36 (b) illustrates the situation for different Fl_{total}, which fits well into this picture, too. When a higher Fl_{total} is applied to an established OPM material growth condition, higher R_D will be generally observed because of higher silane supply (see Fig. 4.16). But the increasing SiH_x radical density and the possible atomic H annihilation effect by the excessive silane molecules results in a lower H/SiH_x ratio, leading to lower i-layer crystallinity. This is confirmed by the Raman scattering measurements (Fig. 4.21) and by the J-V parameters (Fig. 4.17) of the solar cells deposited with different Fl_{total}. In order to maintain the proper ratio of atomic H over SiH_x, one has to go to lower SC at higher Fl_{total}. Note that Fig. 4.36 is just an illustrative picture and the rectangle areas do not represent the true radical densities.

Similar relation between material crystalline volume fraction and precursor ratio can also be deduced from the optical emission of the plasma. The emission intensities of Si* or SiH* were proposed proportional to the growth rate of a-Si:H and μc-Si:H under certain conditions [*Matsuda 1983a, Howling 1992, Keppner 1999, Guo 1998, Rath 2004*]. In addition, the H_α intensity was found suitable as a measure for the atomic hydrogen density [*Heintze 1993a*]. A monotonic decrease of crystallinity with increasing Si^*/H_α or SiH^*/H_α was found while varying working pressure or discharge power [*Guo 1998, Keppner 1999*]. Furthermore, it was found that, if the H_α/Si* ratio is higher than a threshold value, the transition from amorphous to microcrystalline growth occurs, irrespective of the ion energy and deposition rate [*Rath 2004*]. All these findings support the hypothesis that maintaining a proper H/SiH_x ratio is critical for the optimum phase mixture material growth. The threshold value of H/SiH_x ratio may be different under different conditions. A further investigation about the H/SiH_x ratio for the crystalline growth under various condition is of great interest.

As the variation of SC is the most simple and straightforward method to adjust the

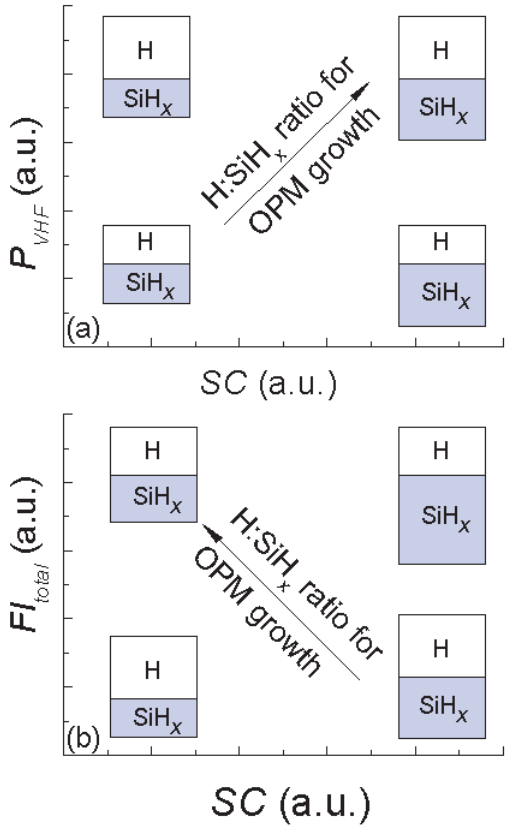

Figure 4.36: *Schematic diagrams of the amount of hydrogen and silane radicals (arbitrary units) (a) in the SC - P_{VHF} parameter space and (b) in Fl_{total} - SC parameter space under hphP conditions. To maintain the necessary H/SiH_x ratio for growth of optimum phase mixture material, the SC has to be adjusted when varying P_{VHF} and Fl_{total}. Areas of rectangles do not represent the exact radical densities.*

H/SiH_x ratio, it is considered mandatory for material and device optimization.

Solar cell performance and *i*-layer properties

This chapter has studied the transport properties of μc-Si:H solar cells, prepared by different techniques and at different deposition rates by dark *J-V* and quantum efficiency measurements and correlated these with the results from Raman and Raman "depth profile" measurements. Based on various earlier reports about high deposition rate processes for intrinsic μc-Si:H absorber layers, including work in the hphP regime [*Rech 2003, Kondo 2003, Niikura 2004, Rath 2003*], one could have expected, that the high rate growth process has negative influences on the material quality, likely due to the high energy ion bombardment resulting from the required high discharge power. In addition, structure

inhomogeneity along the growth axis can be another negative effect induced by the high deposition rate. The results from the structure depth profile clearly show the existence of such a structure in-homogeneity in hphP material at high growth rate. Surprisingly this structure in-homogeneity is not reflected in an overall reduced solar cell efficiency under illumination as compared with low deposition rate material (Fig. 4.19), but only in a lower short wavelength response (Fig. 4.26). Also the evaluations of the dark J-V curves do neither indicate differences in the total defect density nor differences in the interface recombination between solar cells prepared with different regimes. Assuming the validity of the theory for p-n diodes as applied to μc-Si:H solar cells, similar defect densities can be deduced from the similar j_0 in the solar cells with similar crystallinity and thickness (Fig. 4.28 (a)). Thus, a similar diode factor n in the solar cells with the same crystallinity (in Fig. 4.28 (b)) suggests no noticeable difference in the recombination at the interface. Detailed discussion about the j_0 and n in μc-Si:H p-i-n diodes can be found in Ref. [*Brammer and Stiebig 2005*]. Further support for similar bulk layer properties between high (hphP) and low (lplP) deposition rate material is given by the very similar I_{QE_red} values in the quantum efficiency measurements for both types of solar cells.

Another similarity between the lplP and hphP material is that the optimum solar cells are always obtained at the μc-Si:H/a-Si:H transition. In good agreement with previous results that higher defect density was found in the highly crystalline material [*Finger 2002, Baia Neto 2002*], the reduced I_{QE_red} (Fig. 4.26 (a)), the high diode factors $n >$ 1.7 and the high dark saturation current densities (Fig. 4.28) at the highest crystalline volume fractions suggest carrier extraction problems in the devices. In addition to the higher V_{OC} in the solar cells with OPM material, higher FF in such cells suggests lower bulk recombination and better carrier extraction, as compared to the highly crystalline samples.

On the other hand, the considerable difference in blue light response I_{QE_blue} does indicate a difference at the p/i interface in lplP and hphP solar cells with reduced carrier extraction from the interface-near region in hphP solar cells deposited at high R_D. However, the observed structure development may not be pronounced enough to deteriorate the carrier extraction in the bulk. The FF remains at high levels above 70 %, indicating good carrier extraction from the bulk in these cells.

In summary, the combination of high plasma excitation frequencies in PECVD together with high deposition pressure makes it possible to achieve high rate growth of OPM material without negative influence on the solar cell J-V parameters. All results suggest very good bulk layer properties with no indication for differences between high and low growth rate material. This allows high rate growth of high efficiency solar cells. However, there are clear indications for structure in-homogeneity and deteriorated p/i interfaces in the hphP material. This gives hope for even further improved solar cell performance at high deposition rate by reducing the structure development or improving the p/i interface.

4.5 Summary of this chapter

4.5.1 Material properties

Microcrystalline silicon material was deposited at high R_D by VHF-PECVD working at high pressure-high power. The structural, electrical and optical properties of the hphP material with different structural composition were investigated and compared with μc-Si:H films deposited under conventional low pressure-low power conditions. It is found that

- Device grade μc-Si:H material was achieved at high deposition rate above 1.0 nm/s by the combination of VHF and hphP.
- μc-Si:H films deposited with hphP and lplP are similar with respect to material properties, such as conductivity, optical absorption and H content and bonding structure.
- Compared to the lplP material with similar I^{RS}_{C488}, hphP material shows more pronounced structure evolution in the growth direction.
- With similar microstructure factor R at the same I^{RS}_{C488}, hphP material shows more severe post-deposition atmospheric in-diffusion.

4.5.2 μc-Si:H solar cells deposited at high rates

The influences of the deposition parameters and i-layer quality on the solar cell performance were investigated in this chapter. One can conclude that

- A very effective growth regime, using VHF-PECVD at high pressure and high power (hphP), for the deposition of μc-Si:H solar cell absorber layers with excellent quality at high deposition rates was identified.
- Under all deposition conditions used, highest solar cell efficiencies are obtained with optimum phase mixture (OPM) material grown close to the transition from highly crystalline to amorphous growth.
- Growth of OPM material is strongly determined by a proper H over SiH_x ratio in the gas phase. This ratio is most easily controlled by a variation of the silane concentration. Corresponding silane concentration series are considered mandatory for successful device optimization.
- The μc-Si:H material quality is found to be independent on the deposition rate up to 1.5 nm/s under VHF-PECVD hphP growth conditions in the investigated range in this work.
- A high efficiency of 9.8 % was obtained for a single junction p-i-n solar cell with the i-layer deposited at 1.1 nm/s. For a single junction module with aperture area of 8×8 cm^2, an efficiency of 8.8 % was achieved.

• The structure evolution along the growth axis was found in the high deposition rate material. Although without noticeable effect on the total solar cell efficiency, it deteriorates the blue light light response in the solar cells, indicating the potential for further optimization of the presented growth process and, thus, of the device performance.

• Optimum μc-Si:H solar cells deposited close to the transition region were found very stable against light soaking. After more than 1000 hours of AM1.5 illumination, only slight degradation below 7 % was found. Furthermore, no degradation was observed in these optimum cells deposited at high rates after long term storage in the air.

Chapter 5

μc-Si:H films and solar cells deposited by HWCVD and PECVD

PECVD has long been a widely-used deposition method for a-Si:H and μc-Si:H material and solar cells. In the recent decade, great effort has been made to improve the material quality and increase the deposition rate (as mentioned in the former chapter). High efficiencies over 9 % for the single junction μc-Si:H solar cells were achieved by a number of groups. At the same time, different growth regimes, working with high plasma excitation frequency and high pressure high power, were established to achieve high rate deposition [*Feitknecht 2003, Matsui 2004, Gordijn 2005, Kilper 2005*]. In Chapter 4, a high efficiency of 9.8 % was successfully realized for the single junction μc-Si:H solar cells in *p-i-n* configuration at a considerably high deposition rate over 1.0 nm/s by the combination of VHF and hphP. HWCVD is an alternative deposition method for high quality μc-Si:H material and solar cells. The renaissance of HWCVD commenced with the intensive work of Matsumura [*Matsumura 1989, Matsumura 1989a*], which showed that HWCVD was capable of providing high quality a-Si:H and a-Si:H based alloys. High efficiency a-Si:H solar cells were deposited at high rate of 1.65 nm/s [*Mahan 1998*], and a-Si:H material can be deposited at a very high R_D above 10 nm/s by HWCVD [*Mahan 2002*]. Deposition of μc-Si:H material and solar cells using HWCVD became a hot topic in the field in the recent years. Superior properties, such as large grain size, small microstructure factor and low defect density etc., were achieved in HWCVD μc-Si:H material [*Schropp 1997, Rath 1997, Alpuim 1999*], but a breakthrough in the solar cell efficiency was not made until the low substrate temperature deposition process was identified [*Klein 2002a*], benefiting from the sufficient hydrogen passivation of the grain boundaries. However, the low filament temperature in such deposition process, preventing the detrimental radiant heating from the hot filaments, significantly decreases the deposition rate.

Similar in a number of aspects, the material and solar cells deposited by PECVD and HWCVD also have many differences. High quality a-Si:H deposited by PECVD usually has about 10 at.% bonded hydrogen content [*Stutzmann 1989, Mahan 1991*], while a-

Si:H films deposited by HWCVD still maintain a low defect density and a narrow Urbach edge with much lower hydrogen content down to 2 % [*Mahan 1991*]. More pronounced differences were found in μc-Si:H solar cells. μc-Si:H solar cells deposited by PECVD show a poor performance as the open circuit voltage (V_{OC}) exceeds a value of the optimum cells (typically between 500 - 540 mV as can be found in literature *[Vetterl 2000, Roschek 2002]*), while solar cells deposited by HWCVD at low substrate temperature maintain high performance at a higher V_{OC} of up to 600 mV. A comparison of the structural, electrical and optical properties of the PECVD and HWCVD films and solar cells can help to reveal the origins of the above mentioned differences.

5.1 μc-Si:H films deposited by PECVD and HWCVD

μc-Si:H films deposited by PECVD are the same as those presented in Chapter 4 prepared either at low pressure, low power (lplP) or at high pressure, high power (hphP). The data of HWCVD samples was taken from the PhD thesis of S. Klein [*Klein 2004*]. Those samples were deposited at low filament temperature (T_f, 1650 °C) to prevent the detrimental radiant substrate heating. Two different gas pressures (p_{depo}), 3 and 5 Pa, were used. The substrate temperature was fixed at ∼220 °C by varying the heater temperature.

5.1.1 Raman spectroscopy

I^{RS}_{C488} were re-calculated for the HWCVD films with three Gaussian peaks fitted to the Raman spectra in the same way as used for the PECVD material. The values are systematically about 5 % smaller than those calculated by S. Klein in his PhD thesis [*Klein 2004*]. This is probably due to the different baseline subtraction methods.

Besides an easy tool to semi-quantitatively determine the crystallinity, the line width and peak frequency of the crystalline peak at ∼520 cm^{-1} of Raman spectra, associated with the transverse optical (TO) mode, can be used to characterize the lattice order of semiconductors [*Perkowitz 1993*]. In general, a narrower line width and a higher frequency of the TO peak of the crystalline component imply higher order of material or larger crystallite size [*Iqbal 1981, Richter 1981, Campbell and Fauchet 1986, Fauchet and Campbell 1990, Smit 2003*]. The full width at half maximums (FWHM) and the peak frequencies of the crystalline component, determined from the Raman spectra of the PECVD and HWCVD material after an amorphous reference spectrum is subtracted, are shown in Fig. 5.1. For the subtraction procedure, please see Appendix B. Although with remarkable scatter, clear trends can still be found. In the top set of the figure, a dashed line indicates the FWHM value of 11 cm^{-1}. As can be seen, almost all PECVD samples are located above the dashed line, while the HWCVD samples are found below. In good agreement with the results in the literature [*Iqbal 1981*], higher peak frequency are found in the samples with higher crystallinity (Fig. 5.1 (b)). However, in contrast to the obvious difference in the FWHM

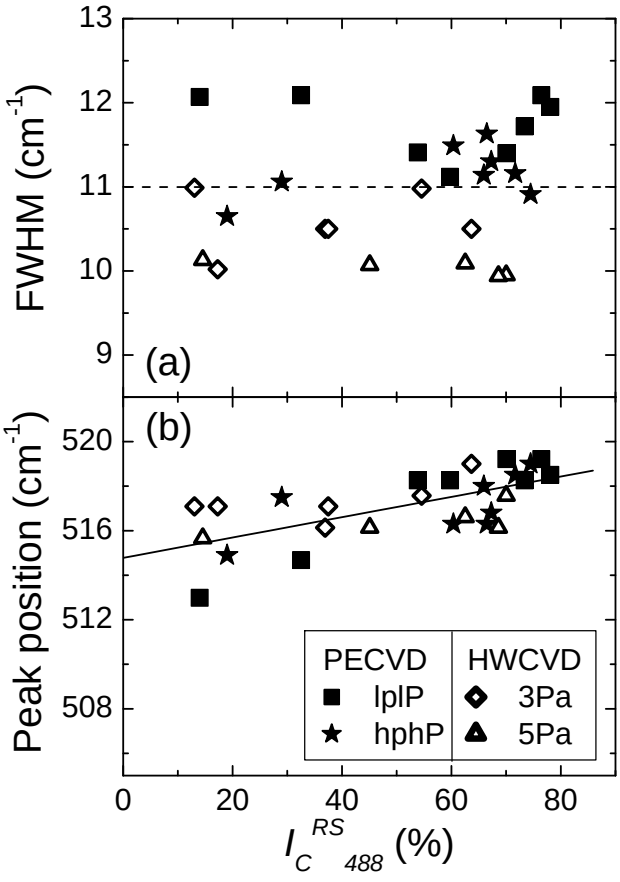

Figure 5.1: *(a), FWHM of the crystalline TO peak of the PECVD and HWCVD material at different I^{RS}_{C488}, (b), frequency of the peak position of the crystalline component.*

values, no clear difference can be seen between the PECVD and HWCVD samples.

5.1.2 Infrared spectroscopy

Passivating the dangling bond defects and reducing the intrinsic stress of the random network, bonded hydrogen atoms show strong influence on the electrical and optical properties of the material. In this section, the infrared spectroscopy measurements are used to investigate the bonded H content (C_H) and their bonding configuration. The microstructure factor R and C_H of the PECVD and HWCVD films are shown in Fig.5.2 as a function of I^{RS}_{C488}. C_H increases and microstructure factor R decreases with the increasing amorphous volume fraction, which is consistent with the previous findings [*Klein 2001, Lossen 2004*]. Deposited at almost 5 times higher R_D, the PECVD hphP series show slightly

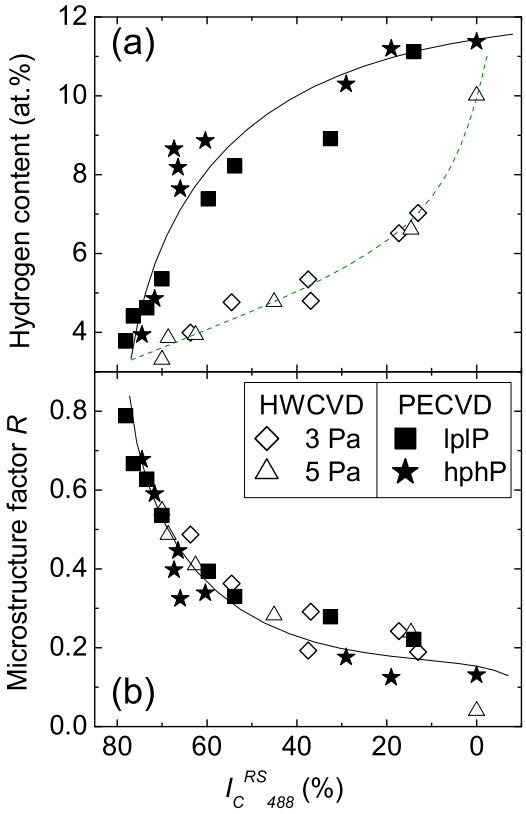

Figure 5.2: *(a), bonded H content of the HWCVD and PECVD films determined from the infrared absorption of the SiH wagging mode center at ∼640 cm^{-1}. (b), Microstructure factor R of the four material series.*

higher C_H than the lplP material with similar I_{C488}^{RS}. This has been stated in the former chapter. An important observation in this figure is the remarkably higher C_H in the two PECVD series, compared to the HWCVD material with similar structure composition. In the I_{C488}^{RS} region between 70 % and 20 %, C_H increases from about 4 % to 6 % in the two HWCVD series, while it increases from ∼5 % to 11 % in the two PECVD series. At the same time, the microstructure factor R was found to be very similar in the μc-Si:H material deposited by PECVD and HWCVD in the whole range of I_{C488}^{RS}.

5.1.3 Conductivity

Fig. 5.3 (a) shows the photo- and dark- conductivities (σ_{photo} and σ_{dark}, respectively) of the four series deposited with HWCVD and PECVD, plotted as a function of I_{C488}^{RS}. With the structure composition shifting from highly microcrystalline (at I_{C488}^{RS} of ∼80 %) to

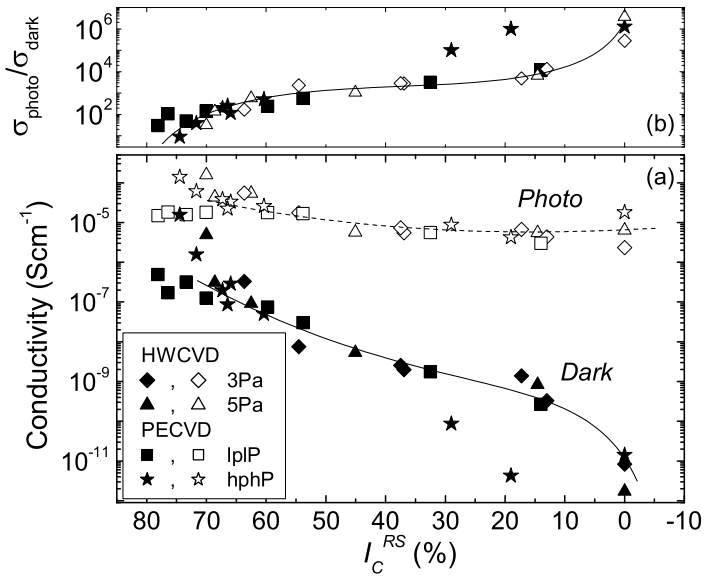

Figure 5.3: *(a), σ_{photo} and σ_{dark} of the PECVD and HWCVD material at different I^{RS}_{C488}, (b), photosensitivity of these samples.*

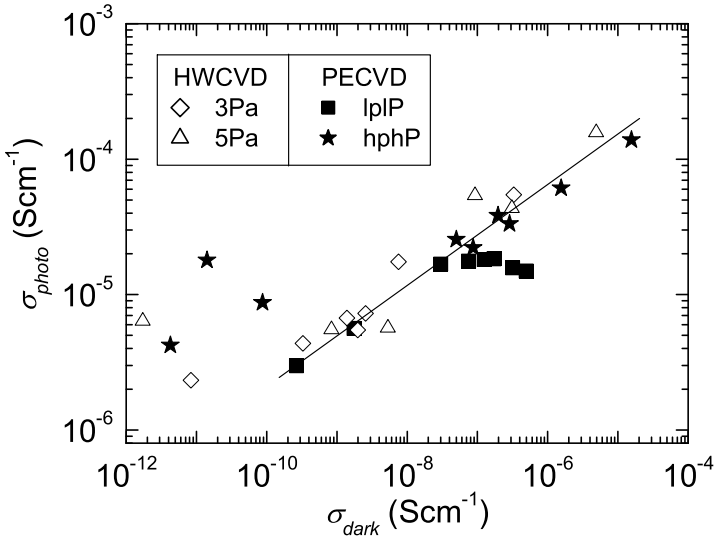

Figure 5.4: *σ_{photo} of the PECVD and HWCVD films plotted as a function of σ_{dark}.*

fully amorphous growth, σ_{dark} decrease by several orders of magnitude in all PECVD and HWCVD series, and photo-conductivities decrease by about a factor of ten. This results in an increase in photosensitivity ($\sigma_{photo}/\sigma_{dark}$) with decreasing crystallinity, as shown in Fig. 5.3 (b).

Although with distinct differences in the growth process, PECVD and HWCVD film show surprising similarities in σ_{photo}, σ_{dark} and photo-sensitivities in a wide range of I_{C488}^{RS}, as indicated by the two guidelines in Fig. 5.3 (b). The increased σ_{photo} and σ_{dark} at I_{C488}^{RS} $>$ 65 % found in PECVD hphP material can also be observed in the two HWCVD series.

Fig. 5.4 shows σ_{photo} as a function of σ_{dark}. Although there is considerable scatter, especially for the samples with low crystalline volume fraction, μc-Si:H films deposited by PECVD and HWCVD exhibit a similar relationship between σ_{photo} and σ_{dark}. Such correlation was previously established for a-Si:H [*Beyer and Hoheisel 1983*] and was postulated valid for the μc-Si:H material [*Finger 2002, Brüggemann and Main 1998*]. High σ_{photo} and high σ_{dark} are usually found in μc-Si:H with high crystallinity. According to the above literature, the higher defect density and/or impurity content, which can shift the Fermi-level to the conduction band and charge deep defects, enhance the σ_{photo} and σ_{dark} at the same time.

5.2 μc-Si:H solar cells deposited by PECVD and HWCVD

From the previous section, one can see that the PECVD and HWCVD material at constant I_{C488}^{RS} are very similar in the σ_{photo} and σ_{dark}, suggesting similar properties in the carrier generation, transport and recombination. However, an unambiguous and direct correlation between the material and solar cells is still not available. In addition, substrate and depth dependent growth of μc-Si:H and the complicate operating principles of the solar cells make it necessary to make a direct comparison between the PECVD and HWCVD solar cells. In our previous research [*Mai 2006*], the illuminated and dark *J-V* characteristics and spectral response of the PECVD and HWCVD cells were compared. In addition, it was proposed that the *i*-layer material deposited by PECVD or HWCVD is very similar to each other, and that a better p/i interface quality may be responsible for the differences in the solar cell performance. However, more systematic and precise studies, such as the characterization of structure development and p/i interface quality, are still necessary. For this purpose, two solar cell series, with the only difference in the *i*-layers deposited with HWCVD or PECVD, prepared on similar ZnO substrates, with similar doped layers and *i*-layer thickness were compared. The PECVD *i*-layers were deposited under lplP conditions with R_D at about 0.2 nm/s. A low substrate temperature process was used to deposit HWCVD *i*-layers with low T_f of 1650 °C and low p_{depo} of 3 Pa, resulting in T_S of about 180 °C. The deposition rate of HWCVD *i*-layer is about 0.1 nm/s. The *i*-layers are about 1.1 μm thick for all solar cells with standard deviation of about 10 %. R_D of PECVD *i*-layers were determined from the films deposited on glass substrates. This

somewhat underestimated the real R_D values on conductive ZnO substrates. This made the average thickness of PECVD solar cells about 5 % larger than that of the HWCVD cells. To separate the strong effect of the i-layer crystallinity on the V_{OC} values, the SC in both cases was varied to obtain solar cells with crystallinities covering the range from highly crystalline to fully amorphous.

5.2.1 *J-V* parameters versus V_{OC}

Fig. 5.5 shows the efficiency, fill factor (FF) and short circuit current density (J_{SC}) of the solar cells with i-layers deposited by PECVD and HWCVD, plotted as a function of V_{OC}. High efficiencies of ~8 % are obtained for the optimum solar cells in both series, indicating that both techniques are capable to provide high quality absorber material. In good agreement with our previous results [*Mai 2006*], PECVD and HWCVD cells are quite similar as V_{OC} is smaller than 550 mV. Efficiencies of PECVD cells decrease sharply as the V_{OC} exceed 550 mV, resulting from the deteriorated FF and J_{SC}. On the contrary,

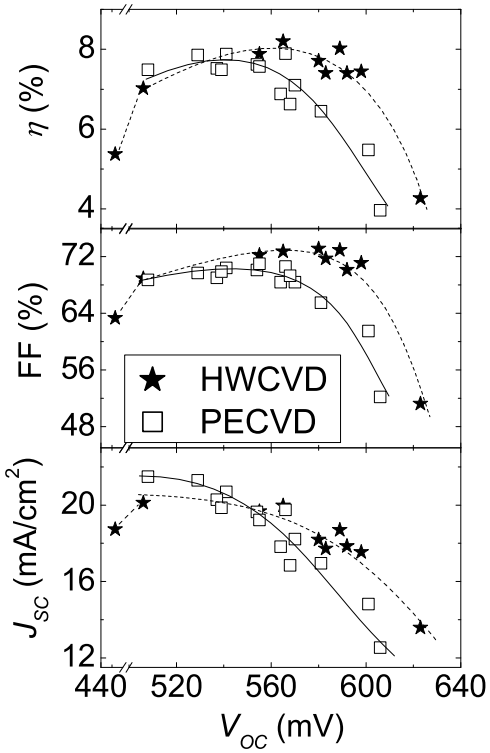

Figure 5.5: *Efficiency, FF and J_{SC} of the solar cells with* i*-layers deposited by PECVD and HWCVD, plotted as a function of V_{OC}. Lines are guides to the eye.*

the FF of HWCVD cells continues to increase with the increasing V_{OC} and maintains very high value at 598 mV. At the same time, the HWCVD cells show higher J_{SC} than the PECVD cells with the same V_{OC} at $V_{OC} > 550$ mV, although the J_{SC} decrease with the increasing V_{OC} in both series. As a result, high solar cell performance is still maintained in the HWCVD series at high V_{OC} close to 600 mV, indicating distinct difference from the sharp deterioration in the PECVD series. For example, a solar cell with V_{OC} of 589 mV shows an efficiency of 8.02 % and a FF of 72.9 %. Another HWCVD cell with V_{OC} up to 598 mV still show a high efficiency of 7.44 % and FF of 71.1 %. Note that all solar cells are with simple Ag back contacts.

5.2.2 *J-V* parameters versus I^{RS}_{C488}

Raman scattering measurement was conducted directly on the solar cells after the removal of the a-Si:H n-layers by KOH etching. Although the excitation laser used here with a wavelength of 488 nm can just show the structure properties of the top several hundred nm of the μc-Si:H i-layer (see section 3.1), a homogeneous growth in these two series of solar cells was confirmed by other methods later in this chapter. The normalized Raman spectra of the two series are indicated in Fig. 5.6. The TO peaks of the amorphous phase increase steadily with the increasing SC in the feedstock gases. Although the crystallinity is very sensitive to SC at the transition from μc-Si:H to amorphous growth, especially in the PECVD process, there is no expected difficulty in obtaining a wanted crystallinity if

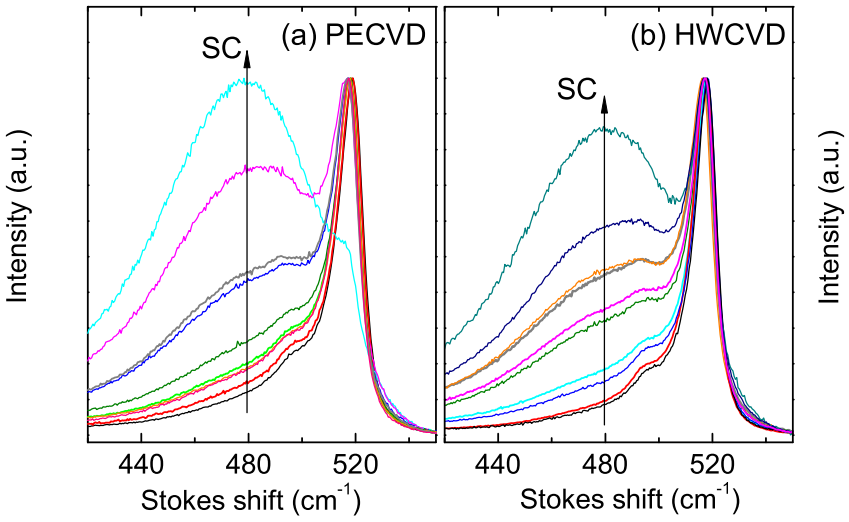

Figure 5.6: *Raman spectra of the PECVD and HWCVD solar cells. It is possible to obtain any desired crystallinity if sufficient fine tuning of SC is applied.*

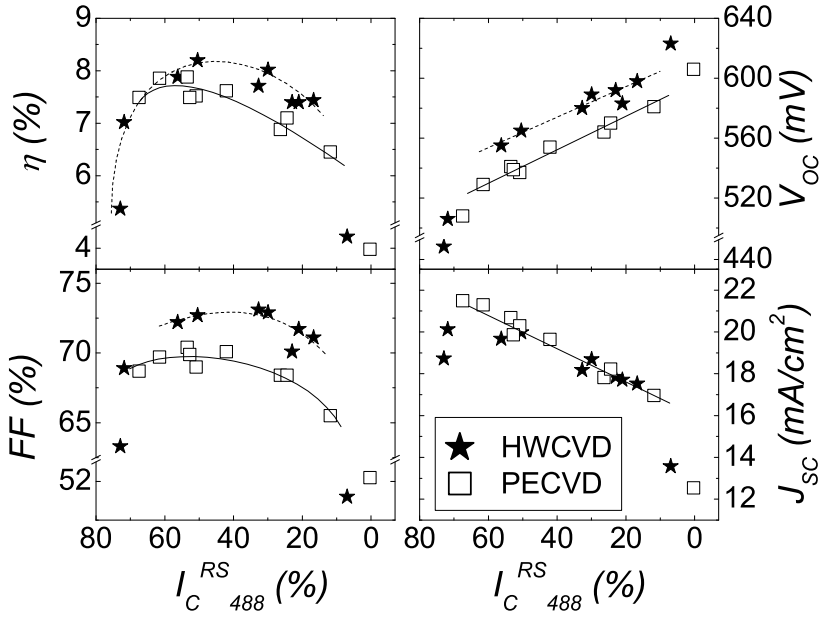

Figure 5.7: J-V *characteristics, η, V_{OC}, FF and J_{SC}, of μc-Si:H solar cells with* i*-layers deposited by PECVD or HWCVD, plotted as a function of I_{C488}^{RS}. The intrinsic HW* p/i *buffer layers in PECVD solar cells nearly eliminates the differences between the PECVD and HWCVD solar cells. Lines are guides to the eye.*

the pace of SC variation is small enough.

The efficiency (η), V_{OC}, FF and J_{SC} of the two series in Fig. 5.5 are re-plotted in Fig. 5.7 as a function of i-layer I_{C488}^{RS}. V_{OC} in both series depends critically on the i-layer crystallinity and increases with decreasing I_{C488}^{RS}. But, too high or too low crystallinity in the i-layer leads to bad solar cell quality, indicated by the inferior FF and J_{SC}, resulting in highest efficiencies at intermediate I_{C488}^{RS}. J_{SC} are very similar in both series in the entire range of I_{C488}^{RS}. It is valuable to remind that the PECVD cells are about 5 % thicker than the HWCVD cells. The decreasing J_{SC} at $I_{C488}^{RS} < 60$ % can be attributed to the low absorption coefficient of the long wavelength light in the increasing amorphous phase in the i-layer. The low J_{SC} in the high I_{C488}^{RS} region has been discussed in Chapter 4 in terms of the strong bulk recombination. An important observation in this figure is that the HWCVD series shows ~25 mV higher V_{OC} and ~3 % (abs.) higher FF than the PECVD samples in the I_{C488}^{RS} region between 60 % and 10 %. A HWCVD sample with low I_{C488}^{RS} of 17 % and thus high V_{OC} of 598 mV still maintains high FF of 71.1 %, indicating a remarkable difference between the two series. However, the higher FF can not be simply attributed to the better carrier extraction in the solar cells, since a larger FF can be mathematically

obtained from a J-V curve with higher V_{OC} [*Stiebig 2005, Green 1992*].

5.2.3 PECVD solar cells with HW p/i buffers

Since the above differences in V_{OC} and FF was previously attributed to the better p/i interface quality in the HWCVD solar cells [*Mai 2006*], incorporating an intrinsic μc-Si:H p/i buffer layer deposited by HWCVD into PECVD cells may improve the cell performance. In the following, the effects of such HW buffer layers will be studied. The deposition parameters of the HW buffer are the same as those for the HWCVD i-layer preparation, except that the SC was kept between 3 and 5 % to obtain sufficient crystallinity, which is crucial to obtain good nucleation in the bulk layer deposited by PECVD. The thicknesses of the HW-buffers were varied between 10 and 100 nm. When different buffer layer thickness is used, the deposition time of the bulk i-layer was simultaneously changed to maintain a constant total thickness of about 1.1 μm. Note that the HW-buffer cells are of similar thickness to the PECVD cells, and thus are approximately 5 % thicker than the HWCVD samples. Different structural compositions were obtained for the bulk layers by the variation of SC to avoid the influence of i-layer crystallinity on V_{OC} and FF values.

The J-V parameters under illumination of the HW-buffer cells are also plotted in Fig. 5.7 together with the two series with i-layers deposited entirely by PECVD and HWCVD, as a function of I_{C488}^{RS}. As can be seen in this figure, inserting an intrinsic μc-Si:H HWCVD buffer layer between the p- and i-layer of the PECVD solar cells nearly eliminates the differences between the PECVD and HWCVD cells. The solar cells with HW-buffers obtain very similar V_{OC} and FF as the HWCVD cells at the same I_{C488}^{RS}, although more than 90 % of the 1100 nm thick bulk i-layer was deposited by PECVD. In addition, HW-buffer layers lead to an increase in J_{SC} at fixed I_{C488}^{RS}, resulting in higher efficiencies up to 8.5 % for the 1.1 μm thick single junction solar cells with only simple Ag back contact. Another exceptional effect of the HW-buffers is that solar cell performance can be maintained at a high level as V_{OC} exceeds 550 mV (Fig. 5.8). Two solar cells with a low I_{C488}^{RS} of 28 % and 10 %, corresponding to V_{OC} values of 585 mV and 586 mV, respectively, still exhibits surprisingly high solar cell performance with efficiency over 8.0 % and FF over 72 %, which up to now could only be obtained with i-layers prepared entirely by HWCVD. It was also found that varying the SC and thickness of the buffer layer to some extent make no visible difference in the solar cell performance. It will be discussed in detail about the effects of the HW-buffer deposition parameters in the following section.

To confirm the hypothesis that better p/i interface quality is the reason for the higher V_{OC} and FF of the HWCVD and HW-buffer cells, J-V characteristics measurements with short and long wavelength illumination were conducted. As the blue light will be nearly totally absorbed in the p-layer and at the p/i interface, the blue light response, therefore, can be regarded as the criterion for the p-layer and p/i interface. The long wavelength light generates a homogeneous absorption profile in the ∼1.1 μm thick i-layer, thus the red light

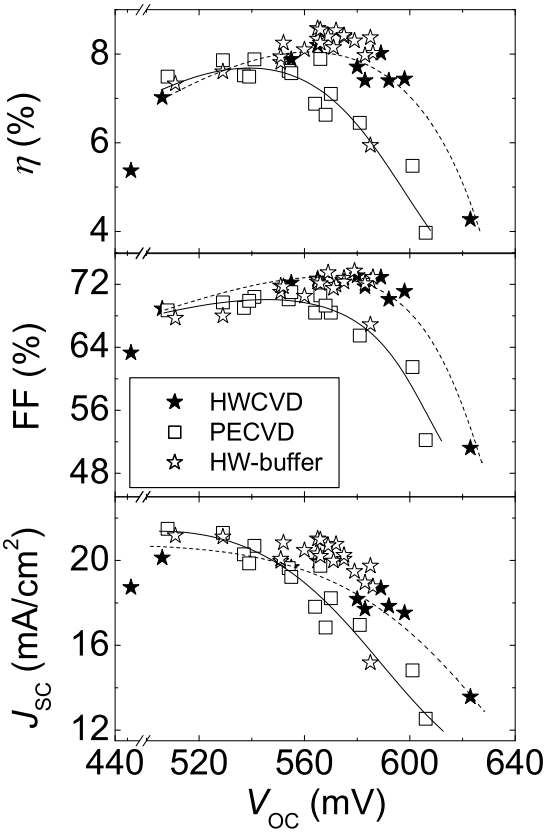

Figure 5.8: Efficiency, FF and J_{SC} of the solar cells with i-layers deposited by PECVD and HWCVD, plotted as a function of V_{OC}. The intrinsic microcrystalline HW-buffers nearly eliminate the differences between the two series with i-layer deposited completely by PECVD or HWCVD. Lines are guides to the eye.

response will shed light on the bulk material quality in the solar cells. Fig. 5.9 shows the FF and J_{SC} of the PECVD and HWCVD series under blue and red light illuminations. The blue and red light illuminations were created with an AM1.5 illumination through a band-pass filter (bg7, centered at 480 nm) and a cut-on filter (og590, >590 nm), respectively. The evolutions of blue light and red light FF upon the variation of I^{RS}_{C488} are very similar to those under AM1.5 illumination. The FF of the PECVD cells starts to drop as the I^{RS}_{C488} decrease below 50 %, while that of the HWCVD cells continues to increase and maintain at a high level at a low I^{RS}_{C488} of 17 %. The blue light J_{SC} (J_{SCbg7}) decrease with decreasing I^{RS}_{C488} in both series, indicating that too high amorphous volume fraction at the p/i interface limit the extraction efficiency for the carriers generated in this region. Compared to the PECVD cells, the HWCVD cells show higher J_{SCbg7} and FF$_{bg7}$in the I^{RS}_{C488} range between 60 % and 10 %, where they simultaneously show higher V_{OC} and FF under AM1.5 illumination. Our

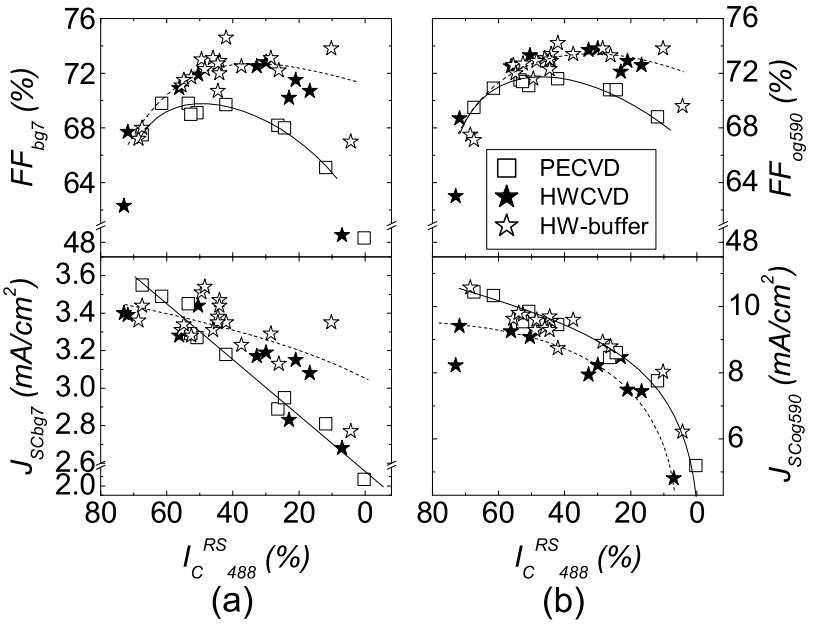

Figure 5.9: *(a), FF and J_{SC} under blue light illumination of the solar cells with* i*-layers deposited by PECVD and HWCVD, plotted as a function of I_{C488}^{RS}. The application of the HW-buffer layers improve the blue light response. (b), FF and J_{SC} under red light illumination of these cells. Lines are guides to the eye.*

previous research [*Klein 2002, Mai 2006*] yielded similar results that HWCVD cells with high V_{OC} of 600 mV still maintain high blue light quantum efficiency. The two series with the bulk i-layer deposited with PECVD and with similar i-layer thickness have very similar red light response. The relatively lower $J_{SCog590}$ in the HWCVD cells, compared to those of the PECVD and HW-buffer cells, can be attributed to the thinner i-layers. With higher blue light or red light J_{SC} than the PECVD or HWCVD cells, HW-buffer cells obtain higher AM1.5 J_{SC}. In addition to the higher FF_{bg7}, HW-buffer cells also show high red light FF. However, a better extraction for carrier generated in the bulk of the HWCVD and HW-buffer cells can not be unambiguously concluded from higher FF_{og590} alone, as they might be, at least partly, a result of the larger V_{OC} values [*Stiebig 2005, Green 1992*]. The PECVD and HW-buffere series have i-layers deposited by PECVD with almost the same thickness. The strong resemblance between the $J_{SCog590}$ of these two series in turn give a hint that the HW p/i buffer layers have no significant effect on the extraction efficiency for the carriers generated in the bulk.

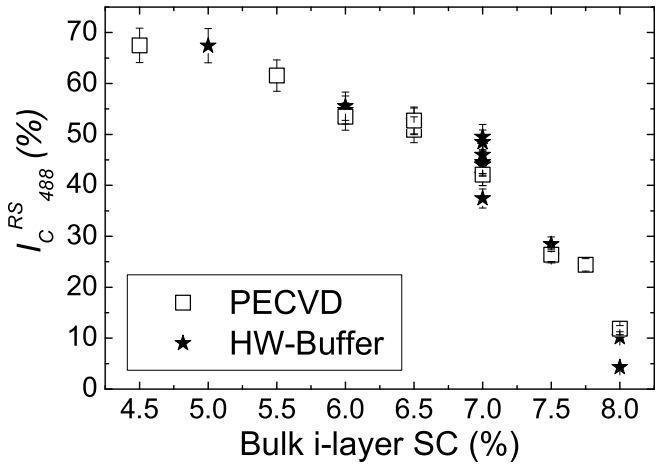

Figure 5.10: I_{C488}^{RS} *of the solar cells with or without HW-buffers plotted as a function of the bulk i-layer SC.*

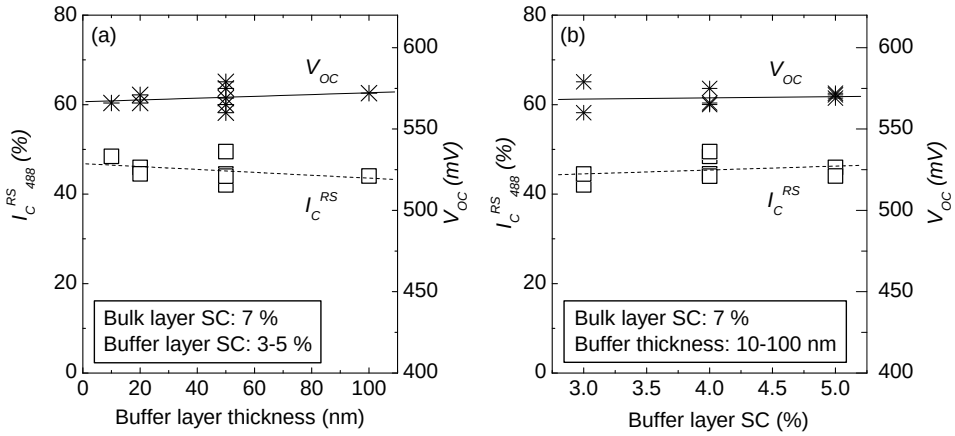

Figure 5.11: *Bulk i-layer* I_{C488}^{RS} *and* V_{OC} *of the solar cells plotted as a function of the buffer layer thickness (a) and SC (b). The i-layers were deposited with the same SC of 7 %*

5.2.4 Influences of HW-buffer deposition parameters

Fig. 5.10 shows the I_{C488}^{RS} values of the PECVD cells and the HW-buffer cells as a function of bulk layer SC. SC was varied from 3 to 5 % and thickness was varied from

10 to 100nm in these HW-buffer cells. It can be seen that the bulk layer crystallinities of HW-buffer cells are mainly determined by the bulk layer SC and are almost identical to those solar cells without buffer layers deposited with the same SC. If SC for bulk layer deposition is kept at 7 %, the bulk layer I^{RS}_{C488} and V_{OC} are nearly constant (Fig. 5.11), as the buffer layer thickness is varied from 10 to 100 nm, and SC from 3 to 5 %.

5.3 The function of HW-buffers

Compared to PECVD cells, solar cells with i-layers deposited entirely by HWCVD show superior performance at high V_{OC} and higher V_{OC} and FF at the same I^{RS}_{C488}. Such differences were attributed to the more effective carrier extraction at the p/i interface in the HWCVD solar cells [*Mai 2006*]. The implementation of a buffer layer prepared by HWCVD leads to a noticeable improvement of FF and V_{OC} in p-i-n solar cells where the bulk i-layer is prepared by PECVD. The better p/i interface quality in the resulted solar cells were confirmed by the enhanced blue light response. However, the reasons for this improvement are not yet understood. There are several possible effects. Firstly, less disordered incubation layer deposited with the HWCVD process improved the nucleation [*Klein 2004*]. Secondly, as the advantage of an ion-free deposition for thin film device fabrication has been already suggested in earlier reports [*Matsumura 1989a, Stannowski 2003*], absence of ion damage during HWCVD growth may result in a better p/i interface quality. In the following of this section, the two likely explanations will be experimentally testified and evaluated.

5.3.1 Facilitating nucleation

The presence of a more amorphous incubation layer and the thickness-dependent crystallinity evolution was found pertaining to the growth of μc-Si:H by a variety of techniques [*Houben 1998, Ross 2000, Luysberg 2001, Collins 2003, and chapter 3*]. The amorphous p/i interface layers and structural development along the growth axis were previously found in the μc-Si:H solar cells deposited by PECVD and regarded to be the origin of deteriorated blue light response [*Stiebig 2000, Vetterl 2001a, and chapter 3*]. On the contrary, the crystalline growth was found starting directly from the microcrystalline p-layers and homogeneously extending to the whole thickness of the i-layers in the HWCVD solar cells deposited with low T_f and T_s [*Klein 2004*]. Furthermore, strong structural development along the growth axis is more commonly seen in the material and solar cells deposited at high R_D. Thus, the 2 - 3 times higher R_D in the PECVD cells make the structural development a suspicious factor that should be firstly verified.

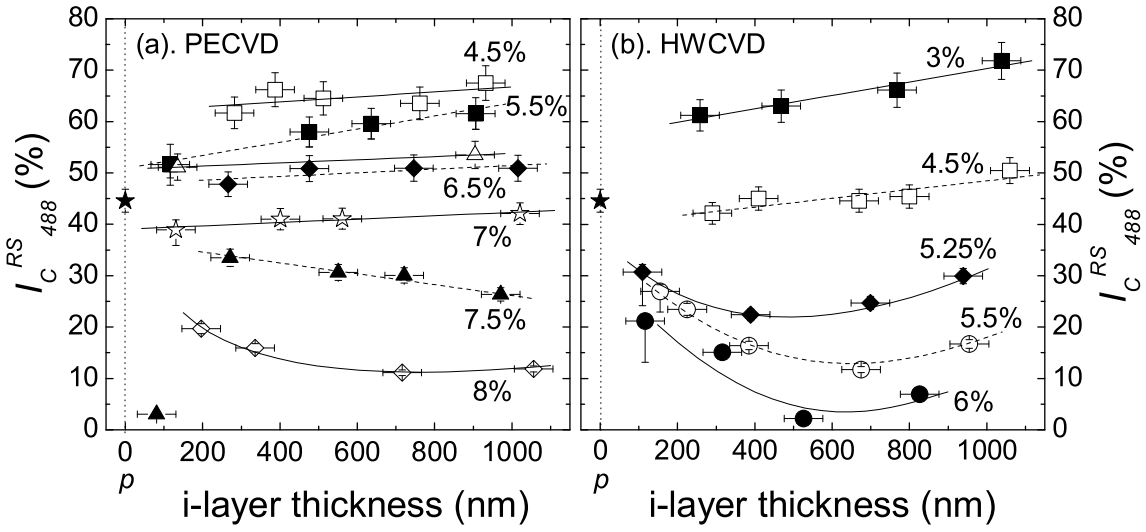

Figure 5.12: *Structure development during the i-layer growth in PECVD (a) and HWCVD (b) solar cells obtained by the Raman structural depth profile. Numbers indicated in the figures are SC for the bulk i-layer deposition. The crystallinity of the ∼20 nm thick μc-Si:H* p*-layer is indicated at the position of x = 0. Lines are guides to the eye.*

Raman structure depth profile

The Raman structure profile method described in the previous chapter is used here to acquire the crystallinity evolution along the growth axis. The I_{C488}^{RS} values at different stages of growth of the PECVD and HWCVD solar cells are shown in Fig. 5.12 (a) and (b), respectively. Numbers indicated in the figure are SC for the bulk layer deposition. The ∼20 nm thick μc-Si:H *p*-layer shows a high crystalline volume fraction of about 45 %, indicated at the position of x = 0. Note that the *p*-layer was deposited on chromium coated glass with the same parameters as the normal *p*-layers in the solar cells. The chromium substrate was used here to reduce the contribution from the substrate in Raman scattering measurement. It is important to remind that the use of chromium substrate may lead to a change in the crystalline volume fraction and film thickness, which in turn will also affect the crystallinity. From these two diagrams, an increasing I_{C488}^{RS} with the thickness is observed in the solar cells with crystallinity near or higher than that of the *p*-layer. In the solar cells with low crystallinity, higher I_{C488}^{RS} is observed in the region close to the *p*-layer in both PECVD and HWCVD series. The contributions of the μc-Si:H *p*-layers to the Raman signal have been taken into account and are indicated by the larger error bars for the data points near the *p*-layers. Data points with thickness > 200 nm can hardly be affected by the *p*-layers,

although $\pm$50 nm error might happen in the thickness measurement (See Chapter 3 for details). The more developed crystallite formation at the p/i interface can be explained by the microcrystalline growth facilitated by the nuclei of microcrystalline p-layers. But the high SC for the i-layer preparation could not maintain the crystalline growth and thus led to a decreasing crystallinity with the increasing thickness. The termination of crystallite growth was also previously observed in high SC samples [*Houben 1998*]. Some solar cells show a minimum crystallinity at the middle of the i-layer, but its origin is not clear. The I^{RS}_{C488} difference between the top and the bottom of the i-layer are typically within 10 % in almost all PECVD and HWCVD solar cells in Fig. 5.12. Note that such a difference is not as big as the values in the former research [*Vetterl 2001a, Klein 2004*]. The structure evolution along the growth axis previously observed in the PECVD μc-Si:H solar cells [*Vetterl 2001a*] can be ascribed to the relatively lower crystallinity of the p-layers prepared in another system of our institute [*Lambertz 2005*].

Raman structure depth profile measurements were also carried out in selected HW-buffer samples (shown in the coming section). Very homogeneous growth, similar to those in PECVD and HWCVD samples, was also found in HW-buffer cells. To confirm the measurement results of the Raman structure depth profile, transmission electron diffraction measurements were performed on the PECVD, HWCVD and HW-buffer cells.

sample	bulk layer by	SC (%)	I_{C488}^{RS} (%)	η (%)	V_{OC} (mV)	FF (%)	J_{SC} (mA/cm^2)	Remark
PECVD	PECVD	7.5	26.4	6.9	564	68.4	17.8	– –
HWCVD	HWCVD	5.25	29.9	8.0	589	72.9	18.9	– –
HW-buffer	PECVD	7.5	28.4	8.4	585	72.4	19.7	100 nm buffer SC: 5 %

Table 5.1: *Deposition parameters, structural and* J-V *parameters of the PECVD, HWCVD and HW-buffer cells.*

Transmission electron microscopy

To confirm the results obtained form Raman scattering measurements, transmission electron microscopy (TEM) pictures measured on three solar cells (one PECVD, one HWCVD and one HW-buffer cell) with similar I_{C488}^{RS} of about 30 %. The deposition parameters, structure properties and J-V characteristics of these cells are summarized in Table 5.1. With very similar i-layer crystallinities with the PECVD cells, the HWCVD and HW-buffer cells show higher V_{OC} ($>$ 20 mV) and FF ($>$ abs. 4 %). The PECVD cell has slightly higher red light J_{SC} ($J_{SCog590}$) than the HWCVD cell, likely due to the thicker i-layer. But its relatively poor blue light J_{SC} results in a smaller total J_{SC} than the HWCVD cell. The HW-buffer cell consists of a 100 nm thick p/i buffer deposited at a SC of 5 %, which is a bit smaller than the SC value (5.25 %) of the HWCVD i-layer. The bulk layer of the HW-buffer cell was deposited with the same SC of 7.5 % as the i-layer in the PECVD cell. With the improved J_{SCbg7} and the higher $J_{SCog590}$ coming from the thicker bulk layer, the HW-buffer cell exhibits the highest AM1.5 J_{SC} in the three samples. As a result, high efficiencies of 8.0 % and 8.4 % are observed in the HWCVD and HW-buffer cells.

Fig. 5.13 shows the cross sectional TEM pictures of these three samples. In the left column are the bright-field images, and in the right column are the dark-field images. Images (bright-field and dark-field) of the PECVD sample are shown in diagrams (a) and (b). Diagrams (c) and (d) belong to the HWCVD cell, and pictures in (e) and (f) are taken from the HW-buffer cell. From the bright- and dark-field images, one can see clearly the aluminum-doped ZnO substrates. The silicon layers looks very similar from the TEM bright-field pictures, featuring with small fiber-like columnar grains. These grains start directly from the ZnO substrates and almost extend through the whole i-layer. The i-layers show a very homogeneous growth and no incubation layer was observed in all these samples. The absence of the incubation layer in the solar cells was believed to be induced by the better nucleation on the microcrystalline p-layers, though the p-layer themselves

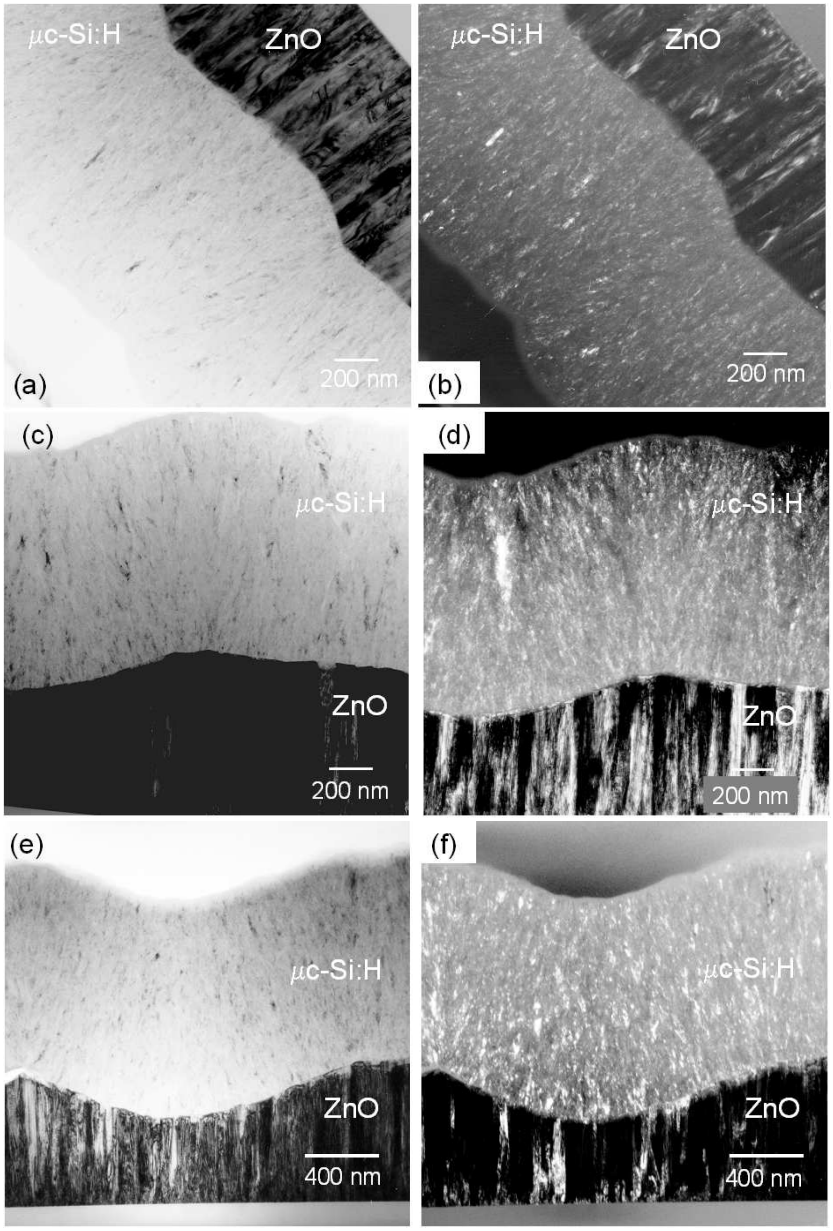

Figure 5.13: *Cross sectional TEM pictures of three selected samples. In the left column are the bright-field images, and in the right column are the dark-field images. Images (bright-field and dark-field) of the PECVD sample are shown in diagrams (a) and (b). Diagrams (c) and (d) belong to the HWCVD cell, and pictures in (e) and (f) are taken from the HW-buffer cell.*

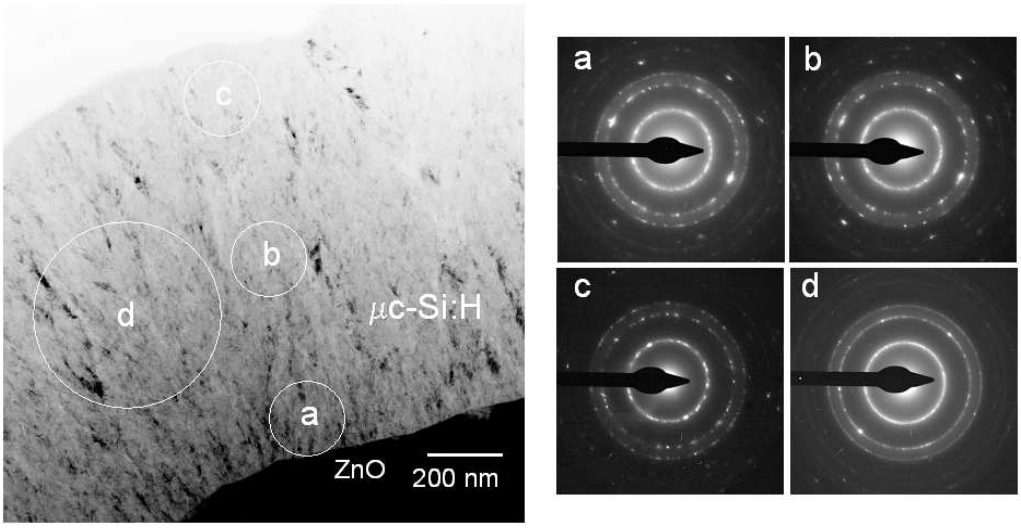

Figure 5.14: *SAED patterns [(a), (b), (c) and (d) on the right-hand side] taken in the HWCVD cell in the indicated regions (left).*

can't be identified in these images between the μc-Si:H i-layers and ZnO substrates.

To quantitatively obtain the structure information at different stages of i-layer growth, selective area electron diffraction (SAED) experiments were carried out on these three samples. It can be seen that SAED patterns of these samples at different selected area are similar to each other, which is consistent with the homogeneous crystallite distribution in the i-layers. Fig. 5.14 exemplarily shows the four ED patterns taken from the different areas in the HWCVD cell. Among them, pattern (a) is taken from the circular area with diameter of 200 nm close to the bottom of the i-layer, and (b) close to the middle, (c) close to the top and (d) from the center part of the i-layer. All diffraction patterns show the spotty rings, which corresponds to the {111}, {220} and {311} lattice planes, and the diffuse halo pattern of a-Si:H.

Crystalline volume fraction at different areas can be estimated from the ratio of the integrated power of the crystalline and amorphous contributions in azimuthally averaged Debye-Scherrer diffraction patterns [*see section 3.5.4 or Luysberg and Houben 2005*]. Fig. 5.15 shows the crystallinity (X_c) of the three solar cells. In good agreement with the measurement results by the Raman structure depth profile (Fig. 5.12], all solar cells have a very homogeneous growth with X_c difference between the top and bottom within 10 %. Actually, the PECVD cell is even more homogeneous than HWCVD cell. The 100 nm thick HW-buffer in the HW-buffer cell is deposited with SC of 5 %, which is lower than that used for the HWCVD cell deposition. The HW-buffer doesn't seem to disturb the

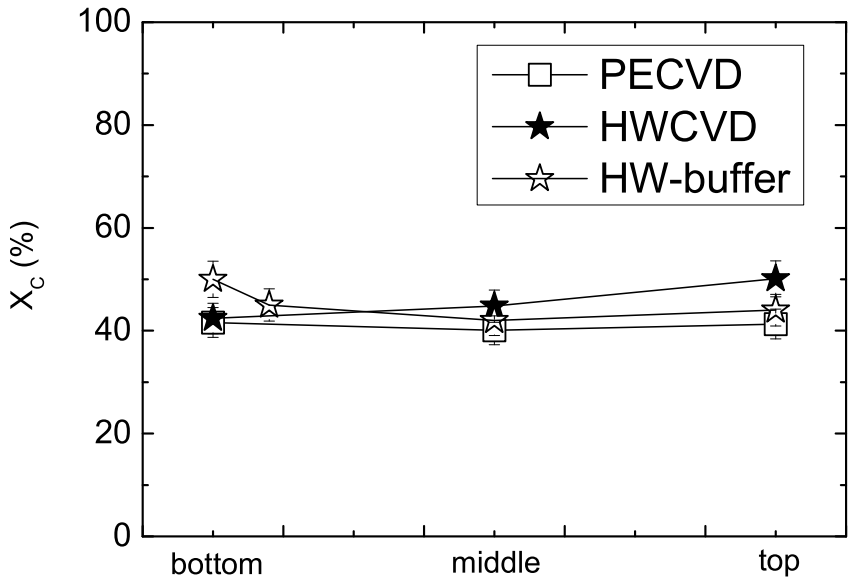

Figure 5.15: *X_c of the PECVD, HWCVD and HW-buffer cells in the regions close to the bottom, middle and top. X_c are estimated from the ED patterns taken from the circular region with diameter of 200 nm.*

bulk layer growth, and the PECVD and HW-buffer cell have similar X_C in almost the whole i-layer. Note that the absolute X_c values calculated from ED patterns are about 10 % higher than the I^{RS}_{C488} values measured from the top of the same solar cells. As both X_c and I^{RS}_{C488} are semi-quantitative measures for crystalline volume fraction, the absolute values are not comparable.

The above TEM and SAED results show that the three cells are all very homogenous along the i-layer growth axis. However, X_c estimated from this method is only an averaged crystallinity of a circular area with a diameter of 200 nm. This make this method also not sensitive enough for the region very close to the p-layer. Therefore, the possibility of a very thin and less crystalline layer at the p/i interface shall not be excluded.

Amorphous HW-buffer layers

From the Raman structural depth profile and TEM measurement presented above, very homogeneous growth is found in both HWCVD and PECVD cells with various structural composition. Therefore, the difference in the V_{OC} and FF in the two types of solar cells should not be attributed to the structure development. But it is notable that the presence

of a several ten nm thick amorphous layer at the p/i interface might worsen the interface properties but is not easily detectable. Without a well-defined surface after the KOH etching and a crystallite distribution function in the incubation layer, it is very difficult to precisely separate the contribution from the p-layers in the Raman depth profile method. As mentioned above, the sensitivity of SAED is also not sufficient for this purpose. It is also difficult for other techniques like high resolution TEM measurement due to its poor contrast on amorphous material. In order to investigate the influence of the possible amorphous p/i interface, HW-buffers with high amorphous volume fraction were intentionally incorporated in PECVD cells.

The solar cells consist of normal doped layers, an intrinsic PECVD bulk layer and a HW-buffer layer. The bulk layers were deposited with lplP at a SC of 7 %. The thickness of the HW-buffer was kept at 10 nm, which was proven to be sufficient to yield higher V_{OC} and FF. Different SC from 4 % to 10 % were used to obtain different structure composition in HW-buffers. The SC of 4 %, yielding highly microcrystalline buffer layers, is one of the typical values for the standard μc-Si:H HW-buffer deposition. To our experience, the HWCVD 'solar cell' deposited at SC = 7 % is fully amorphous. But it is notable that it might not be the case in the very thin layers grown through the local epitaxy on the

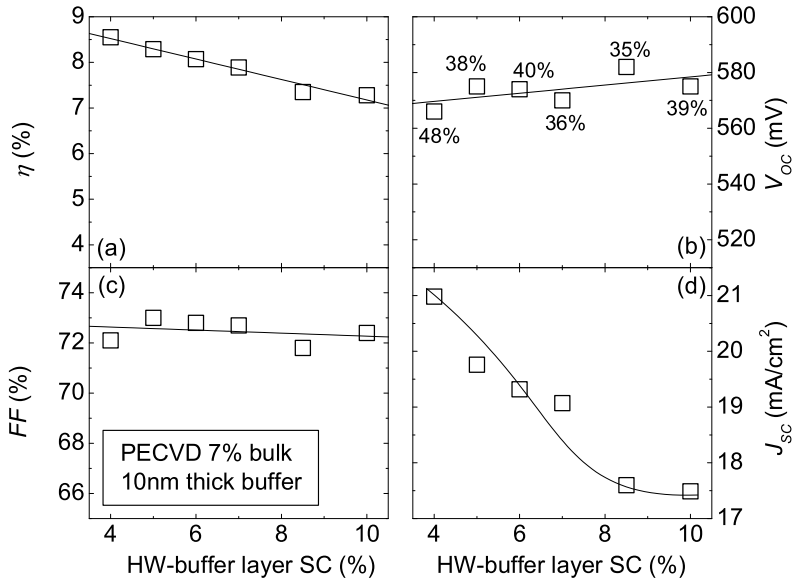

Figure 5.16: *The* J-V *characteristics, (a): η, (b): V_{OC}, (c): FF and (d): J_{SC} of the solar cells with HW-buffer layers deposited at different SC. The percentage numbers in diagram (b) are I^{RS}_{C488} values of the samples. The amorphous HW-buffer layers deteriorated J_{SC} but have almost no effect on V_{OC} and FF. Lines are guides to the eye.*

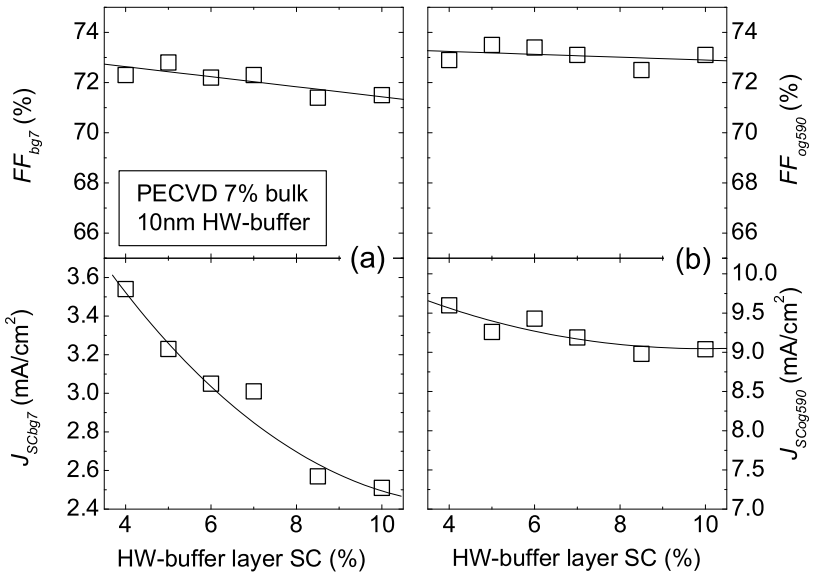

Figure 5.17: *(a), FF and J_{SC} of the solar cells with HW-buffer deposited with different SC under short wavelength light illumination. (b), FF and J_{SC} of these cells under long wavelength light illumination. Lines are guides to the eye.*

microcrystalline p-layers. For this reason, higher SC of 8.5 % and 10 % were also used.

Fig. 5.16 shows the J-V parameter of these solar cells. As the buffer layer SC increases from 4 % to 10 %, very constant FF and slightly increased V_{OC} are observed. A sharp decrease in the J_{SC} from ~21 mA/cm^2 to ~17.5 mA/cm^2 results in a decrease in the efficiency from 8.5 % to 7.3 %. The percentage numbers indicated in Fig. 5.16 (b) are I^{RS}_{C488} values for the corresponding samples measured after the removal of the amorphous n-layers. As the HW-buffer layer is shifted from highly microcrystalline to fully amorphous growth, a slight decrease in the I^{RS}_{C488} is observed, which can explain the increasing V_{OC} values.

However, the marginal change in the i-layer crystallinity can not explain the sharp decrease in J_{SC}. To gain detailed information, the blue and red light responses of these solar cells were measured. As mentioned above, the blue light J_{SC} and FF can be used as the criterion of p/i interface quality, and the red light response will provide the information of light absorption and carrier extraction in the bulk. Fig. 5.17 shows the FF and J_{SC} under the blue and red light illumination. The blue light J_{SC} (J_{SC_bg7}) decreases sharply from ~3.54 mA/cm^2 to ~2.5 mA/cm^2, while FF_{bg7} only decreases slightly from 72.8 % to 71.4 % as the 10 nm HW-buffer shifts to fully amorphous growth. The decrease of red light J_{SC} (J_{SC_og590}) can be partly ascribed to the increased amorphous volume fraction. Note

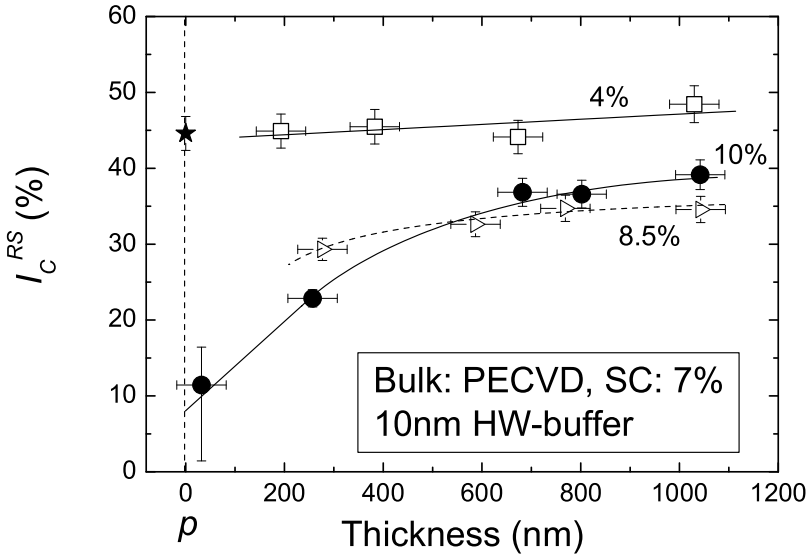

Figure 5.18: *Structure development during the i-layer growth in the solar cells with HW-buffer layers deposited at different SC. Numbers indicated in the figure are SC used for the buffer layer deposition. SC for the PECVD bulk layer deposition is fixed at 7 %. The crystallinity of the ∼20 nm thick μc-Si:H* p*-layer is indicated at the position of x = 0. Lines are guides to the eye.*

that the structural development which incorporates more amorphous volume fraction in the bulk than the I_{C488}^{RS} measured just beneath the top-most region shall not be excluded as a possible reason for the decreasing J_{SC_og590}. To our experience, a reduction of 1 mA/cm^2 in J_{SC_bg7} leads to an approximate loss of 3.2 mA/cm^2 in the total J_{SC} of a 1 μm thick μc-Si:H solar cell under AM1.5 illumination, while the 0.6 mA/cm^2 loss in J_{SC_red} decreases the AM1.5 J_{SC} by about 0.6 mA/cm^2. Thus, one can conclude that the decreased J_{SC} in the solar cells with amorphous HW-buffer layers mainly comes from the loss in the short wavelength light response.

With the use of an amorphous buffer layer, structural evolution along the growth axis is expected in the solar cells. Raman depth profile measurements were performed on three selected cells with different HW-buffer SC of 4 %, 8.5 % and 10 %. The results are shown in Fig. 5.18. The crystallinity of the p-layer deposited on the chromium substrate is also indicated in the figure at x = 0. The solar cell with highly crystalline buffer layer deposited at 4 % SC shows a very homogeneous growth with I_{C488}^{RS} of about 45 % in the i-layer. Coincident with the worsened blue light response, remarkable increase of crystalline volume fraction from 11 % at the bottom of i-layer to 39 % at the top is observed in

the solar cell with the HW-buffer deposited at the SC of 10 %. Also showing poor blue light response, the solar cell with the 8.5 % SC HW-buffer exhibits a moderate structure development as compared to the other two samples. But due to the absence of the data points with smaller distance to the p-layer, no information about p/i interface is available.

In summary, the structural development in the growth axis in the PECVD and HWCVD solar cells were investigated by Raman structural depth profile, TEM measurement and selective area electron diffraction. The PECVD and HWCVD cells were found to be very similar in the microstructure, and crystallites are homogeneously distributed in the whole i-layer. For comparison, a PECVD cell with 10 nm thick amorphous HW-buffer was prepared to study the effect of nucleation. A fully amorphous HW buffer layer leads to a severe structure evolution in the i-layer and worsens the blue light response. However, enhanced V_{OC} and FF are still found in the resulting solar cells. Although previously found critical to the p/i interface quality, a homogeneous i-layer growth seems not to be the prerequisite of the high V_{OC} and FF in the HWCVD and HW-buffer cells. This hypothesis is also consistent with the observations in the PECVD lplP and hphP cells in the former chapter. With remarkable structure evolution in the growth direction, hphP cells do not show reduced V_{OC} and FF, with respect to the lplP cells deposited at low R_D (Fig. 4.19).

5.3.2 ion-bombardment-free deposition

The absence of high-energy ion bombardment in the HWCVD process was regarded to be beneficial to the material quality and device performance [*Matsumura 1989a, Stannowski 2003, Schropp 2004*]. The ion bombardment inherent in the PECVD process may damage the p-layer and cause defect formation at the p/i interface. However, it is currently difficult in the author's lab to directly investigate the effect of ion bombardment on the p/i interface. If one can assume that defect formation is the major effect of the ion bombardment, inserting a defective HWCVD p/i buffer into PECVD cells is an alternative way to understand the function of HWCVD buffer layers.

'Bad' quality material used for HW-buffers

To study the quality of the HWCVD material deposited at high p_{depo} and high T_S, such material were prepared up to ~500 nm thick on glass and c-Si substrates. Table 5.2 shows the deposition parameters of these samples. Sample A was deposited under the standard low T_S conditions with low p_{depo} of 3.5 Pa and low T_f of 1650 °C. SC of 4 % leads to an intermediate crystallinity of 47 %. It is used as the reference for comparison. The deposition conditions for the rest samples were previously found to yield low quality

μc-Si:H films [*Klein 2005*].

sample	T_f (°C)	p_{depo} (Pa)	SC (%)	D (nm)	I^{RS}_{C488} (%)	σ_{dark} (Scm^{-1})	σ_{photo} (Scm^{-1})	$\sigma_{photo}/\sigma_{dark}$
A	1650	3.5	4	434	47	1.72E-7	1.05E-6	6.1
B	1800	3.5	4	569	68	2.90E-8	6.50E-6	224.2
C	1800	10	4	552	6.9	3.80E-8	4.71E-5	1241.1
D	1800	10	3	524	58	6.74E-7	2.06E-5	30.6
E	1650	10	2.5	443	46	5.93E-7	3.93E-5	66.2
F	1650	20	1.5	488	49	1.45E-6	1.80E-5	12.4

Table 5.2: *Deposition parameters, structural and electrical properties of HWCVD material used for HW-buffer layers.*

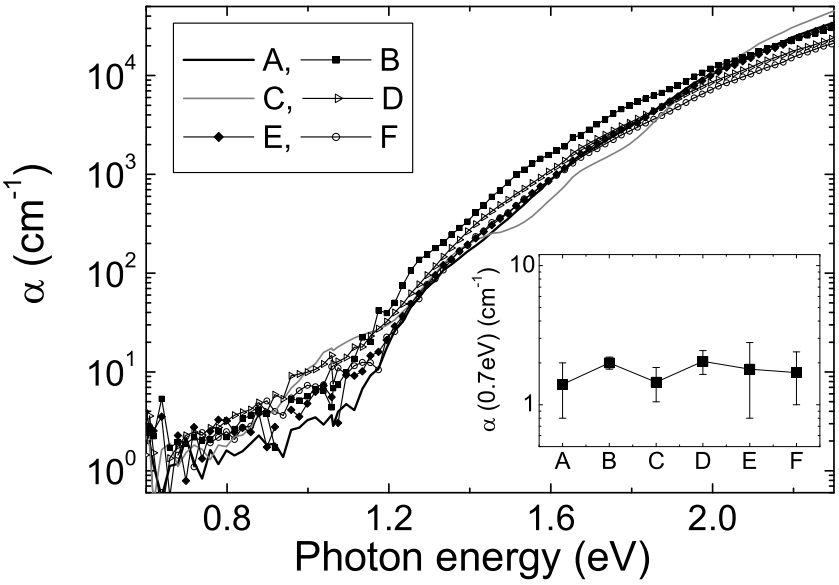

Figure 5.19: *Optical absorption measured by PDS of the samples in Table 5.2 . Inset: Absorption coefficient at 0.7 eV.*

σ_{photo}, σ_{dark} and photosensitivity ($\sigma_{photo}/\sigma_{dark}$) together with the structural composition can be regarded as indications for material quality [*Vetterl 2002, Lossen 2004*]. However, the standard sample A shows a very poor photosensitivity at a medium crystallinity. The reason is not very clear yet. A possible explanation is that it was the first sample deposited in the HWCVD chamber just after a long period of deposition of p-type SiC. Secondary ion mass spectroscopy measurement, however, found almost no enhanced B, C and O content in the film. Sample B deposited at high T_f but low p_{depo} still maintain a good photosensitivity at a high crystallinity of 68 %, indicating high material quality. The rest several samples show inferior photosensitivity at the corresponding I^{RS}_{C488}, as compared to the standard HWCVD and PECVD material presented in Fig. 5.3. A strong post-deposition atmospheric in-diffusion was observed by FTIR measurement in samples C - F, suggesting a porous structure in these films. No noticeable change could be seen in the FTIR spectra of sample A and B after 60 days storage in air.

Optical absorption of these samples are shown in Fig. 5.19. The difference in the above-gap absorption between these samples can be attributed to their different structure compositions. In contrast with the remarkable porous microstructure in sample C, D, E and F, these samples do not indicate higher sub-gap absorption, as compared to the stable sample A and B. The absorption coefficient at 0.7 eV (α(0.7 eV)) is plotted in the inset. If the measurement error is taken into account, difference can hardly be discerned from these six samples. Therefore, although sample C-F were found to have high porosity and low photosensitivity, no direct evidence show that they are highly defective.

PECVD cells with 'bad' quality HW-buffers

In this subsection, the 'bad' quality HWCVD material will be employed in the PECVD solar cells as p/i buffer layers. All solar cells in this experiment have the same doped layers. The bulk i-layers are also deposited with the same parameters with PECVD under hphP condition. The discharge power (P_{VHF}) is 20 W, and total flow rate (Fl_{total}) was 100 sccm. SC were kept at 5.5 % for all solar cells. The HWCVD buffer (same as samples B-F in Table 5.2) with different thickness between 5 and 100 nm were used in the solar cells. The deposition time of the bulk layer was correspondingly varied to keep total i-layer thickness of ∼1 μm. For comparison, two solar cells, one with no buffer layer at all and another with 20 nm normal HW-buffer (material same as sample A), were deposited at the same period of time. Fig. 5.20 shows the J-V parameters (η, FF, V_{OC} and J_{SC}) of these cells as a function of buffer layer thickness. The solar cell without buffer layer is presented by a close square (■) at x = 0. It shows a V_{OC} of 553 mV and a FF of 72 %, which are marked by dashed lines in the figure. Labels in Fig. 5.20 (b) indicate the HW-buffer material used in corresponding cells. As can be seen, similar efficiency of about 8 % are obtained for all solar cells, independent of buffer material and buffer thickness. Most cells with HW-buffers show higher V_{OC} than the reference cell, except the two cells with 50 and 100 nm thick "material C" as buffers. Even in these two cells, V_{OC} is only marginally 4-5 mV lower. In

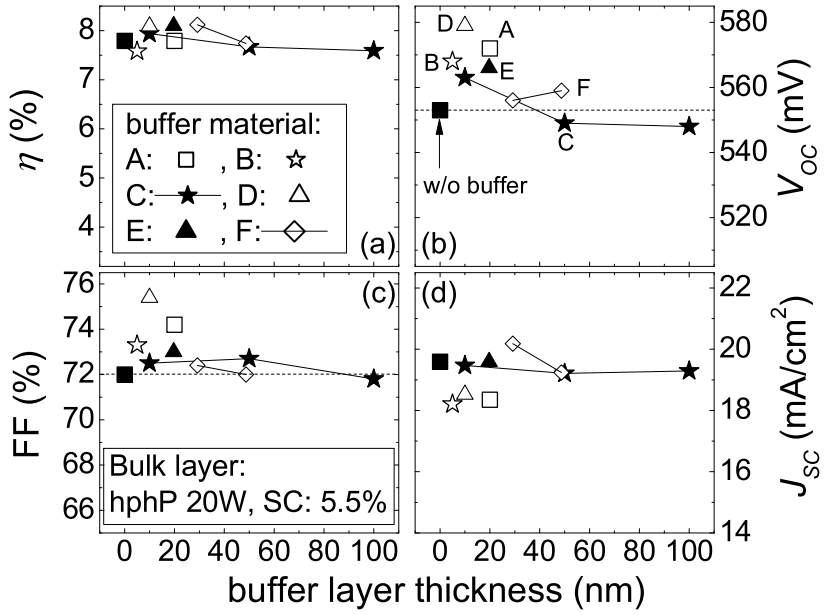

Figure 5.20: J-V *parameters, (a), η, (b), V_{OC}, (c), FF and (d), J_{SC}, of solar cells with different HW-buffer material, plotted as a function of buffer layer thickness. For comparison, a solar cells without buffer layer is indicated by a full square at x=0. Labels in diagram (b) show the HW-buffer material used in corresponding cells. Deposition parameters of the buffer layers can found in Table 5.2.*

addition, all cells with buffers show higher or equivalent FF, as compared to the reference cell. From diagram (b) and (c), lower V_{OC} and FF are typically observed in the cells with thick buffer layers. However, the effect of *i*-layer crystallinity is necessary to be taken into account to analyze the influences of buffer layer quality and thickness.

J-V parameters of these cells (Fig. 5.20) are re-plotted in Fig. 5.21 as a function of I^{RS}_{C488}. Raman scattering measurements were carried out after the removal of the amorphous *n*-layer by KOH etching. One solar cells series with *i*-layers deposited entirely by PECVD with hphP 20W is also shown in the figure. Different structural composition was achieved for this series by the variation of SC. For other deposition parameters of this series, see Table 3.1. The solar cells with HW-buffer layers (Fig. 5.20) are distributed in the I^{RS}_{C488} range between 38 % and 57 %. Note that there is no correlation between the *i*-layer crystallinity and buffer thickness. A nearly linear increase of V_{OC} with the decreasing I^{RS}_{C488} is observed for the cells with HW-buffers. At constant I^{RS}_{C488}, HW-buffer layers even with 'bad' quality still enhance the V_{OC}. But compared with the cells in Fig. 5.7, the effect is less noticeable, and there is no obvious improvement in FF. These results contradict the common views

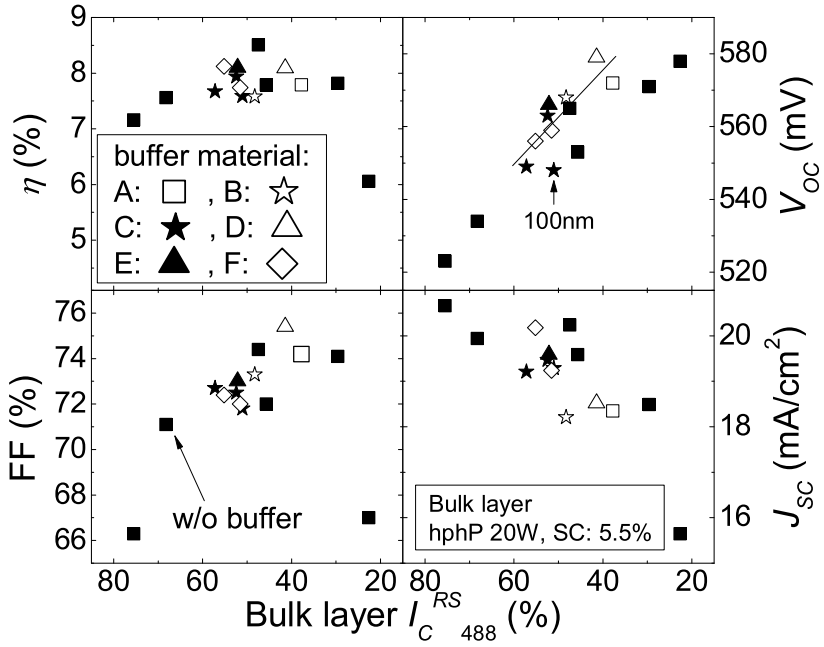

Figure 5.21: J-V *parameters, (a),* η*, (b),* V_{OC}*, (c), FF and (d),* J_{SC}*, of solar cells with different HW-buffer material, plotted as a function of i-layer* I_{C488}^{RS}*. For comparison, a solar cell series with* i*-layers deposited entirely with PECVD hphP 20W are also presented. Deposition parameters of the buffer layers can found in Table 5.2.*

about the importance of high quality p/i interface. However, interpretation of these results shall be very cautious, since there is no clear evidence proving the high defect density in the 'bad' interface layers, although their deposition conditions were previously found not suitable for high quality i-layer.

5.4 Thickness dependence and high efficiency solar cells

As can be seen above, a thin μc-Si:H HWCVD p/i buffer improves the V_{OC} and FF of the PECVD cells deposited with lplP at low R_D of about 0.2 nm/s. It is also very interesting to apply this HW-buffer concept to the solar cells prepared by high deposition rate process. For this purpose, optimum phase mixture material of the hphP 20 W and hphP 400 sccm series with different thickness between 0.5 and 4 μm were used for the bulk i-layer. For the deposition parameters of the hphP 20 W and hphP 400 sccm series, see Table 3.1. The HW-buffer layers are 10 nm thick and were deposited at a SC of 4 %. The illuminated J-V parameters of these two solar cells series are shown in Fig. 5.22.

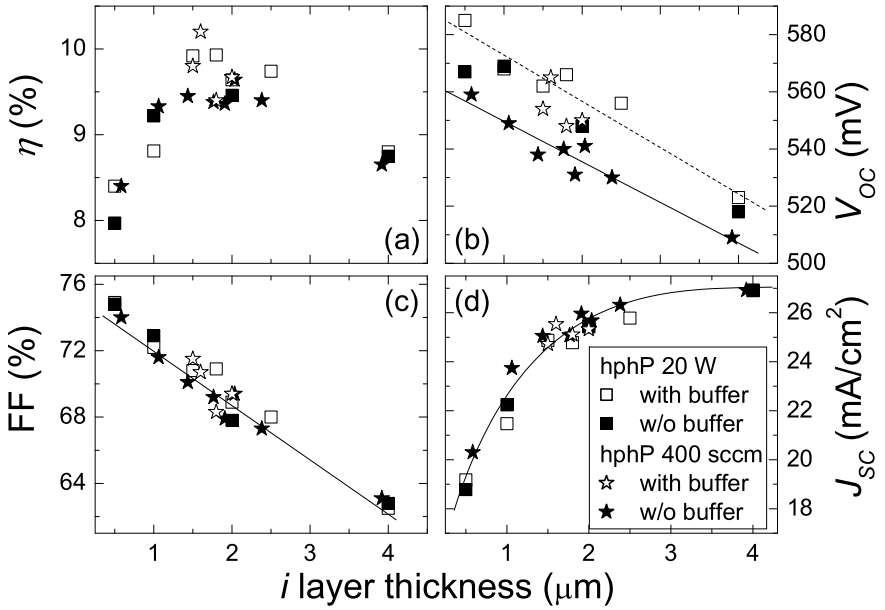

Figure 5.22: J-V *parameters, (a),* η*, (b),* V_{OC}*, (c), FF and (d),* J_{SC}*, of solar cells with different i-layer thickness. The bulk* i*-layers were deposited with PECVD hphP process at high* R_D*. Two solar cell series with HW-buffers are indicated by open symbols. Lines are guide to the eye.*

Two series with *i*-layers deposited entirely by PECVD with the optimum material are also presented for comparison. Highly reflective ZnO/Ag back contacts are used in all solar cells in this figure. Short circuit current densities J_{SC}, depending critically on light absorption, increase with the *i*-layer thickness and start to saturate at about 2.5 μm in all series. Solar cells with the same thickness are very similar in J_{SC}, which seem to be independent of the deposition conditions and the use of buffer layers. Consistent with previous results (Fig. 4.29, *Vetterl 2001, Klein 2002*), FF decrease almost linearly with the increasing thickness. Unlike the significantly enhanced FF by the use of HW-buffer as indicated in Fig. 5.7, FF are only slightly higher in the two series with buffers in this figure. Inserting a μc-Si:H HW-buffer increase the V_{OC} noticeably, thus leads to higher conversion efficiencies. With lower initial V_{OC}, the hphP 400 sccm series gain more evident V_{OC} enhancement with the use of buffer layers. Very high efficiency close or even above 10 % are obtained for the HW-buffer solar cells with bulk layer thickness between 1 and 2.5 μm.

Fig. 5.23 shows the J-V curve of the cell with maximum efficiency in Fig. 5.22, which consists of a HW-buffer and an hphP 400 sccm bulk. A similar cell also with an hphP 400 sccm bulk but without the HW-buffer layer is also shown in this figure. Thanks to the

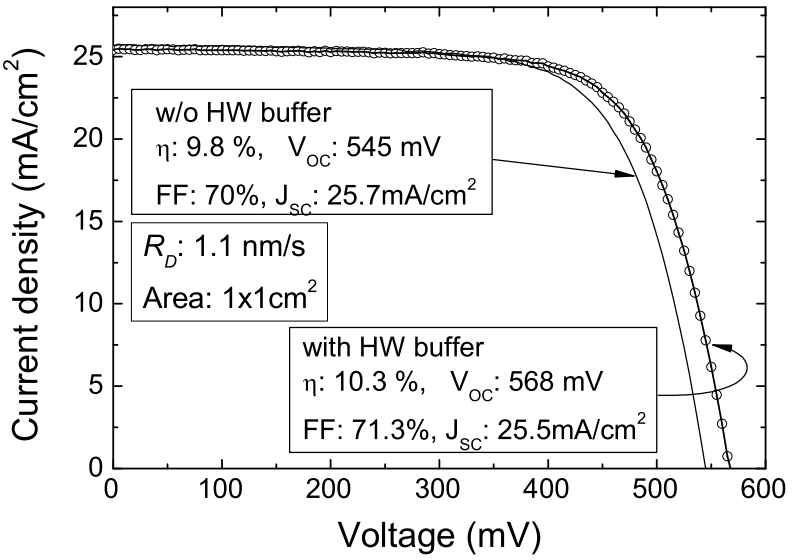

Figure 5.23: *A HW* p/i *buffer layer improves the V_{OC} and FF of a μc-Si:H single junction solar cell and achieves high efficiency of 10.3 % with the bulk i-layer deposited at a R_D of 1.1 nm/s.*

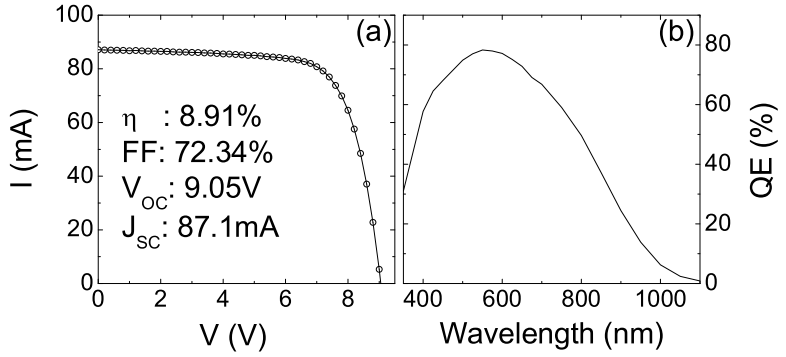

Figure 5.24: *J-V curve (a) and quantum efficiency (b) of a single junction μc-Si:H module with HW-buffer layer. Aperture area: 8×8 cm^2. The bulk i-layer was deposited by PECVD with hphP at a P_{VHF} of 20 W, resulting in a R_D of about 0.6 nm/s.*

improved V_{OC} and FF (568 mV and 71.3 %, respectively), the high efficiency of 10.3 % was achieved for the cell with HW-buffer. To our knowledge, this is the record efficiency for the μc-Si:H single junction solar cells in p-i-n configuration. Note that extended annealing at 160 °C up to two hours increases the solar cell efficiency by 0.2 % (abs.), compared to the results in Fig. 5.23, which were measured after 0.5 hour annealing.

A single junction μc-Si:H mini-module with HW-buffer was also fabricated. The aperture area is 8×8 cm^2. The module consist of a 10 nm thick HW-buffer layer and 1.6 μm bulk layer deposited by hphP 20 W. The R_D for the bulk is 0.6 nm/s. The J-V curve and quantum efficiency of module is shown in Fig. 5.24 (a) and (b), respectively. High efficiency of 8.91 % was obtained. To our knowledge, this is the highest reported efficiency for the single junction μc-Si:H module. Compared to the module without the HW-buffer (in Fig. 4.33), the module with HW-buffer shows higher V_{OC}, higher FF but lower J_{SC}.

5.5 Discussion

5.5.1 μc-Si:H films deposited by PECVD and HWCVD

In section 5.1, the structural and electrical properties of the μc-Si:H material deposited by PECVD and HWCVD were compared. σ_{photo}, σ_{dark} and photo-sensitivity are found similar for the material at constant I^{RS}_{C488}, independent of deposition techniques and conditions.

Analysis of the Raman spectra yields conflicting results in determining the grain size from FWHM or peak frequency of the TO peak. FWHM is independent of the material crystallinity but is governed by the deposition techniques (namely, PECVD and HWCVD), while the peak frequency just shows a dependence on I^{RS}_{C488}. Although links between FWHM, peak frequency and grain size have been proposed by several researchers [*Iqbal 1981, Campbell and Fauchet 1986, Fauchet and Campbell 1990*], but a straightforward and clear-cut correlation between them has not been established. Furthermore, it was argued that Raman spectroscopy alone can not provide unambiguous results regarding crystallite size [*Ossadnik 1999*]. Therefore, although some trends were observed, difference in the grain size can not be reliably deduced from the Raman scattering measurement. More work, such as XRD or TEM analysis, is necessary to compare the microstructure of μc-Si:H deposited by PECVD and HWCVD.

Infrared spectroscopy shows that HWCVD material has very similar microstructure factor R with the PECVD samples. However, the HWCVD films indicate a much lower bonded H content at the same I^{RS}_{C488}. Terminating the point defects, H atoms are very important for the high quality thin film silicon material. The HWCVD material deposited at low substrate temperature, however, maintain high quality with similar low spin density of 1×10^{16} cm^{-3} as in the PECVD μc-Si:H material. Solar cells with such material as absorber layer have high efficiency over 9 % [*Klein 2001*]. It is not difficult to understand

since the number of bonded H atoms in the thin film silicon material (usually about 10^{21} cm^{-3}) is typically two orders of magnitude higher than the number of dangling bonds (10^{19} cm^{-3}) in the pure amorphous silicon without H atom [*Luft and Tsuo 1993*]. However, there still can be peculiarity in the Si-Si network of amorphous tissue in HWCVD μc-Si:H which results in a more effective dangling bond passivation with such a low C_H. Since most of the H atoms are located in the amorphous phase and at the grain boundaries, the remarkable difference in C_H suggests that the material deposited by HWCVD and PECVD may show distinctions in the amorphous tissue and grain boundaries. Device quality a-Si:H material deposited by PECVD typically contains 10 at.% H atoms [*Stutzmann 1989, Mahan 1991*], and too high or too low C_H leads to larger Urbach characteristic energy and higher defect density. On the contrary, a-Si:H material deposited by HWCVD maintain high quality at a much lower C_H of about 2 % [*Mahan 1991*]. The PECVD and HWCVD material in this section show very similar microstructure factor R at fixed I^{RS}_{C488} (Fig. 5.2). These results suggest that the hydrogen bonding configuration or bonding site should be similar in the PECVD and HWCVD material. The different C_H in PECVD and HWCVD μc-Si:H films may come from the different Si-Si bond network in the amorphous phase. This was previously proposed by Mahan et al. for amorphous silicon *Mahan 1991*. They found that Raman TO peaks at 480 cm^{-1} is narrower in the HWCVD a-Si:H, which was attributed to the less bond angle deviations. But in the material in this work with considerable crystalline volume fractions, it is hard to separate the dominant crystalline TO peaks from the total Raman signal and analyze the a-Si:H contribution independently. Thus more precise method is still necessary for the comparison between the amorphous phase in the μc-Si:H. The H distribution in the device quality a-Si:H material deposited by HWCVD was found by ^{1}H NMR measurement to be more inhomogeneous than that in the a-Si:H material deposited by PECVD [*Wu 1996*]. The results suggest that the HWCVD a-Si:H network could consists of regions with high structural order containing nearly no H atoms and regions with lower structural order and high H concentration.

Even with the remarkable difference in C_H, which suggests different amorphous phase in the material, the PECVD and HWCVD films are very similar in the photo- and dark-conductivities if they are compared at the same I^{RS}_{C488}. However, this is not difficult to explain since the conduction in the crystal grains may mainly determine the conductivity in μc-Si:H.

5.5.2 The effect of p/i interface and its characterization

Many groups have reported to improve V_{OC} and efficiency by the use of p/i buffer layer or the so-called "interface treatment" in a-Si:H or μc-Si:H solar cells [*Arya 1986, Hack 1986, Hegedus 1988, Sakai 1990, Xi 1994, Rech 1997, Wada 2002, Grunsky 2004*]. In most cases, an improved p/i interface quality was observed in the experiment or predicted in the computational models. However, none of them gave clear answers how the p/i interface is improved by the buffer layers. This work made some attempt to answer this question and

some possibilities were excluded by experiments, like the nucleation facilitating effect etc. Some possibilities, like ion bombardment, have be investigated but could not be confirmed. There are still some other possibilities which haven't been taken into account in this work, for example, built-in potential and band banding at the p/i interface.

It was found that V_{OC} of thin film silicon solar cells increase with the increasing built-in potential (V_{bi}), if V_{bi} is smaller than a threshold value ($\sim$1 eV for a-Si:H solar cells, depending on the i-layer quality) [*Hegedus 1987, Hack and Shur 1985*]. The reason is that a smaller V_{bi} leads to a larger bulk recombination current, and thus reduces the V_{OC}. As for the solar cells presented in this work, it is assumed that the i-layer deposition does not change the underlying p-layer. However, it can not be excluded that the ion bombardment breaks some Si-Si and Si-B bonds in the p-layer and thus increases the defect density and reduces the doping efficiency. These two effects can decrease the activation energy of the p-layer and the built-in potential of the solar cells. In addition, the out-diffusion of doping element in the p-layer can result in a band bending at the interface and reduce the electric field at the interface. Note that these are all speculations and could not easily verified in the solar cells. In the following some experiments are proposed to checked the unconfirmed possibilities.

Here goes the first one. If the HWCVD p/i interface layer in PECVD cells reduces

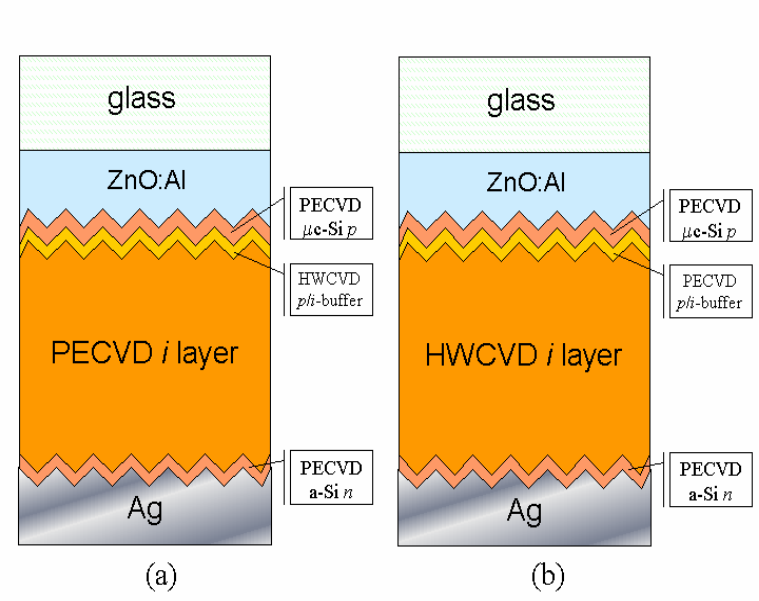

Figure 5.25: *Schematic diagrams of (a), a PECVD cell with HWCVD p/i interface layer, (b), a HWCVD cell with PECVD p/i interface layer.*

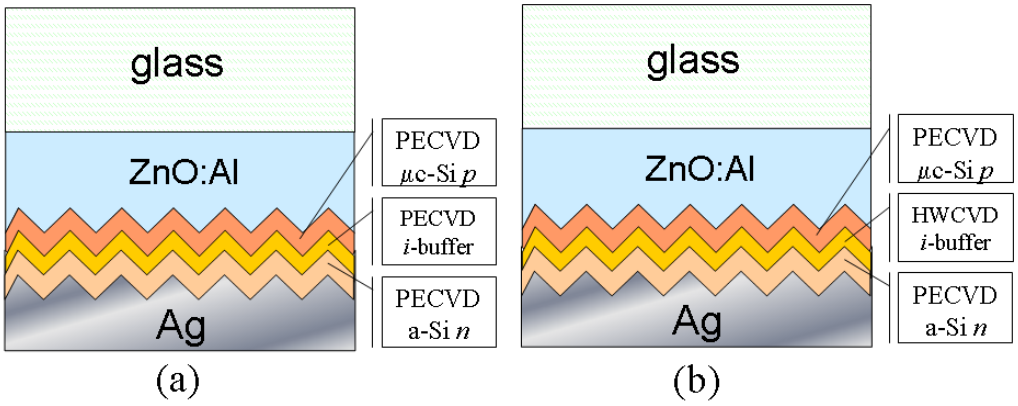

Figure 5.26: *The p-i buffer-n structure with p- and n-layer deposited by PECVD and i buffer by (a) PECVD or (b) HWCVD.*

the ion bombardment on the p/i interface, a PECVD interface layer in HWCVD cells will deteriorate the interface quality. A comparison of the solar cells with these two structure (as shown in Fig. 5.25) can help to understand the effect of the ion bombardment. Actually, such experiment has already been started, but hasn't yielded systematic results yet.

The i-layer thickness of the PECVD and HWCVD cells are usually around 1 μm or even bigger. The thick i-layer has strong effect on the J-V characteristics of a solar cell, and some what shadow that of the p/i interface. Therefore, a p-n structure is more suitable for the interface properties investigation than the p-i-n structure of normal solar cells. To investigate the effect of the interface layers, a thin intrinsic layer deposited by PECVD or HWCVD can be inserted between the p-layer and the n-layer, as indicated in Fig. 5.26 (a) and (b), respectively. Without the influences of the i-layer, the dark J-V curves of these two structure may clearly represent the differences at the interface. However, this structure has its own disadvantage that no photo J-V parameters, like V_{OC} and FF, can not be extracted from it.

5.6 Summary of this chapter

- Microcrystalline silicon films deposited by PECVD and HWCVD were compared at the same crystallinity. Similar in many aspects, such as conductivity and microstructure factor R etc., they also show distinction in H content.
- HWCVD cells maintain high efficiency at a V_{OC} up to 600 mV, while the efficiency of PECVD cells start to drop when V_{OC} exceed 550 mV.

• HWCVD cells show higher V_{OC} and FF than the PECVD cells with the same I_{C488}^{RS} in a wide range of crystallinity between 10 and 60 %.

• The above differences were attributed to the better p/i interface quality in the HWCVD cells, which was concluded from the better blue light responses in these cells.

• Improving the p/i interface quality of PECVD cells, an intrinsic μc-Si:H HW-buffer in PECVD cells nearly eliminated the differences between the two types of solar cells.

• Raman structure depth profile method and transmission electron microscopy revealed that all PECVD, HWCVD and HW-buffer cells are very homogeneous in the crystallinity along the growth axis. Thus, the positive effect of HW-buffer for facilitating nucleation was not observed. Further investigation HW-buffer with different crystallinity led to conclusion that incubation layer and structure development are not the origination for the performance differences between the PECVD and HWCVD cells.

• The HW-buffer deposited at high T_f and/or high p_{depo} still improve the solar performance. Further investigation is still necessary to draw the conclusion that ion bombardment is not responsible for the p/i interface deterioration in PECVD cells.

• By the use of HW-buffer layers, record efficiency of 10.3 % and 8.9 % were achieved for a single junction μc-Si:H solar cell and module, respectively.

Chapter 6

Summary and outlook

This thesis works on two subject of hydrogenated microcrystalline silicon (μc-Si:H) and solar cells. In chapter 4, high quality μc-Si:H films and high performance μc-Si:H solar cells were obtained by VHF-PECVD working at high pressure, high power(hphP). At the same time, the influences of deposition parameters on the material and solar cell properties were also investigated. μc-Si:H films and solar cells deposited by PECVD and HWCVD were compared in Chapter 5. It was found that the intrinsic films deposited by the two methods were quite similar to each other, and that the differences in the solar cell performance could be attributed to the different p/i interfaces. By using a HWCVD p/i interface layer in the PECVD cells eliminated these differences and achieved a high efficiency of 10.3 % in a cell with the i-layer deposited at 1.1 nm/s by PECVD. For comparison, the conversion efficiencies of the high performance cells in this thesis are plotted as a function of R_D in Fig. 6.1 together with the results collected from the literature.

However, there are still many related questions left unanswered.

High deposition rate up to 1.5 nm/s has been achieved in the solar cells without significant deterioration in the efficiency. Further increase in R_D needs higher power for gas molecule dissociation. However, P_{VHF} exceeding 60 W leads to bad homogeneity over the 10×10 cm^2 substrates. In the system with small area reactor, voltage distribution due to standing wave shall not be the reason for the inhomogeneity. The back-diffusion of silane molecules from out of the reactor can be a possible explanation [*van den Donker 2005b*]. Under high P_{VHF} conditions, the high dissociation rate decomposes most of the back-diffused silane molecules in the region close to the border, and prevents them entering the center of the electrode. Therefore, the region in the middle has lower deposition rate and higher crystallinity due to the deeper silane depletion. This is consistent with the observations in Chapter 4. A gas showerhead, which delivers more uniform gas supply, may help to solve this problem.

High quality μc-Si:H was obtained by PECVD at high deposition rate. However, the complicated growth process and plasma physics were hardly studied in this work. This deficiency left some important questions unclarified. For example, to which extent is the

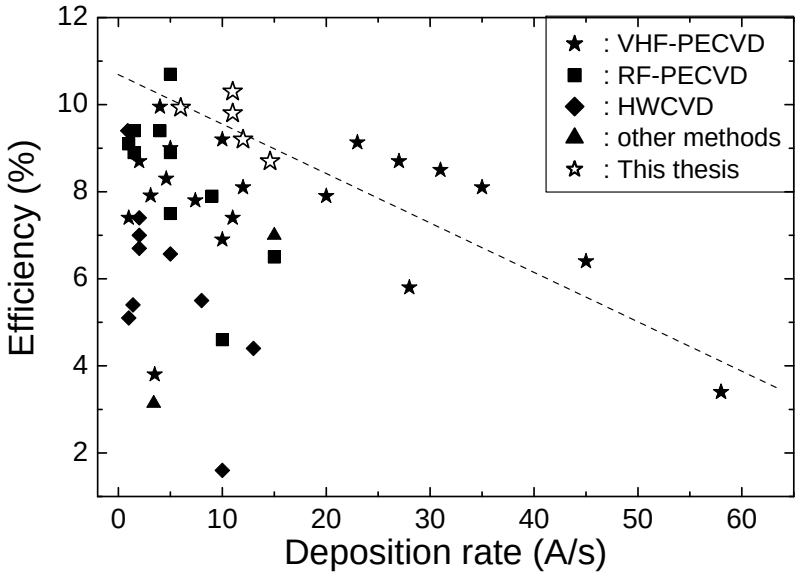

Figure 6.1: *Solar cell efficiencies as a function of deposition rate. Data are taken from this thesis and literature [Rath 2003 and references therein, Gordijn 2005, Niikura 2004, Kilper 2005, Yan 2002, Schropp 2004, Klein 2002, van den Donker 2005b, Roschek 2003, Repmann 2004].*

silane depleted during the growth of μc-Si:H? Are the values of H/Six (x=0,1,2,3) radical ratio the same for the OPM material deposition at different P_{VHF}, Fl_{total} and p_{depo}? What other factors beside ion energy do high pressure and high power have, affecting the material quality? The unveiling of these question can help to improve the material quality and increase R_D further.

Microcrystalline silicon deposited by PECVD and HWCVD was compared in the work, and interesting results was found. Although similar in some aspects, they also show distinct differences, especially in the hydrogen content. These results suggest that the PECVD and HWCVD films may differ from each other in the grain boundaries and amorphous phase. Certainly, some differences in other aspects shall not be excluded. More work needs to be done to find out the differences and their effect on the solar cell performance.

Appendix A

Abbreviation and symbols

Table A.1: ***List of abbreviations***

a-Si:H	hydrogenated amorphous silicon
μc-Si:H	hydrogenated microcrystalline silicon
c-Si	crystalline silicon
ESR	electron spin resonance
hphP	high pressure, high power
HWCVD	hot-wire chemical vapor deposition
J-V	current density vs voltage
lplP	low pressure, low power
OPM	optimum phase mixture
PDS	photothermal deflection spectroscopy
PECVD	plasma-enhanced chemical vapor deposition
QE	quantum efficiency
RF	radio frequency
SAED	selective area electron diffraction
SIMS	secondary ion mass spectroscopy
TCO	transparent conductive oxide
TEM	transmission electron microscopy
TMB	trimethyl boron
VHF	very high frequency

Table A.2: ***List of Symbols***

C_H	bonded hydrogen content
C_O	bonded oxygen content
η	conversion efficiency
Fl_{total}	total flow rate
FF	fill factor
I_C^{RS}	integrated Raman intensity ratio
I_{C415}^{RS}	integrated Raman intensity ratio at the excitation wavelength of 415nm
I_{C488}^{RS}	integrated Raman intensity ratio at the excitation wavelength of 488nm
I_{C647}^{RS}	integrated Raman intensity ratio at the excitation wavelength of 647nm
j_0	saturated dark current density
J_{SC}	short circuit current density
n	diode ideality factor
N_d	defect density
n_i	intrinsic carrier density
p_{depo}	working pressure
P_{VHF}	discharge power
R	microstructure factor
R_D	deposition rate
SC	silane concentration
σ_{dark}	dark conductivity
σ_{photo}	photo-conductivity
$\sigma_{photo}/\sigma_{dark}$	photosensitivity
T_f	filament temperature
T_S	substrate temperature
V_{OC}	open circuit voltage
X_c	crystallinity

Appendix B

The determination of I_C^{RS} by a-Si:H reference spectrum substraction

As described in Chapter 3, a three Gaussian peak fitting procedure to the Raman spectra was used in this work to determine the integrated Raman intensity ratio (I_C^{RS}). However, it is just a semi-quantitative method, and the I_C^{RS} values depend on the choice of fitting restrictions. Therefore, a comparison with the values obtained with other methods is important. In recent years, a new method was proposed to determine the I_C^{RS} [*Smit 2003*, *Carius 2005*]. This method assumes that the shape of the Raman signal of the amorphous phase in a μc-Si:H sample is the same as that of the amorphous films deposited under similar conditions. Thus, one can obtain the crystalline phase contribution to the Raman signal by subtracting a scaled a-Si:H reference spectrum from that of a μc-Si:H sample, as can be seen in Fig B.1. The residue signal consists of a TO vibration peak at around 520 cm^{-1} and another peak at 500 cm^{-1}, which can be associated with the stacking faults or hexagonal silicon (*Kobliska and Solin 1973, Houben 1998*).

The integrated Raman intensity ratio (I_C^{RS}) can be simply obtained by calculating the ratio of the peak intensity associated with crystalline phase (I_C) over the total signal intensity (I_{tot}).

$$I_C^{RS} = \frac{I_C}{I_{tot}}. \tag{B.1}$$

Fig. B.2 shows the I_{C488}^{RS} values of all samples in this work determined from the a-Si:H reference subtraction method, plotted as a function of the corresponding values obtained from the three Gaussian peak fitting. It can be seen that the values determined from the a-Si:H reference subtraction method are about 5 % higher than the value obtained from the latter method in the whole I_C^{RS} range. This suggests that I_C^{RS} values obtained by these two methods are comparable and reproducible.

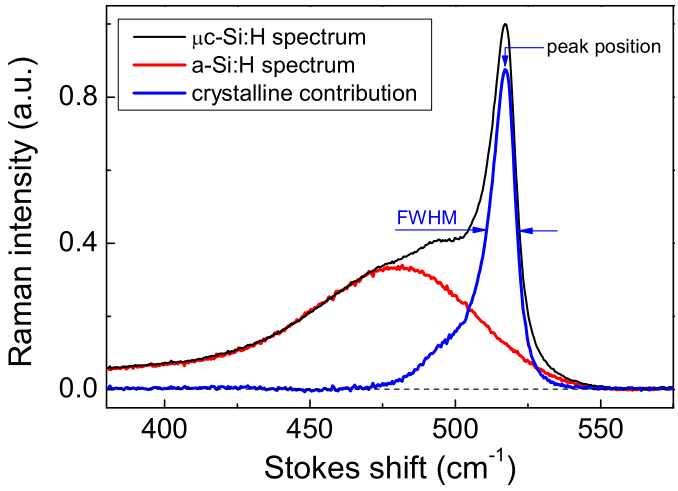

Figure B.1: *The contribution of the crystalline phase in a Raman spectrum of a µc-Si sample can be obtained by subtracting a scaled a-Si:H Raman spectrum.*

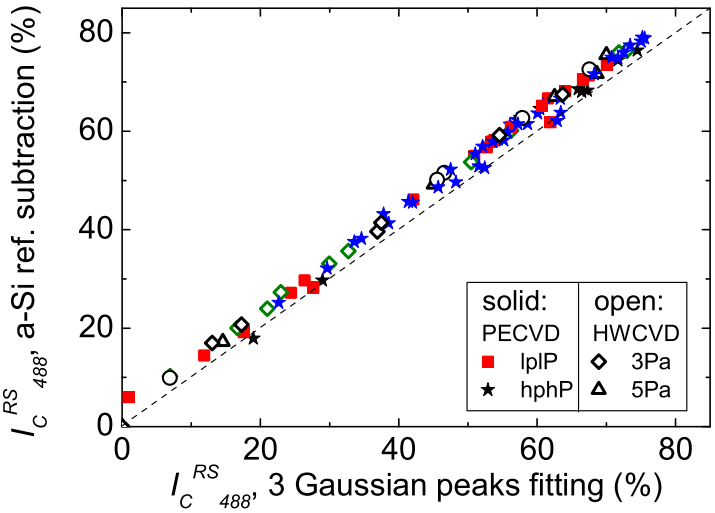

Figure B.2: I_{C488}^{RS} *values of all samples in this work determined from the a-Si:H reference subtraction method, plotted as a function of the corresponding values obtained from the three Gaussian peak fitting.*

The full width at half maximum (FWHM) and the peak position of the crystalline phase TO peak can be explicitly extracted from the residue signal in Fig. B.1. Fig. B.3 (a) and (b) display the crystalline TO peak FWHM and peak position as a function of I_{C488}^{RS}. No clear trend was found in these figures for the samples deposited under different conditions.

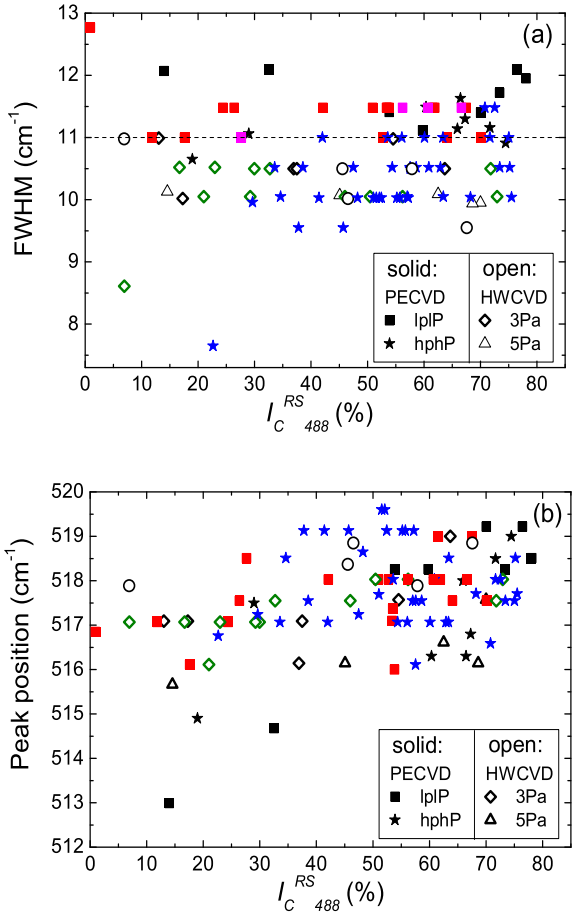

Figure B.3: *(a), FWHM and (b) peak position of the crystalline phase TO peak extracted from all Raman spectra in this work.*

Bibliography

[Alpuim 1999] P. Alpuim, V. Chu, and J. P. Conde, *Amorphous and microcrystalline silicon films grown at low temperatures by radio-frequency and hot-wire chemical vapor deposition*, J. Appl. Phys. **86**, 3812 (1999).

[Amvene-Edjongolo] C. Amvene-Edjongolo, *I-U-Kennlinien von mikcrokristallinen Solarzellen*, Diploma Thesis, Fachhochschule Aachen, 2000. **[Arya 1986]** R. R. Arya, A. Catalano, and R. S. Oswald, *Amorphous silicon p-i-n solar cells with graded interface*, Appl. Phys. Lett. **49**, 1089 (1986).

[Ashok and Pande 1985] S. Ashok and K.P. Pande, *Photovoltaic measurement*, Solar cell **14**, 61 (1985).

[Baia Neto 2002] A.L. Baia Neto, A. Lambertz, R. Carius, F. Finger, *Relationships between structure, spin density and electronic transport in 'solar-grade' microcrystalline silicon films*, J. Non-Cryst. Solids **299-302**, 274 (2002).

[Becquerel 1839] E. Becquerel Mémoire sur les effets électriques produits sous l'influence des rayons solaires. Comptes Rendus de l'Academie de Science, **9**, 561 (1839).

[Beyer and B. Hoheisel 1983] W. Beyer, and B. Hoheisel, *Photoconductivity and dark conductivity of hydrogenated amorphous silicon*, Solid State Commun. **47**, 573 (1983).

[Beyer and Abo Ghazala 1998] W. Beyer and M. S. Abo Ghazala, *Absorption strengths of Si-H vibrational modes in hydrogenated silicon*, Mat. Res. Soc. Proc. **507**, 601 (1998).

[Bouchoule 1991] A. Bouchoule, A. Plain, L. Boufendi, J. P. Blondeau, and C. Laure, *Partical generation and behaviour in a silane-argon low-pressure discharge under continuous or pulsed radio-frequency excitation*, J. Appl. Phys. **70**, 1991 (1991).

[Brammer 2000] T. Brammer, H. Stiebig, A. Lambertz, W. Reetz, and H. Wagner, *Temperature dependent transport in microcrystalline PIN diodes*, Mat. Res. Soc. Symp. Proc. **609**, A32.3 (2000).

[Brammer and Stiebig 2003] T. Brammer, and H. Stiebig, *Defect density and recombination lifetime in microcrystalline silicon absorbers of highly efficient thin-film solar cells determined by numerical device simulations*, J. Appl. Phys. **94**, 1035 (2003).

[Brammer and Stiebig 2006] T. Brammer and H. Stiebig, *Applying analytical and numerical methods for the analysis of microcrystalline silicon solar cells*, (2005) unpublished.

[Brodsky 1977] M.H. Brodsky, Manuel Cardona, and J.J. Cuomo, *Infrared and Raman spectra of the Silicon-hydrogen bonds in amorphous silicon prepared by glow discharge and sputtering*, Phys. Rev. B **16**, 3556 (1977).

[Bronner 2000] W. Bronner, R. Brüggemann, M. Mehring, *Standard and electrically detected magnetic resonance in nanocrystalline silicon*, J. Non-Cryst. Solids **266-269**, 534 (2000).

[Brüggemann and Main 1998] R. Brüggemann, C. Main, *Fermi-level effect on steady-state and transient photoconductivity in microcrystalline silicon*, Phys. Rev. B **57**, R10580 (1998).

[Bruno 1995] G. Bruno, P. Capezzuto and A. Madan, *Plasma deposition of amorphous silicon-based materials*, Academic Press, Boston (1995).

Campbell and Fauchet 1986 I. H. Campbell and P. M. Fauchet, Solid State Commun. **58**, 739 (1986).

[Cardona 1983] M. Cardona, *Vibrational Spectra of Hydrogen in Silicon and Germanium*, Phys. Stat. Sol. (b) **118**, 463 (1983).

[Carius 1997] R. Carius, F. Finger, U. Backhausen, M. Luysberg, P. Hapke, L. Houben, M. Otte, and H. Overhof, *Electronic properties of microcrystalline silicon*, Mat. Res. Soc. Symp. Proc. **467**, 283 (1997).

[Carius 2002] R. Carius, T. Merdzhanova, F. Finger, S. Klein, and O. Vet-

terl, *A comparison of microcrystalline silicon prepared by plasma-enhanced chemical vapor deposition and hot-wire chemical vapor deposition: electronic and device properties*, J. Mater. Sci. - M. El. **14**, 625 (2003).

[Carius 2003] R. Carius, T. Merdzhanova, and F. Finger, *Electronic properties of microcrystalline silicon investigated by photoluminescence spectroscopy on films and devices*, Mat. Res. Soc. Symp. Proc., **762**, A4.2 (2003).

[Carius 2005] R. Carius, private communication. **[Carlson and Wronski 1976]** D. E. Carlson and C. R. Wronski, *Amorphous silicon solar cell*, Appl. Phys. Lett. **28**, 671 (1976).

[Chapin 1954] D. M. Chapin, C. S. Fuller, and G. L. Pearson, *A new silicon p-n junction photocell for converting solar radiation into electrical power*, J. Appl. Phys. **25**, 676 (1954).

[Chapman 1980] B. Chapman, *Glow discharge processes*, John Wiley & Sons, New York, 1980.

[Chittick 1969] R. C. Chittick, J. H. Alexander, and H. F. Stieling, *The preparation and properties of amorphous silicon*, J. Electrochem. Soc. 116, 77 (1969).

[Collins and Yang 1989] R. W. Collins and B. Y. Yang, *In situ ellipsometry of thin-film deposition: Implications for amorphous and microcrystalline Si growth*, J. Vac. Sci. Technol. B **7**, 1155 (1989).

[Collins 2003] R. W. Collins, A. S. Ferlauto, G. M. Ferreira, C. Chen, J. Koh, R.J. Koval, Y. Lee, J.M. Pearce, and C.R. Wronski, *Evolution of microstructure andphase in amorphous, protocrystalline, and microcrystalline silicon studied by real time spectroscopic ellipsometry*, Sol. Energ. Mat. Sol. C. **78**, 143 (2003).

[Curtins 1987] H. Curtins, N. Wyrsch, and A.V. Shah, *High rate deposition of amorphous hydrogenated silicon: effect of plasma excitation frequency*, Electron. Lett. **23**, 228 (1987).

[Diehl 1998] F. Diehl, B. Schröder, and H. Oechsner, *Light scattering and enhanced optical absorption in hot wire microcrystalline silicon*, J. Appl. Phys. **84**, 3416 (1998).

[Dasgupta 2001] A. Dasgupta, A. Lambertz, O. Vetterl, F. Finger, R. Carius, U. Zastrow, and H. Wagner. *P-layers of microcrystalline silicon thin film solar*

cells, In Proc. of the 16^{th} European Photovoltaic Solar Energy Conference, p. 557 (2001).

[Droz 2003] C. Droz, *Thin Film Microcrystalline Silicon Layers and Solar Cells: Microstructure and Electrical Performances*, PhD thesis, Université de Neuchâtel, 2003.

[Duan 2001] H. L. Duan, G. A. Zaharias, and S. F. Bent, *The effect of filament temperature on the gaseous radicals in the hot wire decomposition of silane*, Thin Solid Films **395**, 36 (2001).

[Dylla 2005] T. Dylla, F. Finger and E. A. Schiff, *Hole drift-mobility measurements in microcrystalline silicon*, Appl. Phys. Lett. **87**, 032103 (2005).

[Fang 1980] C.J. Fang, K.J. Gruntz, L. Ley, M. Cardona, F.J. Demond, G. Müller, and S. Kalbitzer, *The hydrogen content of a-Ge:H and a-Si:H as determined by IR spectroscopy, gas evolution and nuclear reaction technology*, J. Non-Cryst. Solids, **35**&**36**, 255 (1980).

[Faraji 1992] M. Faraji, S. Gokhale, S. M. Choudari, M. G. Takwale, and S. V. Ghaisas, *High mobility hydrogenated and oxygenated silicon as a photo-sensitive material in photovoltaic application*, Appl. Phys. Lett. **60**, 3289 (1992).

[Fauchet and Campbell 1990] P. M. Fauchet and I. H. Campbell, *Critical review of Raman spectroscopy as a diagnostic tool for semiconductor microcrystals*, Mater. Res. Soc. Symp. Proc. **164**, 259 (1990).

[Feitknecht 2003] L. Feitknecht, C. Droz, J. Bailat, X. Niquille, J. Guillet, A. Shah, *Towards microcrystalline silicon n-i-p solar cells with 10% conversion efficiency*, Mat. Res. Soc. Symp. Proc. Vol. **762**, A13.5 (2003).

[Feng 2003] Y. Feng, *Stacked solar cells with amorphous silicon germanium red absorber layers*, PhD thesis, Forschungszentrum Jülich GmbH, 2003.

[Finger 1992] F. Finger, U. Kroll, V. Viret, A. Shah, W. Beyer, X. -M. Tang, J. Weber, A. Howling, and Ch. Hollenstein, *Influences of a high excitation frequency (70 MHz) in the glow discharge technique on the process plasma and the properties of hydrogenated amorphous silicon*, J. Appl. Phys. **71**, 5665 (1992).

[Finger 1994] F. Finger, P. Hapke, M. Luysberg, R. Carius, H. Wagner, and

M. Scheib. *Improvement of grain size and deposition rate of microcrystalline silicon by use of very high frequency glow discharge*, Appl. Phys. Lett. **65**, 2588 (1994).

[Finger 2002] F. Finger, S. Klein, T. Dylla, A. L. Baia Neto, O. Vetterl, and R. Carius, *Defects in microcrystalline silicon prepared with hot wire CVD*, Mat. Res. Soc. Symp. Proc. Vol. **715**, A16.3 (2002).

[Finger 2003] F. Finger, R. Carius, T. Dylla, S. Klein, S. Okur, and M. Günes, *Stability of microcrystalline silicon for thin film solar cell applications*, IEE Proc.-Circuits Devices Syst. **150**, 300 (2003).

[Flückiger 1992] R. Flückiger, J. Meier, H. Keppner, U. Kroll, A. S. O. Greim, M. Morris, J. Pohl, P. Hapke, and R. Carius. *Microcrystalline silicon prepared with the very high frequency glow discharge technique for p-i-n solar cell applications*. In Proc. of the 11th EC Photovoltaic Solar Energy Conference, p. 617 (1992).

[Fukawa 2001] M. Fukawa, S. Suzuki, L. Guo, M. Kondo, A. Matsuda, *High rate growth of microcrystalline silicon using a high-pressure depletion method with VHF plasma*, Sol. Energ. Mat. Sol. C. **66**, 217 (2001).

[Gordijn 2005] A. Gordijn, J. Francke, J. K. Rath, and R. E. I. Schropp, *Influence of pressure and plasma potential on high growth rate microcrystalline silicon growth by VHF PECVD*, Mat. Res. Soc. Proc. **862**, A10.3 (2005).

[Graf 2003] U. Graf, J. Meier, U. Kroll, J. Bailat, C. Droz, E. Vallat-Sauvain, and A. Shah, *High rate growth of microcrystalline silicon by VHF-GD at high pressure*, Thin Solid Films **427**, 37 (2003).

[Green 1992] M. A. Green, *Solar cells*, the University of New South Wales, 1992.

[Green 2002] M. A. Green, *Third generation photovoltaics: solar cells for 2020 and beyond*, Physica E 14, 65 (2002).

[Gross 2001] A. Gross, O. Vetterl, A. Lambertz, F. Finger, H. Wagner, and A. Dasgupta, *N-side illuminated microcrystalline silicon solar cells*, Appl. Phys. Lett. **79**, 2841 (2001).

[Grunsky 2004] D. Grunsky, P. Kumar, M. Kupich and B. Schröder, *Optimization of hot wire deposited microcrystalline p-layers for thin film silicon solar*

cell structures, Proc. of 19th European Photovoltaic Solar Energy Conference, (7-11 June 2004, Paris, France), p.1560.

[Guo 1998] L. Guo, M. Kondo, M. Fukawa, K. Saitoh, A. Matsuda, *High Rate Deposition of Microcrystalline Silicon Using Conventional Plasma Enhance Chemical Vapour Deposition*, Jpn. J. Appl. Phys. **37**, L1116 (1998).

[Hack and Shur 1985] M. Hack and M. Shur, *Physics of amorphous silicon alloy p-i-n solar cells*, J. Appl. Phys. **58**, 997 (1985).

[Hack and Shur 1986] M. Hack and M. Shur, *Limitations to the open circuit voltage of amorphous silicon solar cells*, Appl. Phys. Lett. **49**, 1432 (1986).

[Hamakawa 2000] Y. Hamakawa, *40 years trajectory of amorphous semiconductor research*, Mat. Res. Soc. Symp. Proc. **609**, A17.2 (2000).

[He 2000] L.-N. He, D.-M. Wang, S. Hasegawa, *A study of plasma-deposited amorphous SiO_x:H ($0<x<2.0$) films using infrared spectroscopy*, J. Non-Cryst. Solids **261**, 67 (2000).

[Hegedus 1987] S. S. Hegedus, M. Schmidt, and N. Salzman, *Measurement of the built-in potential in amorphous silicon p-i-n solar cells*, Proceedings of the 19th IEEE Photovoltaic Specialists Conference (IEEE, New York, 1987), p.210.

[Hegedus 1988] S. S. Hegedus, N. Salzman, and E. Fagen, *The relation of dark and illuminated diode parameters to the open-circuit voltage of amorphous silicon p-i-n solar cells*, J. Appl. Phys. **63**, 5126 (1988).

[Heintze 1993] M. Heintze, R. Zedlitz and G. H. Bauer, *Analysis of high-rate a-Si:H deposition in a VHF plasma*, J. Phys. D: Appl. Phys. 26 1781 (1993).

[Heintze 1993a] M. Heintze, W. Westlake, and P. V. Santos, *Surface controlled plasma deposition and etching of silicon near the chemical equilibrium*, J. Non-Cryst. Solids, **164-166**, 985 (1993).

[Heintze 1996] M. Heintze, R. Zedlitz, H. N. Wanka, and M. B. Schubert, *Amorphous and microcrystalline silicon by hot wire chemical vapor deposition*, J. Appl. Phys. **79**, 2699 (1996).

[Houben 1998] L. Houben, M. Luysberg, P. Hapke, R. Carius, F. Finger,

and H.Wagner, *Structural properties of microcrystalline silicon in the transition from highly crystalline to amorphous growth*, Philos. Mag. A **77**, 1447 (1998).

[Houben 1998a] L. Houben, *Plasmaabscheidung von mikrokristallinem Silizium: Merkmale der Mikrostruktur und deren Deutung im Sinne von Wachstumsvorgängen*, Ph.D. thesis, Heinrich-Heine-Universität Düsseldorf, 1998a.

[Houben 2002] L. Houben, C. Scholten, M. Luysberg, O. Vetterl, F. Finger, R. Carius, *Growth of microcrystalline nip Si solar cells: role of local epitaxy*, J. Non-Crystal. Solids **299-302**, 1189 (2002).

[Howling 1992] A. A. Howling, J. -L. Dorier, Ch. Hollenstein, U. Kroll, and F. Finger, *Frequency effect in silane plasma for plasma enhanced chemical vapor deposition*, J. Vac. Sci. Technol. A**10**, 1080, (1992).

[Howling 1993] A. A. Howling, L. Sansonnes, J. -L. Dorier, and Ch. Hollenstein, *Negative hydrogenated silicon ion clusters as partical precursors in RF silane plasma experiments*, J. Phys. D: Appl. Phys. **26**, 1003 (1993).

[Iqbal 1981] Z. Iqbal, S. Vepřek, A. P. Webb, and P. Capezzuto, *Raman scattering from small particale size polycrystalline silicon*, Solid State Commun. **37**, 993 (1981).

[Iqbal and Vepřek 1982] Z. Iqbal and S. Vepřek, *Raman scattering from hydrogenated microcrystalline and amorphous silicon*, J. Phys. C: Solid State Phys. **15**, 377 (1982).

[Iqbal 1983] Z. Iqbal, F-A Sarrot, and S. Vepřek, *Optical absorption in hydrogenated microcrystalline silicon*, J. Phys. C: Solid State Phys. **16**, 2005 (1983).

[Jackson 1981] W. B. Jackson, N. M. Amer, A. C. Boccara, and D. Fournier, *Photothermal deflection spectroscopy and detection*, Appl. Optics **20**, 1333 (1981).

[Jackson and Amer 1982] W. B. Jackson, N. M. Amer, *Direct measurement of gap-state absorption in hydrogenated amorphous silicon by photothermal deflection spectroscopy*, Phys. Rev. B **25**, 5559 (1982).

[Jun 2002] K. H. Jun, R. Carius, and H. Stiebig, *Optical characteristics of intrinsic microcrystalline silicon*, Phys. Rev. B **66**, 115301 (2002).

[Kamei 1996] T. Kamei, N. Hata, A. Matsuda, T. Uchiyama, S. Amano,

K. Tsukamoto, Y. Yoshioka, and T. Hirao, *Deposition and extensive light soaking of highly pure hydrogenated amorphous silicon*, Appl. Phys. Lett. **68**, 2380 (1996).

[Keppner 1999] H. Keppner, J. Meier, P. Torres, D. Fischer, A. Shah, *Microcrystalline silicon andmicromorph tandemsolar cells*, Appl. phys. A: Mater. Sci. Process. **69**, 169 (1999).

[Kilper 2005] T. Kilper, T. Repmann, B. Rech, G. Bräuer, S. Wieder, *Development of microcrystalline silicon solar cells using large area capacitively coupled planar electrodes*, Proc. of 20th European Photovoltaic Solar Energy Conference, June 2005, Barcelona, p. 1554.

[Klein 2001] S. Klein, F. Finger, R. Carius, O. Kluth, L. Baia Neto, H. Wagner, and M. Stutzmann, *Intrinsic microcrystalline silicon by hot-wire chemical vapour deposition for solar cell applications*, in Proceedings 19th European Photovoltaic Solar Energy Conference, Munich, Germany, edited by B. Mc Nellis, W. Palz, A. Ossenbrink and P. Helm (WIP, Munich, 2001), p. 2965.

[Klein 2002] S. Klein, F. Finger, R. Carius, B. Rech, L. Houben, M. Luysberg, M. Stutzmann, *High Efficiency Thin Film Solar Cells with Intrinsic Microcrystalline Silicon Prepared by Hot Wire CVD*, Mat. Res. Soc. Symp. Proc. Vol. **715**, A26.2 (2002).

[Klein 2002a] S. Klein, J. Wolff, F. Finger, R. Carius, H. Wagner, and M. Stutzmann, *Microcrystalline Silicon Prepared by Hot-Wire Chemical Vapour Deposition for Thin Film Solar Cell Applications*, Jpn. J. Appl. Phys., Part II: Letters **41**, L10 (2002a).

[Klein 2003] S. Klein, F. Finger, R. Carius, T. Dylla, B. Rech, M. Grimm, L. Houben and M. Stutzmann, *Intrinsic microcrystalline silicon prepared by hot-wire chemical vapour deposition for thin film solar cells*, Thin Solid Films, **430**, 202 (2003).

[Klein 2004] S. Klein, *Microcrystalline silicon prepared by hot wire CVD - Preparation and characterisation of material and solar cells*, Ph.D. thesis, Technische Universität Müchen (2004).

[Klein 2004a] S. Klein, F. Finger, R. Carius, H. Stiebig, *Light-induced degradation of microcrystalline silicon thin film solar cells prepared by hot-wire CVD*, in Proceedings 19th European Photovoltaic Solar Energy Conference, Paris, France 2004, edited by W. Hoffmann, J.-L. Bal, H. Ossenbrink, W. Palz, and P. Helm (WIP, Munich, 2004), p. 1579.

[Klein 2005] S. Klein, F. Finger, R. Carius, and M. Stutzmann, *Deposition of microcrystalline silicon prepared by hot-wire chemical-vapor deposition: The influence of the deposition parameters on the material properties and solar cell performance*, J. Appl. Phys. **98**, 024905 (2005).

[Kluth 1997] O. Kluth, A. Löffl, S. Wieder, C. Beneking, W. Appenzeller, L. Houben, B. Rech, H. Wagner, S. Hoffmann, R. Waser, J. A. Anna-Selvan, and H. Keppner, *Texture etched Al-doped ZnO: A new material for enhanced light trapping in thin film solar tells*, in: Proceedings of the 26th IEEE Photovoltaic Specialists Conference, Anaheim, 1997, p. 715.

[Kluth 1999] O. Kluth, B. Rech, L. Houben, S. Wieder, G. Sch?öpe, C. Beneking, H. Wagner, A. Löffl, and H. W. Schock, *Texture etched ZnO:Al coated glass substrates for silicon based thin film solar cells*, Thin Solid Films **351**, 247 (1999).

[Kluth 2001] O. Kluth, Texturierte Zinkoxidschichten für Silizium-Dünnschichtsolarzellen, Ph.D. thesis, Rheinisch-Westfälische Technische Hochschule Aachen, (2001).

[Kobliska and Solin 1973] R. Kobliska, and S. Solin, *Raman spectrum of wurtzite silicon*, Phys. Rev. B **8**, 3799 (1973).

[Kocka 2003] J. Kocka, A. Fejfar, H. Stuchlikova, J. Stuchlik, P. Fojtik, T. Mates, B. Rezek, K. Luterova, V. Svrcek, I. Pelant, *Basic features of transport in microcrystalline silicon*, Sol. Energ. Mat. Sol. C. **78**, 493 (2003) 493.

[Koh 1998] J. Koh, Y. Lee, H. Fujiwara, C. R. Wronski, and R. W. Collins, *Optimization of hydrogenated amorphous silicon p-i-n solar cells with two-step i layers guided by real-time spectroscopic ellipsometry*, Appl. Phys. Lett. **73**, 1526 (1998).

[Köhler 1985] K. Köhler, D.E. Horne, and J.W. Coburn, *Frequency dependence of ion bombardment of grounded surfaces in rf argon glow discharges in a planar system*, J. Appl. Phys. **58**, 3350 (1985).

[Kondo 1996] M. Kondo, Y. Toyoshima, A. Matsuda, and K. Ikuta, *Substrate dependence of initial growth of microcrystalline silicon in plasma-enhanced chemical vapor deposition*, J. Appl. Phys. **80**, 6061 (1996).

[Kondo 2000] M. Kondo, M. Fukawa, L. Guo, A. Matsuda, *High rate growth of microcrystalline silicon at low temperature*, J. Non-Cryst. Solids **266-269**, 84 (2000).

[Kondo 2003] M. Kondo, S. Suzuki, Y. Nasuno, M. Tanda and A. Matsuda, *Recent developments in the high growth rate technique of device-grade microcrystalline silicon thin film*, Plasma Sources Sci. Technol. **12**, S111 (2003).

[Kroll 1996] U. Kroll J. Meier, A. Shah, S. Mikhailov and J. Weber, *Hydrogen in amorphous and microcrystalline silicon films prepared by hydrogen dilution*, J. Appl. Phys. **80**, 4971 (1996).

[Lambertz 2001] A. Lambertz, O. Vetterl and F. Finger, *High deposition rate for μc-Si:H absorber layers using VHF PECVD at elevated discharge power and deposition pressure*, Proc. of the 17th European Photovoltaic Solar Energy Conference, Edited by B. McNelis, W. Palz, H.A. Ossenbrink and P. Helm (WIP-Renewable Energies, Munich), 2977 (2001).

[Lambertz 2005] A. Lambertz, private communication.

[Langford 1992] A. A. Langford, M. L. Fleet, B. P. Nelson, W. A. Langford, and N. Maley, *Infrared absorption strength and hydrogen content of hydrogenated amorphous silicon*, Phys. Rev. B **45**, 13367 (1992).

[Lossen 2003] J. Lossen, *Hot-Wire Schichten bei hohen Raten: Der Einfluss von Drahttemperatur, Depositionsabstand und Katalysatoroberfläche*, Diploma Thesis, Universität Köln, 2003.

[Lossen 2004] J. Lossen, S. Klein, and F. Finger, *Optimization of the filament arrangement at constant radiant heat in HWCVD for the preparation of compact μc-Si:H at high deposition rates*, Thin Solid Films **451-452**, 531 (2004).

[Lucovsky 1983] G. Lucovsky, J. Yang, S. S. Chao, J. E. Tyler, and W. Czubatyj, *Oxygen-bonding environments in glow-discharge-deposited amorphous silicon-hydrogen alloy films*, Phys. Rev. B **28**, 3225 (1983).

[Luft and Tsuo 1993] W. Luft and Y. S. Tsuo, *Hydrogenated amorphous silicon alloy deposition process*, Marcel Dekker, Inc., 1993.

[Luysberg 1997] M. Luysberg, P. Hapke, R. Carius, and F. Finger, *Structure and growth of microcrystalline silicon: Investigation by TEM and Raman spectroscopy of films grown at different plasma excitation frequencies*, Philos. Mag. A **75**, 31 (1997).

[Luysberg 2001] M. Luysberg, C. Scholten, L. Houben, R.Carius, F.Finger and O. Vetterl, *Structural properties of microcrystalline Si Solar cells*, Mat. Res. Soc. Symp. Vol. **664**, A15.2 (2001).

[Luysberg and Houben 2005] M. Luysberg and L. Houben, *Structure of microcrystalline solar cell materials: What can we learn from electron microscopy?* Mater. Res. Soc. Symp. Proc. Vol. **862**, A24.1 (2005).

[Mahan 1991] A. H. Mahan, B. P. Nelson, S. Salamon, and R. S. Crandall, *Deposition of device quality, Low H content a-Si:H by the hot wire technique*, J. Non-Cryst. Solids **137&138**, 657 (1991).

[Mahan 1998] A. H. Mahan, R. C. Reedy Jr., E. Iwaniczko, Q. Wang, B. P. Nelson, Y. Xu, A. C. Gallagher, H. M. Branz, R.S. Crandall, J. Yang, and S. Guha, Mat. Res. Soc. Symp. Proc. **507**, 119 (1998).

[Mahan 2000] A. H. Mahan, L. M. Gedvilas, and J. D. Webb, *SiĺCH bonding in low hydrogen content amorphous silicon films as probed by infrared spectroscopy and x-ray diffraction*, J. Appl. Phys. **87**, 1650 (2000).

[Mahan 2002] A. H. Mahan, Y. Xu, E. Iwaniczko, D. L. Williamson, B. P. Nelson, and Q. Wang, *Amorphous silicon films and solar cells deposited by HWCVD at ultra-high deposition rates*, J. Non-Crystal. Solids **299-302**, 2 (2002).

[Mai 2006] Y. Mai, S. Klein, X. Geng, M. Hülsbeck, R. Carius, and F. Finger, *Differences in the structure composition of microcrystalline silicon solar cells deposited by HWCVD and PECVD: Influence on open circuit voltage*, Thin Solid Films **501**, 272 (2006).

[Maley 1992] N. Maley, *Critical investigation of the infrared-transmission-data analysis of hydrogenated amorphous silicon alloys*, Phys. Rev. B **46**, 2078 (1992).

[Matsuda 1983] A. Matsuda, *Formation kinetics and control of microcrystallite in μc-Si:H from glow discharge plasma*, J. Non-Cryst. Solids **59&60**, 767

(1983).

[Matsuda 1983a] A. Matsuda, T. Kaga, H. Tanaka, L. Malhotra, and K. Tanaka, *Glow-discharge deposition of a-Si:H from pure Si_2H_6 and pure SiH_4*, Jpn. J. Appl. Phys. **22**, L115 (1983).

[Matsuda 2003] A. Matsuda, M. Takai, T. Nishimoto,M. Kondo, *Control of plasma chemistry for preparing highly stabilized amorphous silicon at high growth rate*, Solar Energy Materials & Solar Cells **78**, 3 (2003).

[Matsui 2004] T. Matsui, A. Matsuda and M. Kondo, *High-Rate Plasma Process for Microcrystalline Silicon: Over 9% Efficiency Single Junction Solar Cells*, Mat. Res. Soc. Symp. Proc. **808**, A8.11 (2004).

[Matsumura 1989] H. Matsumura, *Study on catalytic chemical vapor deposition method to prepare hydrogenated amorphous silicon*, J. Appl. Phys. **65**, 4396 (1989).

[Matsumura 1989a] H. Matsumura, *Low Temperature Deposition of Silicon Nitride by the Catalytic Chemical Vapor Deposition Method*, Jpn. J. Appl. Phys. **28**, 2157 (1989).

[Matsumura 1991] H. Matsumura, *Formation of polysilicon films by catalytic chemical vapor deposition (Cat-CVD) method*, Jpn. J. Appl.Phys. **30**, L1522 (1991).

[Matsumura 1998] H. Matsumura, *Formation of silicon-based thin films prepared by catalytic chemical vapor deposition (Cat-CVD) method*, Jpn. J. Appl. Phys. **37**, 3175 (1998).

[Matsuoka 1999] Y. Matsuoka, M. Shiratani, T. Fukuzawa, Y. Watanabe, and K. Kim, *Effects of Gas Flow on Particle Growth in Silane RF Discharges*, Jpn. J. Appl. Phys. **38**, 4556 (1999).

[Meier 1994] J. Meier, R. Flückiger, H. Keppner, and A. Shah, *Complete microcrystalline* p-i-n *solar cell-Crystalline or amorphous cell behavior?* Appl. Phys. Lett. **65**, 860 (1994).

[Meier 1996] J. Meier, P. Torres, R. Platz, S. Dubail, U. Kroll, J. A. Anna Selvan, N . Pellaton Vaucher, Ch. Hof, H. Keppner, A. Shah, K. D. Ufert, P.

Giannoules And J. Koehler. *On the way towards high efficiency thin film silicon solar cells by the "micromorph" concept*. Mater. Res. Soc. Symp. Proc., p. 3 (1996).

[Metzdorf 1987] J. Metzdorf, *Calibration of solar cells: the differential spectral responsivity method and characterization: simplified DSR apparatus*, Appl. Optics, **26**, 1701 (1987).

[Morris 1990] J. Morris, R. R. Arya, J.G. O'Dowd, S. Wiedemann, *Absorption enhancement in hydrogenated amorphous silicon (a-Si:H) based solar cells*. J. Appl. Phys. **67**, 1079 (1990).

[Mueck 2000] A. Mück, U. Zastrow, O. Vetterl, and B. Rech, *SIMS depth profile analysis of oxygen contamination in hydrogenated amorphous and microcrystalline silicon*, in: A. Benninghoven, P. Bertrand, H. N. Migeon, and H. W. Werner (eds.), proceeding of the 12^{th} International Conference in Secondary Ion Mass Spectroscopy, P. 689, Brussels, Belgium (2000).

[Müller 2004] J. Müller, B. Rech, J. Springer, M. Vaněček, *TCO and light trapping in silicon thin film solar cells*, Solar Energy **77**, 917 (2004).

[Nakamura 1995] K. Nakamura, K. Yoshino, S. Takeoka, and I. Shimizu, *Roles of atomic hydrogen in chemical annealing*, Jpn. J. Appl. Phys. **34**, 442 (1995).

[Niikura 2004] C. Niikura, M. Kondo, and A. Matsuda, *Preparation of microcrystalline silicon films at ultra high-rate of 10 nm/s using high-density plasma*, J. Non-Cryst. Solids **338-340**, 42 (2004).

[Nozaki 2000] Y. Nozaki, K. Kongo, T. Miyazaki, M. Kitazoe, K. Horii, H. Umemoto, A. Masuda, H. Matsumura, *Identification of Si and SiH in catalytic chemical vapor deposition of SiH_4 by laser induced fluorescence spectroscopy*, J. Appl. Phys. **88**, 5437 (2000).

[Oda and Noda 1988] S. Oda, and J. Noda, *Preparation of a-Si:H films by VHF plasma CVD*, Mat. Res. Soc. Sym. Proc. **118**, 117 (1988).

[Ossadnik 1999] Ch. Ossadnik, S. Vepřek, and I. Gregora, *Applicability of Raman scattering for the characterization of nanocrystalline silicon*, Thin Solid Films **337**, 148 (1999).

[Paesler 1978] M. A. Paesler, D. A. Anderson, E. C. Freeman, G. Moddel,

and W. Paul, *New development in the study of amorphous silicon hydrogen alloys: The story of O*, Phys. Rev. Lett. **41**, 1492 (1978).

[Perkowitz] S. Perkowitz, *Optical characterization of semiconductors: infrared, Raman, and photoluminescence spectroscopy*, Academic Press, (1993).

[Perrin 1991] J. Perrin, *Plasma and surface reaction druing a-Si:H film growth*, J. Non-Cryst. Solids **137&138**, 639 (1991).

[Poruba 2000] A. Poruba, A. Fejfar, O. Salyk, M. Vaněček, and J. Kocka, *Surface and bulk light scattering in microcrystalline silicon for solar cells*, J. Non-Cryst. Solids **271**, 152 (2000).

[Prasad 1990] K. Prasad, F. Finger, H. Curtins, A. Shah, and J. Bauman, *Preparation and characterization of highly conductive (100S/cm) phosphourus doped μc-Si:H films deposited using the VHF-GD technique*, Mat. Res. Soc. Symp. Proc. **164**, 27 (1990).

[Rath 1997] J. K. Rath, H. Meiling, and R. E. I. Schropp, *Purely intrinsic poly-Silicon films for n-i-p solar cells*, Jpn. J. Appl. Phys. **36**, 5436 (1997).

[Rath 2003] J. K. Rath, *Low temperature polycrystalline silicon: a review on deposition, physical properties and solar cell applications*, Sol. Energ. Mat. Sol. C. **76**, 431 (2003).

[Rath 2004] J. K. Rath, R. H. J. Franken, A. Gordijn, R. E. I. Schropp, and W. J. Goedheer, *Growth mechanism of microcrystalline silicon at high pressure conditions*, J. Non-Cryst. Solids **338-340**, 56 (2004).

[Rech 1997] B. Rech, C. Beneking, S. Wieder, and H. Wagner, *Initial and stablized open-circuit voltage of a-Si:H solar cells: a discussion on the basis of dark I-V curves*, In proceeding of 14th European Photovoltaic Solar Energy Conference, Barcelona, Spain, 30 June-4 July, 1997, p 574.

[Rech 1997a] B. Rech, *Solarzellen aus amorphem Silizium mit hohem stabilem Wirkungsgrad*, PhD thesis, RWTH Aachen, 1997.

[Rech 2002] B. Rech, T. Roschek, T. Repmann, J. Müller, R. Schmitz, and W. Appenzeller, *Microcrystalline silicon for large area thin film solar cells*, Thin Solid Films **427**, 157 (2003).

[Rech 2005] B. Rech, T. Repmann, J. Hüpkes, M. Berginski, H. Stiebig, W. Beyer, V. Sittinger, and F. Ruske, *Recent progress in amorphous and microcrystalline silicon based solar cell technology*, Proc. of 20th European Photovoltaic Solar Energy Conference, 6-10 June 2005, Barcelona, Spain, p.1481.

[Reimer 1993] L. Reimer. *Transmission electron microscopy*, Springer, Berlin, Heidelberg, New York (1993).

[Repmann 2004] T. Repmann, W. Appenzeller, B. Sehrbrock, H. Stiebig, B. Rech, *Advanced PECVD processes for thin-film silicon solar cells on glass*, in Proceedings of 19th European Photovoltaic Solar Energy Conference, Paris, France 2004, edited by W. Hoffmann, J.-L. Bal, H. Ossenbrink, W. Palz, and P. Helm (WIP, Munich, 2004), p. 1334.

[Richter 1983] H. Richter, Z.P. Wang, and L. Ley, *The one phonon Raman spectrum in microcrystalline silicon*, Solid State Commun. **39**, 625 (1981).

[Richter 1983] H. Richter, J. Trodahl, and M. Cardona, *The strecthing modes of the Si-H and Ge-H bonds in amorphous and crystalline Ge and Si*, J. Non-crystal. Solids, **59&60**, 181 (1983).

[Rosckek 2002] T. Roschek, T. Repmann, J. Müller, B. Rech, and H. Wagner, *Comprehensive study of microcrystalline silicon solar cells deposited at high rate using 13.56 MHz plasma-enhanced chemical vapor deposition*, J. Vac. Sci. Technol. A **20**, 492 (2002).

[Rosckek 2003] T. Roschek, *Microcrystalline silicon solar cells prepared by 13.56 MHz PECVD - Prerequisites for high quality material at high growth rate*, Ph.D. Thesis, Heinrich-Heine Universität Düsseldorf (2003).

[Rosckek 2004] T. Roschek, B. Rech, J. Muller, R. Schmitz, H. Wagner, *Influence of the total gas flow on the deposition of microcrystalline silicon solar cells*, Thin Solid Films **451-452**, 466, (2004).

[Ross 1984] R. C. Ross, *Plasma polymerization and deposition of amorphous hydrogenated silicon from rf and dc silan plasmas*, J. Appl. Phys. **55**, 3785 (1984).

[Ross 2000] C. Ross, J. Herion, R. Carius, and H. Wagner, *Nucleation and growth of low-temperature fine-crystalline silicon: a scanning probe microscopy and*

Raman spectroscopy study of the influence of hydrogen and different substrates, Mat. Sci. Eng. B **72**, 1 (2000).

[Ross 2005] C. Ross, Y. Mai, R. Carius, and F. Finger, *'Seed Layers' for the preparation of hydrogenated microcrystalline silicon with defined structural properties on glass*, Mat. Res. Soc. Symp. Proc. **862**, A10.4 (2005).

[Sah 1957] C. T. Sah, R. N. Noyce, and W. Shockley, *Carrier gerneration and recombination in p-n junction and p-n junction characteristics*, In Proc. of the IRE, Bd. **45**. S., 1228 (1957).

[Sakai 1990] H. Sakai, T. Yoshida, S. Fujikake, T. Hama, and Y. Ichikawa, *Effect of p/i interface layer on dark J-V characteristics and V_{OC} in p-i-n a-Si solar cells*, J. Appl. Phys. **67**, 3494 (1990).

[Sault and Goodman 1990] A. G. Sault and D. W. Goodman, *Reations of silane with the W(110) surface*, Surface Science **235**, 28 (1990).

[Schropp 1997] R.E.I. Schropp, K.F. Feenstra, E.C. Molenbroek, H. Meiling, J.K. Rath, *Device-quality polycrystalline and amorphous silicon films by hot-wire chemical vapour deposition*, Phil. Mag. B **76**, 309 (1997).

[Schropp and Zeman 1998] R. E. I. Schropp and M. Zeman, *Amorphous and microcrystalline silicon solar cells: modelling, material and device technology*, Kluwer Academic Publishers, 1998.

[Schropp 2004] R. E. I. Schropp, *Present status of micro- and polycrystalline silicon solar cells made by hot-wire chemical vapor deposition*, Thin Solid Films **451-452**, 455 (2004).

[Sendova-Vassileva 2004] M. Sendova-Vassileva, S. Klein, A. Lambertz, and F. Finger, *Stability of microcrystalline solar cells under treatment in water, air and vacuum*, in Proc. of 19th European Photovoltaic Solar Energy Conference, 7-11 June 2004, Paris, France, p. 1423.

[Shimizu 2004] T. Shimizu, *Staebler-Wronski effect in hydrogenated amorphous silicon and related alloy films*, Jpn. J. Appl. Phys. **43**, 3257 (2004).

[Shirai 1991] H. Shirai, J. Hanna, and I. Shimizu, *Role of atomic hydrogen during growth of hydrogenated amorphous silicon in the "Chemical Annealing"*, Jpn.

J. Appl. Phys. **30**, L679 (1991).

[Smit 2003] C. Smit, R. A. C. M. M. van Swaaij, H. Donker, A. M. H. N. Petit, W. M. M. Kessels, and M. C. M. van de Sanden, *Determining the material structure of microcrystalline silicon from Raman spectra*, J. Appl. Phys. **94**, 3582 (2003).

[Spear and LeComber 1975] W. E. Spear and P. G. LeComber, *Substitutional doping of amorphous silicon*, Solid State Comm. **17**, 1193 (1975).

[Staebler 1977] D. L. Staebler and C. R. Wronski, *Reversible conductivty changes in discharge-produced amorphous Si*, Appl. Phys. Lett. **31**, 292 (1977).

[Stannowski 2003] B. Stannowski, J. K. Rath, and R. E. I. Schropp, *Growth process and properties of silicon nitride deposited by hot-wire chemical vapor deposition*, J. Appl. Phys. **93**, 2618 (2003).

[Stiebig 2000] H. Stiebig, T. Brammer, J. Zimmer, O. Vetterl, and H. Wagner, *Investigation of the optoelectronic properties of μc-Si:H pin solar cells*, J. Non-Cryst. Solids **266-269**, 1104 (2000).

[Stiebig 2005] H. Stiebig, Private communication.

[Stutzmann 1989] M. Stutzmann, *The defect density in amorphous silicon*, Philos. Mag. B **60**, 531 (1989).

[Suzuki 2002] S. Suzuki, M. Kondo, and A. Matsuda, *Growth of device grade μc-Si film at over 50 (Å/s) using PECVD*, Sol. Energ. Mat. Sol. C. **74**, 489 (2002).

[Sze 1981] S. M. Sze, *Physics of Semiconductor Devices*, 2nd Edition, John Wiley & Sons, New York, (1981).

[Tange 2001] S. Tange, K. Inoue, K. Tonokura, M. Koshi, *Catalytic decomposition of SiH_4 on a hot filament*, Thin Solid Films 395, 42 (2001).

[Tsai 1989] C. C. Tsai, G. B. Anderson, R. Thompson, B. Wacker, *Control of silicon network structure in plasma deposition*, J. Non-Cryst. Solids **114**, 151 (1989).

[Tzolov 1997] M. Tzolov, F. Finger, R. Carius, and P. Hapke, *Optical and*

transport studies on thin microcrystalline silicon films prepared by very high frequency glow discharge for solar cell applications, J. Appl. Phys. **81**, 7376 (1997).

[Usui and Kikuchi] S. Usui and M. Kikuchi, *Properties of heavily doped gd-Si with low resistivity*, J. Non-Cryst. Solids **34**, 1 (1979).

[Vallat-Sauvain 2000] E. Vallat-Sauvain, U. Kroll, J. Meier, N. Wyrsch, A. Shah, *Microstructure and surface roughness of microcrystalline silicon prepared by very high frequency-glow discharge using hydrogen dilution*, J. Non-Cryst. Solids **266-269**, 125 (2000).

[van den Donker 2005] M. N. van den Donker, E. A. G. Hamers, and G. M. W. Kroesen, *Measurements and semi-empirical model describing the onset of powder formation as a function of process parameters in an RF silane-hydrogen discharge*, J. Phys. D: Appl. Phys. **38**, 2382 (2005).

[van den Donker 2005a] M.N. van den Donker, R. Schmitz, W. Appenzeller, B. Rech, W.M.M Kessels, M.C.M. van de Sanden, presented at the E-MRS spring meeting, Strasbourg, France (2005), to be published in Thin Solid Films.

[van den Donker 2005b] M. N. van den Donker, B. Rech, F. Finger, W.M.M. Kessels, and M.C.M. van de Sanden, *Highly efficient microcrystalline silicon solar cells deposited from a pure SiH_4 flow*, Appl. Phys. Lett. **87**, 263503 (2005).

[Vaněček 1998] M. Vaněček, A. Poruba, Z. Remeš, N. Beck, M. Nesládek, *Optical properties of microcrystalline materials*, J. Non-Cryst. Solids **227-230**, 967 (1998).

[Vaněček 2000] M. Vaněček, A. Poruba, Z. Remeš, J. Rosa, S. Kamba, V. Vorlíček, J. Meier, A. Shah, *Electron spin resonance and optical characterization of defects in microcrystalline silicon*, J. Non-Cryst. Solids **266-269**, 519 (2000).

[Vepřek and Mareček 1968] S. Vepřek and V. Mareček, *The preparation of thin layers of Ge and Si by chemical hydrogen plasma transport*, Solid-State Electron. **11**, 683 (1968).

[Vepřek 1981] S. Vepřek, Z. Iqbal, H. R. Oswald and A. P. Webb, *Properties of polycrystalline silicon prepared by chemical transport in hydrogen plasma at temperatures between 80 and 400 °C*, J. Phys. C: Solid State Phys. **14**, 295 (1981).

[Vepřek 1983] S. Vepřek, Z. Iqbal, R. O. Kühne, P. Capezzuto, F. A. Sarott, and J. K. Gimzewski, *Properties of microcrystalline silicon: IV. Electrical conductivity, electron spin resonance and the effect of gas adsorption*, J. Phys. C: Solid State Phys. **16**, 6241 (1983).

[Vepřek 1989] S. Vepřek, F. -A. Sarrot, S. Rambert, and E. Taglauer, *Surface hydrogen content and passivation of silicon deposited by plasma induced chemical vapor deposition from silane and the implications for the reaction mechanism*, J. Vac. Sci. Technol. A **7**, 2614 (1989).

[Vepřek 1990] S. Vepřek, *Chemistry and solid state physics of microcrystalline silicon*, Mat. Res. Soc. Symp. Proc. **164**, 39 (1990).

[Vetterl 2000] O. Vetterl, F. Finger, R. Carius, P. Hapke, L. Houben, O. Kluth, A. Lambertz, A. Mück, B. Rech, and H. Wagner, *Intrinsic microcrystalline silicon: A new material for photovoltaics*, Sol. Energ. Mat. Sol. C. **62**, 97 (2000).

[Vetterl 2001] O. Vetterl, A. Lambertz, A. Dasgupta, F. Finger, B. Rech, O. Kluth, H. Wagner, *Thickness dependence of microcrystalline silicon solar cell properties*, Sol. Energ. Mat. Sol. C. **66**, 345 (2001).

[Vetterl 2001a] O. Vetterl, *On the physics of microcrystalline silicon thin film solar cells - From the material to devices with high conversion efficiencies.* Ph.D. thesis, Heinrich-Heine-Universität Düsseldorf (2001a).

[Vetterl 2002] O. Vetterl, A. Groß, T. Jana, S. Ray, A. Lambertz, R. Carius, and F. Finger, *Changes in electric and optical properties of intrinsic microcrystalline silicon upon variation of the structural composition*, J. Non-Cryst. Solids **299-302**, 772 (2002).

[Vetterl 2003] O. Vetterl, M. Hülsbeck, J. Wolff, R. Carius, and F. Finger, *Preparation of microcrystalline silicon seed-layers with defined structural properties*, Thin Solid Films **427**, 46 (2003).

[Wada 2002] T. Wada, M. Kondo, and A. Matsuda, *Improvement of V_{OC} using carbon added microcrystalline Si p-layer in microcrystalline Si solar cells*, Sol. Energ. Mat. Sol. C. **74**, 533 (2002).

[Wagner and Beyer 1983] H. Wagner, and W. Beyer, *Reinterpretation of the silicon-hydrogen stretch frequencies in amorphous silicon*, Solid State Comm. **48**,

585 (1983).

[Wang and Lucovsky 1990] C. Wang and G. Lucovsky, *Intrinsic microcrystalline silicon deposited by remote PECVD: a new thin-film photovoltaic material*. In Proceedings of the 21st IEEE Photovoltaic Specialists Conference, p. 1614 (1990).

[Watanabe 1996] Y. Watanabe, M. Shiratani, T. Fukuzawa, H. Kawasaki, Y. Ueda, S. Singh, and H. Ohkura, *Contribution of short lifetime radicals to the growth of particles in SiH_4 high frequency discharges and the effects of particles on deposited films*, J. Vac. Sci. Technol. A **14**, 995 (1996).

[Wu 1996] Y. Wu, J. T. Stephen, D. X. Han, J. M. Rutland, R. S. Crandall, and A. H. Mahan, *New Hydrogen Distribution in a-Si:H: An NMR Study*, Phys. Rev. Lett. **77**, 2049 (1996).

[Wyrsch 1991] N. Wyrsch, F. Finger, T. J. McMahon, and M. Vanecek, *How to reach more precise interpretation of subgap absorption spectra in terms of deep defect density in a-Si:H*, J. Non-Cryst. Solids, **137**&**138**, 347 (1991).

[Xi 1994] J. Xi, D. Shugar, and H. Volltrauer, *Large area module performance and identification and control of P-I interface-correlated device degradation and further improvement in stablize efficiency of single-junction a-Si solar cell*, First WCPEC; DeC. 5-9, 1994 Hawaii, Proc. 24th IEEE PV Specialists Conference, p.401.

[Yacobi 1981] B. G. Yacobi, R. W. Collins, G. Moddel, P. Viktorovitch, and W. Paul, *Effect of oxygen on the optoelectronics properties of amorphous hydrogenated silicon*, Phys. Rev. B **24**, 5907 (1981).

[Yamamoto 2000] K. Yamamoto, M. Yoshimi, Y. Tawada, Y. Okamoto, and A. Nakajima, *Thin film Si solar cell fabricated at low temperature*, J. Non-Cryst. Solids **266-269**, 1082 (2000).

[Yamamoto 2003] K. Yamamoto, A. Nakajima, M. Yoshimi, T. Sawada, S. Fukuda, T. Suezaki, M. Ichikawa, Y. Koi, M. Goto, H. Takata, T. Sasaki, and Y. Tawada, *Novel hybrid thin film silicon solar cell and module*, Proc. 3rd World Conference on Photovoltaic Energy Conversion, Osaka, Japan, 11-18 May 2003. p. S2B903.

[Yan 2002] B. Yan, K. Lord, J. Yang, S. Guha, J. Smeets and J. Jacquet,

Hydrogenated microcrystalline silicon solar cells made with modified very-high-frequency glow discharge, Mat. Res. Soc. Symp. Proc. **715**, A26.4 (2002).

[Yan 2004] B. Yan, G. Yue, J. M. Owens, J. Yang, and S. Guha, *Light-induced metastability in hydrogenated nanocrystalline silicon solar cells*, Appl. Phys. Lett. **85**, 1925 (2004).

[Yang 1997] J. Yang, A. Banerjee, and S. Guha, *Triple-junction amorphous silicon alloy solar cell with 14.6% initial and 13.0% stable conversion efficiencies*, Appl. Phys. Lett. **70**, 2975 (1997).

[Zhao 1999] J. Zhao, A. Wang, and M. A. Green, *24.5% Efficiency Silicon PERT Cells on MCZ Substrates and 24.7% Efficiency PERL Cells on FZ Substrates*, Prog. Photovolt: Res. Appl. **7**, 471 (1999).

Acknowledgments

At the end of this thesis, I would like to acknowledge those people who kindly offer help during this work.

First of all, I express my appreciation to Prof. X. Geng of Nankai University. She has been my supervisor for more than 6 years even since I became a master student in 1999. I thank her for her continuous guidance and consideration.

My deepest gratitude will be given to Dr. F. Finger. He has been a fantastic supervisor and friend whose comments and criticism were always so mild, so precise and so valuable. I also deeply appreciate his great patience and wisdom in the experiment design, result discussion and manuscript correction.

I thank Dr. S. Klein for his selfless help with the experiments and result analysis. The discussion with Dr. R. Carius helped to solve many difficulties. I also thank him a lot.

I thank Dr. W. Beyer, Dr. B. Rech, Dr. H. Stiebig, Dr. T. Brammer, Dr. T. Repmann and Mr. A. Lambertz for the constructive discussions in the material and solar cell physics.

Mr. J. Wolff and Mr. A. Lambertz are greatly appreciated for their technical assistance.

I would like to thank Mr. J. Klomfass for the PDS and CPM measurements, Mr. M. Hülsbeck for the Raman scattering measurements. Mr. F. Birmanns, Mr. W. Reetz, and Mr. Ch. Zahren are acknowledged for their helps with the J-V, QE measurements and light-induced degradation experiments.

I thank Mrs. H. Siekmann, Ms. S. Michel, Mr. G. Schöpe, Mrs. B. Zwaygardt, Dr. J. Hüpeks, and Dr. O. Kluth for the ZnO:Al substrate and back contact preparation.

I appreciate Dr. M. Luysberg and Dr. L. Houben for the TEM measurements on the solar cells.

Dr. S. Klein, Dr. A. Gordijn, Dr. Ch. Ross and Mr. M. van den Donker carefully read this thesis and gave many constructive suggestions. Here, I say thanks to them.

Mrs. A. Mühlheims was very helpful with many organizational and administrative problems and I thank her very much.

I thank all colleagues from IPV. The three years together with them is a wonderful period to be remembered in my whole life.

I dedicate this work to my parents and my wife.

Forschungszentrum Jülich
in der Helmholtz-Gemeinschaft

Jül-4254
September 2007
ISSN 0944-2952